Stony Brook University

Classical Strongly Coupled Quark-Gluon Plasma

A Dissertation Presented

by

Sung Tae Cho

to

The Graduate School

in Partial Fulfillment of the Requirements

for the Degree of

Doctor of Philosophy

in

Physics

Stony Brook University

December 2009

Stony Brook University

The Graduate School

Sung Tae Cho

We, the dissertation committee for the above candidate for the Doctor of Philosophy degree, hereby recommend acceptance of this dissertation.

Ismail Zahed - Dissertation Advisor
Professor, Department of Physics and Astronomy

Edward Shuryak - Chairperson of Defense
Distinguished professor, Department of Physics and Astronomy

Vladimir Goldman
Professor, Department of Physics and Astronomy

Roy Lacey
Professor, Department of Chemistry

This dissertation is accepted by the Graduate School.

Lawrence Martin
Dean of the Graduate School

Abstract of the Dissertation

Classical Strongly Coupled Quark-Gluon Plasma

by

Sung Tae Cho

Doctor of Philosophy

in

Physics

Stony Brook University

2009

In the first part of this thesis, we focus on the equilibrium properties of the SU(N) classical quark-gluon plasma (cQGP). We define the partition function of the cQGP through three expansions: A low density expansion, a cumulant expansion, and a high temperature expansion or loop expansion. We derive the equation of state of the cQGP and compare it to the SU(2) and SU(3) lattice data.

In the second part of the thesis, we address the non-equilibrium issues of the SU(2) cQGP. We derive generalized relations for the multiple color structure factors and compare them to results from molecular dynamics simulation. We use the classical Liouville

equations to derive non-pertubative expressions for the transport coefficient, e.g, the viscosity and diffusion constant.

In the third part of the thesis, we address the issue of the energy loss of heavy jet quarks in the SU(2) cQGP. We compare our results to molecular dynamics simulation results at intermediate and strong Coulomb coupling.

To my family.

Contents

List of Figures

List of Tables

Acknowledgements

I would like to thank my advisor, Prof. Zahed. Without his patience and guidance during my research, this thesis would not have been possible. I also would like to thank members of Nuclear Theory Group, especially Prof. Shuryak and Prof. Brown for their encouragement and support. I am grateful to committee members, Prof. Goldman and Prof. Lacey.

I am very fortunate to have been a graduate student of Nuclear Theory Group. I have learned many things directly or indirectly from faculty members and also from my fellow graduate students. I thank them. I also thank Korean graduate students in physics department for making my life in Stony Brook more enjoyable.

Finally, I am much indebted to my parents, my sister and my brother. This work would not have been possible without their love, encouragement and support.

Chapter 1

Introduction

1.1 Strongly coupled quark-gluon plasma

Relativistic Heavy Ion Collision (RHIC) experiments carried out at Brookhaven National Laboratory (BNL) create new form of matter called quark-gluon plasma (QGP), which cannot exist in nature and is believed to have existed for a moment right after Big Bang. The research on QGP, the high temperature state of quarks and gluons, makes it possible for us to have a deeper understanding about the strong interactions between quarks and gluons and also the properties of the initial state of matter created after Big Bang.

The QGP, also a high temperature state of quantum chromodynamics (QCD), has been studied through various direct and indirect methods. The tools for the research on QGP include photons, dileption pair production from a virtual photon in QGP, bound states of heavy quark systems and so on.

These approaches to QGP have been mostly based on the assumption that the interaction between quasiparticles is weak enough to be treated perturbatively since it has been believed that at high enough temperature, quarks and

gluons in hadrons can overcome the strong forces confining them and become free quasiparticles. But it was recently shown that quarks and gluons in QGP near but above the phase transition temperature T_c are not weakly coupled, which contradicts the main assumption. Thereafter, the QGP near T_c, a system composed of strongly coupled particles, has been named as a strongly coupled QGP (sQGP).

The research on sQGP has been more various than that on QGP. These studies include the research on trapped ultracold atoms, the strongly coupled one-component plasma, the transport theory through the linear response theory, the relativistic hydrodynamics theory, the gauge theory of gravity, and string theory/AdS-CFT correspondence.

The group of physicists doing research through the relativistic hydrodynamics, for example, has succeeded in describing the properties of radial and elliptic flows produced after the collision of heavy ions, which shows that the newly found state of collective particles has the shorter mean-free path and the stronger color dissipation. Theorists studying the $\mathcal{N} = 4$ supersymmetric Yang-Mills theory also have shown that QGP found near T_c is strongly coupled by presenting the ratio of the shear viscosity to the entropy density $\eta/s = 1/4\pi$, the lowest value we have ever found, where η is the shear viscosity and s is the entropy density. And recently, the new approach to describe the particles in QGP as the classical particles of non-Abelian color charges interacting through the color Coulomb force (classical QGP, cQGP) has been developed and the lower $\eta/s \simeq 0.34$ from the molecular dynamics simulations based on cQGP has been known.

1.2 Classical QGP

In this thesis, we adopt the model of classical quark-gluon plasma (cQGP) developed by Gelman, Shuryak and Zahed and study further various properties of cQGP. cQGP consists of classical particles of like-mass m with 3-position $\boldsymbol{r}_i(t)$ and 3-momentum $\boldsymbol{p}_i(t)$ with N_c^2-1 adjoint colored charges $Q_i^\alpha(t)$ and fixed N_c-1 Casimirs. Particle motion in the cQGP is treated classically through

$$\begin{aligned} m\frac{dr_i^\mu(t)}{dt} &= p_i^\mu(t) \\ m\frac{dp_i^\mu(t)}{dt} &= gQ^\alpha F_a^{\mu\nu}(r_i)p_{i\nu}(t) \\ m\frac{dQ_i^\alpha(t)}{dt} &= -gf^{\alpha\beta\gamma}p_i^\mu(t)A_\mu^\beta(r_i)Q_i^\gamma(t) \end{aligned} \tag{1.2.1}$$

The repulsive effects of the core is subsumed. A^μ is the gauge field on the ith particle due to all other particles, $F_\alpha^{\mu\nu}$ is its field strength, and $f^{\alpha\beta\gamma}$ the pertinent structure constant for $SU(N_c)$. The last relation is Wong's equation. The magnetic contribution to the Lorentz force is suppressed by v/c and dropped in the electric cQGP.

The Hamiltonian for the cQGP reads

$$H=\sum_{a,i}\frac{p_{a,i}^2}{2m_a}+\frac{1}{2}\frac{g^2}{4\pi}\sum_{a,i\neq a',j}\frac{Q_{a,i}^\alpha Q_{a',j}^\alpha}{\mid \boldsymbol{r}_{a,i}-\boldsymbol{r}'_{a',j}\mid}+V_{core} \tag{1.2.2}$$

where the core potential is now explicit. The double sum is over species a (to be set to 3 below) and particle index $i=1,..,N$. In terms of the color charge density. Therefore, we use the following equations of motion.

$$\frac{d\boldsymbol{r}_i}{dt} = \frac{\boldsymbol{p}_i}{m} \tag{1.2.3}$$

for the position in space. Repeated indices are summed over. The Newtonian equation of motion is just the colored electric Lorentz force

$$\frac{d\boldsymbol{p}_i}{dt} = Q_i^a \, \boldsymbol{E}_i^a = \boldsymbol{F}_i \tag{1.2.4}$$

with the colored electric field and potentials defined as ($a = 1, 2, \cdots, N_c^2 - 1$)

$$\boldsymbol{E}_i^a = -\boldsymbol{\nabla}_i \Phi_i^a = -\boldsymbol{\nabla}_i \sum_{j \neq i} \frac{Q_j^a}{|\boldsymbol{r}_i - \boldsymbol{r}_j|} \tag{1.2.5}$$

The equation of motion of the color charges is

$$\frac{dQ_i^a}{dt} = \sum_{j \neq i} \frac{Q_i T^a Q_j}{|\boldsymbol{r}_i - \boldsymbol{r}_j|} \tag{1.2.6}$$

for arbitrary color representation.

1.3 Outline of thesis

In the first two chapters, we concentrate on the equilibrium properties of sQGP. We define the most important thermodynamic function, the grand partition function and calculate the free energy of the classical QGP through three expansions. A cumulant expansion, a high temperature expansion and a loop expansion are those. We show explicitly the effect of color charges in each expansion.

Then we construct the equation of the state of cQGP valid for all interaction strength by combining an analytic calculation with the result from

molecular dynamics simulation. We test our result by comparing the running coupling constant extracted from the energy density fit to the running coupling constant directly measured by the lattice. We also predict the pressure and entropy of cQGP for $0 < T/T_c < 5$. We confirm that QGP at equilibrium near T_c is in a liquid state.

In the second part of this thesis, we consider non-equilibrium properties of cQGP. First, we emphasize the importance of correlation functions which play a central role in explaining the dynamics of a system of strongly coupled particles. We generalize the Ornstein-Zernicke relation for cQGP and use it to derive the structure factor, the density correlation function, in an analytic form. We concentrate on the structure factor of the zeroth and first channel. We also present structure factors obtained by the molecular dynamics simulation.

In the next chapter, we focus on the kinetics of cQGP. Starting from the derivation of the colored Liouville operator, we construct the equation of motion for the correlation functions containing the self-energy kernel, which has the information about the non-local collision effects. Finally we show how to extract the transport coefficients from the self-energy kernel through the hydrodynamical modes.

In the last part of thesis, we explain the energy loss of heavy quarks travelling through SU(2) classical colored plasma. We derive the equation for the energy loss using the linear response theory and the fluctuation-dissipation theorem. We investigate the energy loss in various limits and compare our result to results from the molecular dynamics simulation.

Chapter 2

Free energy

2.1 Introduction

Plasmas are statistical classical/quantum systems involving charge constituents. Notable are electromagnetic plasmas whereby the underlying constituents interact through long range Coulomb fields. The simplest theory of electromagnetic plasmas is the One Component Plasma (OCP) whereby the constituents are like (negative) charges embedded in a uniform and neutralizing unlike (positive) background. A number of analytical approaches to the OCP exist in the form of diagrammatic or field theoretical methods [1, 2]. These formal approaches form a useful theoretical corpus for understanding ionic liquids.

Ionic liquids are characterized by a short range repulsive core in addition to the long range Coulomb potential. The core is a scalar with a range of the order of the interparticle distance, while the Coulomb attraction is vectorial with infinite range. Reference liquids are described by a repulsive pair potential $w(x) = \infty$ for $x < \sigma$ and $w(x) = 0$ for $x > \sigma$ where σ is the diameter of a hard sphere. The Coulomb potential is generally viewed as a *perturbation* added

to the repulsive core. Many models of ionic liquids have been developed to accommodate arbitrary charges and cores such as the Primitive Model (PM). Spinoffs are the Restricted Primitive Model (RPM) with opposite charge pairs and the same core, and the Special Primitive Model (SPM) with arbitrary charges and the same core.

The Classical Quark Gluon Plasma (cQGP) as developed by Gelman, Shuryak and Zahed can be regarded as an example of an SPM model in ionic liquids, albeith with *non-Abelian* colored charges [3]. The nature of the core in the CQGP is quantum mechanical and thus assumed. Detailed molecular dynamics simulations of the cQGP [3] have shown a strongly coupled plasma for $\Gamma = V/K \approx 1$, i.e. whenever the potential energy is of the order of the kinetic energy. The classical and colored cQGP maybe in a liquid state at moderate values of Γ prompting us to use methods for classical liquids to analyze it.

This chapter is the first of a series of sequels to [3] to develop analytical methods to address the many-body dynamics of the cQGP. In section 2.2, we define the partition function of the cQGP as a classical but colored liquid. In section 2.3 and 2.4, we work out the partition function in the low density limit through a cumulant expansion after resumming the Debye screening effects. In section 2.5, we discuss a high temperature expansion. In section 2.6, we detail a diagrammatic or loop expansion for the cQGP that is justified at high temperatures. We carry the expansion to three loops. In section 2.7, we unwind the free energies both in the loop and density expansions. In section 2.8, we compare the excess free energies to recent molecular dynamics simulations. Our conclusions are in section 2.9. Useful definitions and color integrations are given in the Appendices 2.10.

2.2 The grand canonical partition function for cQGP

The cQGP has been defined in [3]. It consists of classical particles of like-mass m with 3-position $\boldsymbol{x}_i(t)$ and 3-momentum $\boldsymbol{p}_i(t)$ with N_c^2-1 adjoint colored charges $Q_i^\alpha(t)$ and fixed N_c-1 Casimirs. Because of the constraints, the color variables are Darboux's type as summarized in the Appendix. (see also [4]). Particle motion in the cQGP is treated classically through

$$\begin{aligned} m\frac{dx_i^\mu(t)}{dt} &= p_i^\mu(t) \\ m\frac{dp_i^\mu(t)}{dt} &= gQ^\alpha F_a^{\mu\nu}(x_i)p_{i\nu}(t) \\ m\frac{dQ_i^\alpha(t)}{dt} &= -gf^{\alpha\beta\gamma}p_i^\mu(t)A_\mu^\beta(x_i)Q_i^\gamma(t) \end{aligned} \tag{2.2.1}$$

where we have trivially covariantized the notations. The repulsive effects of the core is subsumed [3]. A^μ is the gauge field on the ith particle due to all other particles, $F_\alpha^{\mu\nu}$ is its field strength, and $f^{\alpha\beta\gamma}$ the pertinent structure constant for $SU(N_c)$. The last relation is Wong's equation [5]. The magnetic contribution to the Lorentz force is suppressed by v/c and dropped in the electric cQGP. cQGP simulations with both electric and magnetic charges can be found in [6].

The Hamiltonian for the cQGP reads

$$H=\sum_{a,i}\frac{p_{a,i}^2}{2m_a}+\frac{1}{2}\frac{g^2}{4\pi}\sum_{a,i\neq a',j}\frac{Q_{a,i}^\alpha Q_{a',j}^\alpha}{\mid \boldsymbol{x}_{a,i}-\boldsymbol{x}'_{a',j}\mid}+V_{core} \tag{2.2.2}$$

where the core potential is now explicit. The double sum is over species a (to

be set to 3 below) and particle index $i = 1, .., N$. In terms of the color charge density

$$\rho^{\alpha}(\boldsymbol{r}) = \sum_{a,i} Q^{\alpha}_{a,i} \delta(\boldsymbol{r} - \boldsymbol{r}_{a,i}) \tag{2.2.3}$$

the grand partition function for the cQGP is

$$\begin{aligned} Z &= \sum_{N_a} \int \prod_a \frac{1}{N_a!} \prod_{a,i}^{N_a} (dQ_{a,i} d^3 r_{a,i} n_a) \\ &\times \prod_{\alpha}^{N_c^2 - 1} \exp\left(-\frac{1}{2} \beta \int d^3 r d^3 r' \rho^{\alpha}(\boldsymbol{r}) v(\boldsymbol{r} - \boldsymbol{r}') \rho^{\alpha}(\boldsymbol{r}') \right) \end{aligned} \tag{2.2.4}$$

with

$$v(\boldsymbol{r} - \boldsymbol{r}') = \frac{g^2}{4\pi} \frac{1}{\mid \boldsymbol{r} - \boldsymbol{r}' \mid} \tag{2.2.5}$$

and the free particle density

$$n_a = g_a \frac{1}{{\Lambda_a}^3} e^{\beta \mu_a} \ . \tag{2.2.6}$$

g_a is the degeneracy factor and μ_a^{α} the chemical potential of species a. The factor of Λ_a^{-3} is the thermal wavelength resulting from the momentum integral over phase space. The repulsive core potential is set to be

$$w(\boldsymbol{r} - \boldsymbol{r}') = \begin{cases} \infty & (\mid \boldsymbol{r} - \boldsymbol{r}' \mid < \sigma) \\ 0 & (\mid \boldsymbol{r} - \boldsymbol{r}' \mid > \sigma) \end{cases}$$

with a core size σ to prevent classical collapse. In reality, the core emerges

from Coulomb repulsion between like-particles or the quantum uncertainty repulsion between unlike/like particles. With this in mind, we can rewrite (2.2.4) in the form

$$
\begin{aligned}
Z = \sum_{N_a} \int \prod_a \frac{1}{N_a!} \prod_{a,i}^{N_a} (dQ_{a,i} d^3 r_{a,i} n_a) \prod_{\alpha}^{N_c^2-1} \\
\times \exp\left(-\tfrac{1}{2}\beta \int d^3r d^3r' \rho^\alpha(\boldsymbol{r}) v(\boldsymbol{r}-\boldsymbol{r}') \rho^\alpha(\boldsymbol{r}') \right) \\
\times e^{\frac{1}{2}w_0} \exp\left(-\tfrac{1}{2} \int d^3r d^3r' \rho(\boldsymbol{r}) w(\boldsymbol{r}-\boldsymbol{r}') \rho(\boldsymbol{r}') \right)
\end{aligned}
\tag{2.2.7}
$$

with the number density $\rho(\boldsymbol{r}) = \sum_{a,i} \delta(\boldsymbol{r} - \boldsymbol{r}_{a,i})$. $w_0 = w(0)$ is identified with the self-energy.

The repulsive core (2.2.7) acts like the potential between two hard spheres with diameter $R = \sigma$. Thus, we may treat each particle classically as a rigid sphere of diameter R with uniform color charge Q^α on the surface,

$$
Q\, q(\boldsymbol{x}) = \frac{Q}{\pi R^2} \delta(|\boldsymbol{x}| - R/2) \tag{2.2.8}
$$

The repulsive core (2.2.7) is now generated classically as the Coulomb repulsion between the rigid spheres [7]. For two spheres located at $\boldsymbol{r}$ and $\boldsymbol{r}'$ this is

$$
W(\boldsymbol{r}-\boldsymbol{r}') = \int d\boldsymbol{x} d\boldsymbol{y} q(|\, \boldsymbol{r} - \boldsymbol{x}\, |) \frac{1}{|\, \boldsymbol{x} - \boldsymbol{y}\, |} q(|\, \boldsymbol{r}' - \boldsymbol{y}\, |)\ . \tag{2.2.9}
$$

The grand canonical partition function follows in the form

$$Z = \sum_{N_a} \int \prod_a \frac{1}{N_a!} \prod_{a,i}^{N_a} (dQ_{a,i} d^3 r_{a,i} n_a) e^{\gamma (N_c^2-1) W_0} e^{-v_{HS}}$$
$$\times \exp\Big(-\tfrac{\beta}{2} \tfrac{g^2}{4\pi} \textstyle\sum_\alpha^{N_c^2-1} \int d^3 r d^3 r' \rho^\alpha(\boldsymbol{r}) W(\boldsymbol{r}-\boldsymbol{r}') \rho^\alpha(\boldsymbol{r}') \Big) \qquad (2.2.10)$$

where the Coulomb self energy is now $W_0 = W(\mathbf{0})/2$ and γ_a

$$\gamma_a = \beta \frac{g^2}{4\pi} \frac{1}{N_c^2 - 1} \sum_\alpha Q_a^{\alpha 2} \qquad (2.2.11)$$

2.3 Liquid of Colored Hard Spheres

To analyze (2.2.10) we first consider a dilute cQGP with N_c colors. Performing $(N_c^2 - 1)$ times the Sine-Gordon transform on (2.2.10) yields

$$\exp\Big(-\frac{\beta}{2} \frac{g^2}{4\pi} \sum_\alpha^{N_c^2-1} \int d\boldsymbol{r} d\boldsymbol{r}' \rho^\alpha(\boldsymbol{r}) W(\boldsymbol{r}-\boldsymbol{r}') \rho^\alpha(\boldsymbol{r}') \Big)$$
$$= \langle \exp\Big(\sum_\alpha^{N_c^2-1} i (\beta \frac{g^2}{4\pi})^{1/2} \int d\boldsymbol{r} \rho^\alpha(r) \phi^\alpha(r) \Big) \rangle_W \qquad (2.3.1)$$

where the averaging on the RHS (right hand side) is carried using the measure

$$\langle \cdots \rangle_W = \frac{\int [\prod_\alpha^{N_c^2-1} d\phi^\alpha] (\cdots) \exp\Big(-\frac{1}{2} \sum_\alpha^{N_c^2-1} \int d\boldsymbol{r} d\boldsymbol{r}' \phi^\alpha(\boldsymbol{r}) W^{-1}(\boldsymbol{r}-\boldsymbol{r}') \phi^\alpha(\boldsymbol{r}') \Big)}{\int [\prod_\alpha^{N_c^2-1} d\phi^\alpha] \exp\Big(-\frac{1}{2} \sum_\alpha^{N_c^2-1} \int d\boldsymbol{r} d\boldsymbol{r}' \phi^\alpha(\boldsymbol{r}) W^{-1}(\boldsymbol{r}-\boldsymbol{r}') \phi^\alpha(\boldsymbol{r}') \Big)} \qquad (2.3.2)$$

To proceed further, we define

$$\tilde{\nu}_a = \beta\tilde{\mu}_a = \beta\mu_a + (N_c^2 - 1)\gamma W_0$$
$$\tilde{n}_a = n_a e^{(N_c^2-1)\gamma W_0} e^{i(\beta\frac{g^2}{4\pi})^{\frac{1}{2}} \sum_{\alpha}^{N_c^2-1} \sum_{a,i} Q_{a,i}^{\alpha} \phi^{\alpha}(\boldsymbol{r}_{a,i})} \tag{2.3.3}$$

as the renormalized chemical potential and species densities respectively. In terms of which the grand canonical partition function is now

$$Z = \sum_{N_a} \int \prod_a \frac{1}{N_a!} \prod_{a,i}^{N_a} (dQ_{a,i} d^3 r_{a,i} \langle \tilde{n}_a \rangle_W) e^{-v_{HS}} \equiv \langle Z_{HS} \rangle_W \tag{2.3.4}$$

$e^{-v_{HS}}$ is short for the Gaussian measure in (2.3.2). (2.3.2) can be Taylor expanded around the mean density n_a (see below). The result is

$$\begin{aligned} \ln\left(\frac{Z}{Z_{HS}}\right) &= \sum_{n=1} \tfrac{1}{n!} \sum_{a_1,a_2,\cdots,a_n} \int (d^3 r_{a_1} dQ_{a_1}) \cdots (d^3 r_{a_n} dQ_{a_n}) \\ &\times \frac{\delta^n \ln Z}{\delta\tilde{n}_{a_1}(\boldsymbol{r}_{a_1}) \cdots \delta\tilde{n}_{a_n}(\boldsymbol{r}_{a_n})} \Big|_{\tilde{n}_{a_i}(\boldsymbol{r}_{a_i}) = n_a} \prod_{i=1}^{n} (\tilde{n}_{a_i}(\boldsymbol{r}_{a_i}) - n_a) \end{aligned} \tag{2.3.5}$$

If we were to assume that the species chemical potentials are all the same $\mu_{a_1} = \cdots = \mu_{a_n} = \mu_a$, then in the free particle case

$$\mu_0 = \mu_a + \frac{1}{\beta}\ln(3), \qquad n_0 = 3n_a = 3\lambda \tag{2.3.6}$$

We have set the particle species to 3 to account classically for quarks, anti-quarks and gluons all of equal constituent thermal mass m for simplicity. In terms of (2.3.6) the integrand in (2.3.3) can be identified with the classical correlation function $h_0^{(n)}$ of a liquid of hard spheres [7]

$$n_a{}^n \frac{\delta^n \ln Z}{\delta\tilde{n}_{a_1}(\boldsymbol{r}_{a_1})\cdots\delta\tilde{n}_{a_n}(\boldsymbol{r}_{a_n})}\Big|_{\tilde{n}_{a_i}(\boldsymbol{r}_{a_i})=n_a} = \frac{\rho_0'^n}{3^n} h_0^{(n)}(\boldsymbol{r}_{a_1},\cdots\boldsymbol{r}_{a_n}) = \rho_0^n h_0^{(n)}(\boldsymbol{r}_{a_1},\cdots\boldsymbol{r}_{a_n}) \tag{2.3.7}$$

with the number density

$$\rho_0' = \frac{1}{V}\frac{\partial \ln Z_{HS}}{\partial \nu_0} \tag{2.3.8}$$

Thus, the partition function for a colored liquid of hard spheres now read

$$\ln\left(\frac{Z}{Z_{HS}}\right) = \langle \exp(-U[\phi^\alpha])\rangle_W = \mathcal{N}_W^{-1}\int [\prod_\alpha d\phi^\alpha]\exp(-S[\phi^\alpha]) \tag{2.3.9}$$

with

$$\begin{aligned}
\mathcal{N}_W &= \int [\prod_\alpha d\phi^\alpha]\exp\Big(-\frac{1}{2}\sum_\alpha^{N_c^2-1}\int d\boldsymbol{r}d\boldsymbol{r}'\phi^\alpha(\boldsymbol{r})W^{-1}(\boldsymbol{r}-\boldsymbol{r}')\phi^\alpha(\boldsymbol{r}')\Big)\\
S[\phi^\alpha] &= \frac{1}{2}\sum_\alpha^{N_c^2-1}\int d\boldsymbol{r}d\boldsymbol{r}'\phi^\alpha(\boldsymbol{r})W^{-1}(\boldsymbol{r}-\boldsymbol{r}')\phi^\alpha(\boldsymbol{r}') + \sum_{n=1}U_n[\phi^\alpha]\\
U_n[\phi^\alpha] &= -\frac{\rho_0^n}{n!}\sum_{a_1,a_2,\cdots,a_n}\int (d^3r_{a_1}dQ_{a_1})\cdots(d^3r_{a_n}dQ_{a_n})h_0^{(n)}\prod_{i=1}^n(\frac{\tilde{n}_{a_i}(\boldsymbol{r}_{a_i})}{n_a}-1)
\end{aligned} \tag{2.3.10}$$

2.4 Cumulant Expansion

To perform a cumulant expansion at low density, we add and subtract the Hartree part in $U[\phi]$ through

$$U[\phi^\alpha] = (U[\phi^\alpha] - U_0[\phi^\alpha]) + U_0[\phi^\alpha] \tag{2.4.1}$$

with

$$U_0[\phi^\alpha] = \frac{1}{2}\rho_0 \sum_a \gamma_a \sum_\alpha \int d\boldsymbol{r} \phi^\alpha(\boldsymbol{r})^2 \ , \tag{2.4.2}$$

yields the identity

$$\langle \exp(-U[\phi^\alpha]) \rangle_W = \frac{\mathcal{N}_X}{\mathcal{N}_W} \langle \exp(-U[\phi^\alpha]) \rangle_X \tag{2.4.3}$$

with $\mathrm{X}^{-1} = \mathrm{W}^{-1} + \rho_0 \sum_a \gamma_a \mathbf{1}$. The normalizations in (2.4.2) is explicitly

$$\frac{\mathcal{N}_X}{\mathcal{N}_W} = \exp\Big(-\frac{V}{2}(N_c^2 - 1) \int \frac{d\boldsymbol{q}}{(2\pi)^3} \ln(1 + \rho_0 \sum_a \gamma_a \tilde{W}(\boldsymbol{q})) \Big) \tag{2.4.4}$$

The Fourier transform of the core $\tilde{W}(q)$ is related to the Fourier transform $\tilde{X}(q)$ as

$$\tilde{X}(q) = \frac{\tilde{W}(q)}{1 + \rho_0 \gamma \tilde{W}(\boldsymbol{q})} = \frac{\sin^2(qR/2)}{(qR/2)^2} \frac{4\pi}{q^2 + \kappa_0^2 \frac{\sin^2(qR/2)}{(qR/2)^2}} \tag{2.4.5}$$

with

$$\kappa_0^2 = 4\pi \sum_a \gamma_a \rho_0 = \beta g^2 \rho_0 \frac{1}{N_c^2 - 1} \sum_a \sum_\alpha Q_a^{\alpha 2} \tag{2.4.6}$$

All in all the partition function for a colored liquid of hard spheres with their color charges smeared on the surface is

$$
\begin{aligned}
-\frac{\ln Z}{V} &= -\frac{\ln Z_{HS}}{V} + \frac{1}{2}(N_c^2-1)\int \frac{d^3\boldsymbol{q}}{(2\pi)^3}\ln(1+\rho_0\sum_a \gamma_a \tilde{W}(\boldsymbol{q})) \\
&\quad -\frac{1}{V}\sum_{n=1}\frac{(-1)^n}{n!}\langle \mathcal{H}^n[\phi^\alpha]\rangle_{X,c}
\end{aligned} \tag{2.4.7}
$$

with $\mathcal{H}[\phi^\alpha] = U[\phi^\alpha] - U_0[\phi^\alpha]$ and $\langle\cdots\rangle_{X,c}$ denotes a cumulant average. At low density, the grand partition function is dominated by the first cumulants

$$
-\frac{\ln Z}{V} = -\frac{\ln Z_{HS}}{V} + w_1 + w_2 + \mathcal{O}(\rho_0^3) \tag{2.4.8}
$$

with

$$
\begin{aligned}
w_1 &= \frac{1}{2}(N_c^2-1)\int \frac{d\boldsymbol{q}}{(2\pi)^3}\ln(1+\rho_0\sum_a \gamma_a \tilde{W}(\boldsymbol{q})) \\
w_2 &= \frac{1}{V}\langle \mathcal{H}[\phi^\alpha]\rangle_X - \frac{\langle \mathcal{H}^2[\phi^\alpha]\rangle_X - \langle \mathcal{H}[\phi^\alpha]\rangle_X^2}{2V} \\
\mathcal{H} &= U_1[\phi^\alpha] + U_2[\phi^\alpha] - U_0[\phi^\alpha]
\end{aligned} \tag{2.4.9}
$$

The leading or zeroth order cumulant is known from hard sphere liquid analysis [1]

$$
-\frac{\ln Z_{HS}}{V} = -\rho_0' - \frac{2\pi}{3}\rho_0'^2\sigma^3 - \frac{5}{18}\pi^2\rho_0'^3\sigma^6 + \mathcal{O}(\rho_0'^4) \tag{2.4.10}
$$

with $\rho_0' = 3\rho_0$. The first cumulant reads

$$
\begin{aligned}
& w_1 - (N_c^2-1)\rho_0 \sum_a \gamma_a W(0) \\
& = -(N_c^2-1)\frac{2}{3}\sqrt{\pi}{\rho_0}^{3/2}(\sum_a \gamma_a)^{3/2} + (N_c^2-1)\frac{7}{15}\pi{\rho_0}^2(\sum_a \gamma_a)^2 R \\
& -(N_c^2-1)\frac{1}{3}\pi^{3/2}{\rho_0}^{5/2}(\sum_a \gamma_a)^{5/2}R^2 + \mathcal{O}(\rho_0^3)\ . \qquad (2.4.11)
\end{aligned}
$$

The Gaussian averaging in the second cumulant can be carried out. The result is

$$
\begin{aligned}
w_2 \quad & = -(N_c^2-1)\frac{\rho_0}{R}\sum_a \gamma_a - \frac{1}{2}(N_c^2-1)\rho_0 \sum_a \triangle_{a0} \\
& +\rho_0\Big(3 - \sum_a e^{-\frac{1}{2}(N_c^2-1)\triangle_{a0}}\Big) - \frac{1}{2}\rho_0^2\Big(3 - \sum_a e^{-\frac{1}{2}(N_c^2-1)\triangle_{a0}}\Big)^2 \tilde{h}_0(0) \\
& -\frac{\rho_0^2}{4}\Big(\sum_a \gamma_a(1 - e^{-\frac{1}{2}(N_c^2-1)\triangle_{a0}})\Big)^2 \int d\boldsymbol{r} X^2(r) \\
& -\frac{1}{4}\rho_0^2(N_c^2-1)\Big(\sum_a \gamma_a e^{-\frac{1}{2}(N_c^2-1)\triangle_{a0}}\Big)^2 \int d\boldsymbol{r} X^2(r) h_0^{(2)}(r) \\
& -\frac{1}{2}\rho_0^2 \sum_{a,a'}\Bigg(e^{-\frac{1}{2}(N_c^2-1)\triangle_{a0}} e^{-\frac{1}{2}(N_c^2-1)\triangle_{a'0}} \int d\boldsymbol{r} dQ_a dQ_{a'} (h_0^{(2)}(r)+1) \\
& \times\Big(e^{-\beta\frac{g^2}{4\pi}X(r)\sum_\alpha Q_a^\alpha Q_{a'}^\alpha} - 1 - \frac{1}{2}(N_c^2-1)\gamma_a\gamma_{a'}X^2(r)\Big)\Bigg) \qquad (2.4.12)
\end{aligned}
$$

with $\triangle_{a0} = \gamma_a X(0) - 2\gamma_a/R$ and $\tilde{h}_0(0)$ the 3D Fourier transform of $h_0^{(2)}(r)$,

$$
\triangle_{a0} = \gamma_a X(0) - 2\frac{\gamma_a}{R} = \gamma_a\Big(-\kappa_0 + \frac{7}{15}\kappa_0^2 R - \frac{5}{24}\kappa_0^3 R^2 + \mathcal{O}(\kappa_0^4)\Big) \qquad (2.4.13)
$$

and

$$\gamma_a X(r) = 2\frac{\gamma_a}{R} - \frac{\gamma_a}{R^2} r - \gamma_a \kappa_0 + \mathcal{O}(\kappa_0^2) \qquad (r < \sigma)$$
$$\gamma_a X(r) = \gamma_a \frac{\sin^2(\kappa_0 R/2)}{(\kappa_0 R/2)^2} \frac{1}{r} e^{(-\kappa_0 r)} + \mathcal{O}(\kappa_0^2) (r > \sigma) \qquad (2.4.14)$$

Collecting all the results up to the second cumulant in powers of the original activity $n_a (= \lambda)$ we have for $N_c = 2$

$$-\frac{\sigma^3 \ln Z}{V} = -3\tilde{\lambda} - 2\sqrt{\pi}\tilde{\lambda}^{3/2}(\sum_a \epsilon_a)^{3/2} - \tilde{\lambda}^2\Big(\frac{9}{2}\pi \sum_a \epsilon_a \sum_a \epsilon_a^2 + {B_2}'\Big) + \mathcal{O}(\tilde{\lambda}^{5/2}) \qquad (2.4.15)$$

up to order $\lambda^{5/2}$, with

$${B_2}' = \frac{\pi}{24\epsilon} \sum_{a,a'} \left(54\epsilon^4 \int_0^{3\epsilon} \frac{\sinh t}{t} dt + e^{3\epsilon}(-2-2\epsilon-3\epsilon^2-9\epsilon^3) + e^{-3\epsilon}(2-2\epsilon+3\epsilon^2-9\epsilon^3) \right) \qquad (2.4.16)$$

where $\epsilon_a = \frac{\gamma_a}{\sigma}$, $\epsilon = \sqrt{\epsilon_a \epsilon_{a'}}$ and $\tilde{\lambda} = \sigma^3 \lambda$. We have set $h_0^{(2)}(r) = -1$ for $r < \sigma$ and $h_0^{(2)}(r) = 0$ otherwise, and used

$$\rho_0 = \frac{\rho_0'}{3} = \frac{n_0}{3} \frac{\partial}{\partial n_0} \Big(\frac{\ln Z_{HS}}{V} \Big) = \frac{n_0}{3} - \frac{1}{3}\frac{4\pi}{3}\sigma^3 n_0^2 + \mathcal{O}(n_0^3) = \lambda - 3\frac{4\pi}{3}\sigma^3 \lambda^2 + \mathcal{O}(\lambda^3) \qquad (2.4.17)$$

The correction of order $\lambda^{5/2}$ is straightforward but tedious. For any N_c we obtain

$$
\begin{aligned}
&-(N_c^2-1)^3\frac{\pi^{\frac{3}{2}}}{4}(\sum_a\gamma_a)^{\frac{1}{2}}(\sum_a\gamma_a^2)^2-(N_c^2-1)^3\frac{\pi^{\frac{3}{2}}}{6}\sum_a\gamma_a^3(\sum_a\gamma_a)^{\frac{3}{2}}\\
&+(N_c^2-1)(\sum_a\gamma_a)^2(\sum_a\gamma_a)^{\frac{1}{2}}2\pi^{\frac{3}{2}}\sigma^2-\frac{1}{2}(N_c^2-1)^2(\sum_a\gamma_a^2)(\sum_a\gamma_a)^{\frac{3}{2}}2\pi^{\frac{3}{2}}\sigma\\
&-\sqrt{\pi}(\sum_a\gamma_a)^{1/2}\sum_{a,a'}\int_\sigma^\infty d^3\boldsymbol{r}\Bigg(\frac{r}{\gamma_{aa'}(N_c^2-1)^{\frac{1}{r}}}\sinh(\gamma_{aa'}(N_c^2-1)\frac{1}{r})\\
&-r\cosh(\gamma_{aa'}(N_c^2-1)\frac{1}{r})+\frac{(\gamma_a+\gamma_{a'0})}{2\gamma_{aa'}\frac{1}{r}}\sinh(\gamma_{aa'}(N_c^2-1)\frac{1}{r})\\
&+\frac{1}{2}(N_c^2-1)(\gamma_a+\gamma_{a'})+\gamma_a\gamma_{a'}(N_c^2-1)\frac{1}{r}-\frac{1}{4}(\gamma_a+\gamma_{a'})\gamma_a\gamma_{a'}(N_c^2-1)^2\frac{1}{r^2}\Bigg)
\end{aligned}
\tag{2.4.18}
$$

The left out integration is divergent. For $N_c=2$, the result is logarithmically divergent

$$
\frac{54}{5}\pi^{\frac{3}{2}}(\sum_a\gamma_a)^{\frac{1}{2}}(\sum_a\gamma_a^2)^2\ln(\frac{\Lambda}{\sigma}) \tag{2.4.19}
$$

where Λ is an infrared cutoff in the radial direction. This result is in total agreement with the result obtained earlier in [8] using a method that did not account for hard spheres and the smearing of the color charge. For $N_c=2$ the order $\lambda^{5/2}$ correction is

$$
\begin{aligned}
&-(N_c^2-1)^3\frac{\pi^{\frac{3}{2}}}{4}(\sum_a\gamma_a)^{\frac{1}{2}}(\sum_a\gamma_a^2)^2-(N_c^2-1)^3\frac{\pi^{\frac{3}{2}}}{6}\sum_a\gamma_a^3(\sum_a\gamma_a)^{\frac{3}{2}}\\
&+(N_c^2-1)(\sum_a\gamma_a)^2(\sum_a\gamma_a)^{\frac{1}{2}}2\pi^{\frac{3}{2}}\sigma^2-\frac{1}{2}(N_c^2-1)^2(\sum_a\gamma_a^2)(\sum_a\gamma_a)^{\frac{3}{2}}2\pi^{\frac{3}{2}}\sigma\\
&+\frac{54}{5}\pi^{\frac{3}{2}}(\sum_a\gamma_a)^{\frac{1}{2}}(\sum_a\gamma_a^2)^2\ln(\frac{\Lambda}{\sigma})
\end{aligned}
\tag{2.4.20}
$$

2.5 High Temperature Expansion

Another useful way to analyze (2.3.9-2.3.10) is through a high temperature expansion which parallels the cumulant (virial) expansion. For that we order the last part of $U_n[\phi^\alpha]$ in (2.3.10) in powers of β as in [9]. For that we define $\gamma' = \beta g^2/4\pi$ so that

$$\begin{aligned}
&\frac{\tilde{n}_{a_i}(\boldsymbol{r}_{a_i})}{n_a} - 1 \\
&= \gamma_a(N_c^2-1)\frac{1}{R} + i\gamma'^{\frac{1}{2}}\sum_\alpha Q_a^\alpha \phi^\alpha(\boldsymbol{r}) - \gamma'\frac{1}{2}\sum_{\alpha,\alpha'} Q_a^\alpha Q_a^{\alpha'}\phi^\alpha(\boldsymbol{r})\phi^{\alpha'}(\boldsymbol{r}) \\
&+\gamma_a^2\frac{1}{2}(N_c^2-1)^2\frac{1}{R^2} - \gamma_a\gamma'\frac{1}{2}(N_c^2-1)\frac{1}{R}\sum_{\alpha,\alpha'} Q_a^\alpha Q_a^{\alpha'}\phi^\alpha(\boldsymbol{r})\phi^{\alpha'}(\boldsymbol{r}) \\
&+\frac{1}{3!}i^3\gamma'^{\frac{3}{2}}\sum_{\alpha,\alpha',\alpha''} Q_a^\alpha Q_a^{\alpha'} Q_a^{\alpha''}\phi^\alpha(\boldsymbol{r})\phi^{\alpha'}(\boldsymbol{r})\phi^{\alpha''}(\boldsymbol{r}) \\
&+\frac{1}{4!}\gamma'^2\sum_{\alpha,\alpha',\alpha'',\alpha'''} Q_a^\alpha Q_a^{\alpha'} Q_a^{\alpha''} Q_a^{\alpha'''}\phi^\alpha(\boldsymbol{r})\phi^{\alpha'}(\boldsymbol{r})\phi^{\alpha''}(\boldsymbol{r})\phi^{\alpha'''}(\boldsymbol{r}) + \mathcal{O}(\beta^{\frac{5}{2}})
\end{aligned} \tag{2.5.1}$$

The rules for color averaging are summarized in Appendix 2.10.2. For instance, using (2.10.18) and (2.10.28) we have

$$\frac{1}{V}\langle U_1[\phi^\alpha]\rangle_X = \frac{1}{2}\rho_0\sum_a \triangle_{a0}(N_c^2-1) - \frac{1}{8}\rho_0\sum_a \triangle_{a0}^2(N_c^2-1)^2 + \mathcal{O}(\gamma^3) \tag{2.5.2}$$

in leading order. In particular, the second cumulant at high temperature is

$$
\begin{aligned}
w_2 = &-(N_c^2-1)\frac{1}{R}\sum_a \gamma_a\rho_0 - \frac{1}{8}(N_c^2-1)^2{\rho_0}^2\tilde{h}_0(0)(\sum_a \triangle_{a0})^2 \\
&-\frac{1}{8}\rho_0(\sum_a \triangle_{a0})^2(N_c^2-1)^2 - \frac{1}{4}(N_c^2-1){\rho_0}^2(\sum_a \gamma_a)^2\int d^3\boldsymbol{r}h_0^{(2)}(r)X^2(\boldsymbol{r}) \\
&+\frac{1}{2}\frac{1}{3!}{\rho_0}^2\gamma'^3\frac{q_3}{4}(\sum_a)^2\int d^3\boldsymbol{r}(h_0^{(2)}(r)+1)X^3(\boldsymbol{r}) + \mathcal{O}(\beta^{\frac{7}{2}}) \ . \qquad (2.5.3)
\end{aligned}
$$

The last term contributes only for $N_c > 2$ with q_3 being the cubic Casimir say for SU(3) as detailed in Appendix 2.10.2.

After collecting all terms and replacing $X(r)$ with $\frac{1}{r}e^{-\kappa_0 r}$ in the limit $R \to 0$, we finally obtain

$$
\begin{aligned}
-\frac{\ln Z}{V} = &-\frac{\ln Z_{HS}}{V} - \frac{2\sqrt{\pi}}{3}(N_c^2-1)\rho_0^{3/2}(\sum_a \gamma_a)^{3/2} \\
&-\frac{1}{4}(N_c^2-1)\rho_0^2(\sum_a \gamma_a)^2\int d^3\boldsymbol{r}h_0^{(2)}(r)\frac{1}{r^2} \\
&+\pi^{\frac{1}{2}}(N_c^2-1){\rho_0}^{\frac{5}{2}}(\sum_a \gamma_a)^{\frac{5}{2}}\int d^3\boldsymbol{r}h_0^{(2)}(r)\frac{1}{r} \\
&-\frac{1}{2}\pi(N_c^2-1)^2\rho_0^3(\sum_a \gamma_a)^3\int d^3\boldsymbol{r}h_0^{(2)}(r) \\
&-2\pi(N_c^2-1)\rho_0^3(\sum_a \gamma_a)^3\int d^3\boldsymbol{r}h_0^{(2)}(r) - \frac{\pi}{2}(N_c^2-1)^2\rho_0^2(\sum_a \gamma_a^2)(\sum_a \gamma_a) \\
&+{\rho_0}^2\frac{1}{2}\frac{1}{3!}\Big(\frac{g^2}{4\pi}\Big)^3(\sum_a)^2\beta^3\frac{q_3}{4}\int d^3\boldsymbol{r}(h_0^{(2)}(r)+1)\frac{1}{r^3}e^{-3(4\pi\rho_0(\sum_a \gamma_a))^{\frac{1}{2}}r} \\
&+\mathcal{O}(\beta^{\frac{7}{2}}) \ . \qquad (2.5.4)
\end{aligned}
$$

Below we show that this result yields a high temperature free energy for the cQGP that is identical to the one following from the loop expansion with an infinite core (2.2.7) with $h_0^{(2)}(r) = -\theta(\sigma - r)$.

2.6 Loop Expansion

The loop expansion of (2.2.7) is best captured by reorganizing the expansion around the Debye-screened solution. This expansion is identical with the high temperature expansion of the hard sphere liquid in the limit of zero size spheres. The finite size case will be derived by inspection. With this in mind, we can perform and perform the Hubbard-Stratonovitch transform on the colored interaction part of (2.2.7),

$$\begin{aligned}
&\exp\left(-\frac{1}{2}\beta\int d\boldsymbol{r}d\boldsymbol{r}'\rho^{\alpha}(\boldsymbol{r})v(\boldsymbol{r}-\boldsymbol{r}')\rho^{\alpha}(\boldsymbol{r}')\right)\\
&=\left(\beta\det(v^{-1})\right)^{\frac{1}{2}}\int[d\phi^{\alpha}]\exp\left(-\frac{\beta}{2}\int d\boldsymbol{r}\phi^{\alpha}(\boldsymbol{r})v^{-1}\phi^{\alpha}(\boldsymbol{r})\right)\\
&\times\exp\left(i\beta\int d\boldsymbol{r}\rho^{\alpha}(\boldsymbol{r})\phi^{\alpha}(\boldsymbol{r})\right)
\end{aligned}\tag{2.6.1}$$

and similarly for the core part in (2.2.7). The partition function for the cQGP reads

$$Z=\left(\beta\det(v'^{-1})\right)^{\frac{1}{2}(N_c{}^2-1)}\left(\det(w^{-1})\right)^{\frac{1}{2}}\int\prod_{\alpha}^{N_c^2-1}[d\phi^{\alpha}][d\psi]e^{-S}\tag{2.6.2}$$

with the induced action

$$\begin{aligned}
S &= \sum_{\alpha}^{N_c^2-1}\frac{\beta}{2}\int d\boldsymbol{r}\phi^{\alpha}(\boldsymbol{r})v^{-1}\phi^{\alpha}(\boldsymbol{r})+\frac{1}{2}\int d\boldsymbol{r}\psi(\boldsymbol{r})w^{-1}\psi(\boldsymbol{r})\\
&- \sum_{a}\int dQ_a d\boldsymbol{r}n_a e^{i\beta\sum_{\alpha}^{N_c^2-1}Q_a^{\alpha}\phi^{\alpha}(\boldsymbol{r})+i\psi(\boldsymbol{r})+\frac{1}{2}w_0}
\end{aligned}\tag{2.6.3}$$

Here w_0 is the divergent self-energy. For simplicity the colored particles are point-like throughout.

If we introduce the screened Coulomb potential

$$v_{DH}(\boldsymbol{r}) = \beta \frac{g^2}{4\pi r} e^{-\kappa_a r} \tag{2.6.4}$$

with the squared Debye wave number,

$$\kappa_a^2 = \frac{g^2}{N_c^2 - 1} \sum_a n_a \beta \sum_\alpha^{N_c^2-1} Q_a^{\alpha 2} \tag{2.6.5}$$

then the induced action (2.6.3) can be split into a screened part S_0 (quadratic in the fields) and an interaction part S_I (rest). Specifically,

$$\begin{aligned} S \quad &= \sum_\alpha^{N_c^2-1} \int d\boldsymbol{r} \Big(- \frac{1}{N_c^2 - 1} \sum_a n_a + \frac{\beta}{2} \phi^\alpha(\boldsymbol{r}) (v^{-1} + \frac{\kappa_a^2}{g^2}) \phi^\alpha(\boldsymbol{r}) \Big) \\ &+ \frac{1}{2} \int d\boldsymbol{r} \psi(\boldsymbol{r}) w^{-1} \psi(\boldsymbol{r}) \\ &- \sum_a \int dQ_a d\boldsymbol{r} n_a \Big(e^{i\beta \sum_\alpha Q_a^\alpha \phi^\alpha(\boldsymbol{r}) + i\psi(\boldsymbol{r}) + \frac{1}{2} w_0} - 1 + \frac{1}{2} (\beta^2 \sum_{\alpha,\alpha'} Q_a^\alpha Q_a^{\alpha'} \phi^\alpha \phi^{\alpha'}) \Big) \\ &= S_0 + S_I \end{aligned} \tag{2.6.6}$$

where we used the color normalization $\int dQ = 1$ and the color averaged squared Debye wave number,

$$\begin{aligned} \kappa_a^2 \equiv \int dQ_a \kappa_a^2 &= \frac{g^2}{N_c^2 - 1} \int dQ_a \sum_a n_a \beta \sum_\alpha^{N_c^2-1} Q_a^{\alpha 2} \\ &= \frac{g^2}{N_c^2 - 1} \int dQ_a \sum_a n_a \beta (N_c^2 - 1) C_{2a} = g^2 \sum_a n_a \beta C_{2a} \end{aligned} \tag{2.6.7}$$

Here C_2 is the quadratic Casimir (q_2) divided by (N_c^2-1),

$$\int dQ_a Q_a^\alpha Q_a^{\alpha'} = C_{2a}\delta^{\alpha\alpha'} = \frac{q_{2a}}{N_c^2-1}\delta^{\alpha\alpha'} \tag{2.6.8}$$

2.6.1 One-Loop

The screened Debye-Huckel partition function follows by setting $S_I = 0$ in the induced action. The corresponding partition function is then

$$Z_0 = \exp\left(V\sum_a n_a\right)\left(\det\left(1+\frac{1}{-\boldsymbol{\nabla}^2}\kappa_a^2\right)\right)^{-\frac{1}{2}({N_c}^2-1)} \tag{2.6.9}$$

The argument of the determinant is the inverse screened Green's function

$$\frac{1}{g^2}\left(-\boldsymbol{\nabla}^2+\kappa_a^2\right)G(\boldsymbol{r}-\boldsymbol{r}') = \delta(\boldsymbol{r}-\boldsymbol{r}') \tag{2.6.10}$$

which is

$$G(\boldsymbol{r}-\boldsymbol{r}') = g^2\int\frac{d\boldsymbol{k}}{(2\pi)^3}\frac{e^{i\boldsymbol{k}\cdot(\boldsymbol{r}-\boldsymbol{r}')}}{\boldsymbol{k}^2+\kappa_a^2} \tag{2.6.11}$$

The apparent singularity for coincidental arguments can be handled by dimensional regularization [10],

$$\lim_{n\to 3} G_n(\mathbf{0}) = G(\mathbf{0}) = -\kappa_a\frac{g^2}{4\pi} \tag{2.6.12}$$

with n being the spatial dimension. The determinant in (2.6.9) can be calculated by standard methods. The identity $\delta\ln\det X = Tr(X^{-1}\delta X)$ yields

$$\ln\det\left(1+\frac{1}{-\boldsymbol{\nabla}^2}\kappa_a^2\right) = \frac{2}{n}G_n(\mathbf{0})\frac{\kappa_a^2}{g^2}V \tag{2.6.13}$$

so that

$$Z_0 = \exp\left(V(\sum_a n_a - \frac{{N_c}^2-1}{n}\frac{\kappa_a^2}{g^2}G_n(\mathbf{0}))\right) \tag{2.6.14}$$

Using (2.6.7) and (2.6.12), we obtain the screened one-loop result as

$$\begin{aligned} Z_0 &= \exp\left(V\sum_a n_a(1+(N_c^2-1)g^2\beta C_{2a}\frac{\kappa_a}{12\pi})\right) \\ &= \exp\left(V\sum_a n_a(1+g^2\beta q_{2a}\frac{\kappa_a}{12\pi})\right) \end{aligned} \tag{2.6.15}$$

2.6.2 Two-Loop

Higher order loop corrections follow from

$$Z = Z_0\prod_\alpha^{N_c^2-1}\exp\left(\frac{1}{2\beta}\int d\boldsymbol{r}_1 d\boldsymbol{r}_2\frac{\delta}{\delta\phi^\alpha}G(\boldsymbol{r}_1-\boldsymbol{r}_2)\frac{\delta}{\delta\phi^\alpha}\right)\exp\left(-S_I(\phi^\alpha)\right)\Big|_{\phi^\alpha=0} \tag{2.6.16}$$

by insering higher G's through S_I as recently discussed in [10] for the Abelian case. The non-Abelian is noteworthy in many respects as we note below. A typical two-loop contribution is shown in Fig. 2.1. Its contribution is

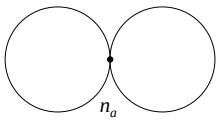

Figure 2.1: Two loop contribution from one particle (2.6.17)

$$\frac{1}{2^3}\beta^2(N_c^2-1)^2\sum_a n_a {C_{2a}}^2\int d\boldsymbol{r}G^2(\mathbf{0}) \tag{2.6.17}$$

The color factors follow from the identity (2.10.18) discussed in Appendix 2.10.2, i.e.

$$\begin{aligned}\int dQQ^\alpha Q^\beta Q^\gamma Q^\delta &= A(\sum_n d^{\alpha\beta n}d^{\gamma\delta n} + \sum_n d^{\alpha\gamma n}d^{\beta\delta n} + \sum_n d^{\alpha\delta n}d^{\beta\gamma n}) \\ &+ B(\delta^{\alpha\beta}\delta^{\gamma\delta} + \delta^{\alpha\gamma}\delta^{\beta\delta} + \delta^{\alpha\delta}\delta^{\beta\gamma}) \end{aligned} \tag{2.6.18}$$

with $A = 0$, $B = 1/15q_2^2$ for SU(2) and $A + 3B = 3/80q_2^2$ for SU(3). Although SU(2) and SU(3) involve considerably different integration measures, the overall result for Fig. 2.1 is the same. Additional contributions to the colored partition function are shown in Fig. 2.2, which contribute

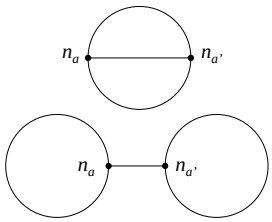

Figure 2.2: Two loop contribution from two particles (2.6.19)

$$\begin{aligned}&-\frac{\beta^3}{2\cdot 3!}\frac{1}{4}q_3\int d\boldsymbol{r}d\boldsymbol{r}'G^3(\boldsymbol{r}-\boldsymbol{r}')\sum_a n_a\sum_{a'}n_{a'} \\ &-\frac{\beta^3}{2\cdot 4}\int d\boldsymbol{r}d\boldsymbol{r}'G(\boldsymbol{r}-\boldsymbol{r}')G^2(\boldsymbol{0})\sum_a n_a\sum_{a'}n_{a'}\frac{1}{4^2}\sum_{\alpha,\beta,\gamma}d^{\alpha\alpha\beta}d^{\beta\gamma\gamma}\end{aligned} \tag{2.6.19}$$

Here q_3 is the cubic Casimir following from the identity

$$\sum_{\alpha,\beta,\gamma}^{N_c^2-1} d_{\alpha\beta\gamma} Q_a^\alpha Q_a^\beta Q_a^\gamma = q_3 = \frac{1}{4} \sum_{\alpha,\beta,\gamma}^{N_c^2-1} d_{\alpha\beta\gamma} d^{\alpha\beta\gamma}$$
$$= \int dQ_a q_3 = \sum_{\alpha,\beta,\gamma}^{N_c^2-1} \int dQ_a d_{\alpha\beta\gamma} Q_a^\alpha Q_a^\beta Q_a^\gamma$$
$$\rightarrow \int dQ_a Q_a^\alpha Q_a^\beta Q_a^\gamma = \frac{1}{4} d^{\alpha\beta\gamma} \tag{2.6.20}$$

as detailed in Appendix 2.10.2. The cubic Casimir exists only for $N_c > 2$ and vanishes identically for SU(2). This is clear from the fact that the contributions in Fig. 2.2 involve 3 colored vertices. Also note that only the irreducible graph of Fig. 2.2 contributtes to (2.6.19) since the reducible graph averages to zero by color integration through the identity

$$\sum_{\alpha,\beta,\gamma} d^{\alpha\alpha\beta} d^{\beta\gamma\gamma} = 0 \tag{2.6.21}$$

Unlike the Abelian case discussed in [10], where tadpoles and disconnected contributions abund, the non-Abelian case has none of these thanks to the color integrations. Also, the effects of the hard core at two loop can easily be recalled by noting that in the 2-particle channel under consideration the distance of minimum encounter is σ. So the radial integrations should be limited to $\sigma < r < \infty$ to account for the hard core. With this in mind, the 2-loop contribution to the partition function reads

$$\frac{\ln Z}{V} = \frac{\ln Z_0}{V} + \frac{1}{2^3}\beta^2 \sum_a n_a {q_{2a}}^2 G^2(\mathbf{0}) - \sum_{a,a'} n_a n_{a'} \Big(\frac{1}{2 \cdot 3!} \beta^3 \frac{1}{4} q_3 \int_\sigma^\infty d\boldsymbol{r} G^3(\boldsymbol{r}) \Big) \tag{2.6.22}$$

where the last term is only present for SU(3). Using (2.6.15) and (2.6.12) we get

$$\begin{aligned}\frac{\ln Z}{V} &= (\sum_a n_a) + \frac{1}{3}\sqrt{4\pi}(\frac{g^2}{4\pi})^{\frac{3}{2}}(N_c^2-1)(\sum_a n_a \beta C_{2a})^{\frac{3}{2}} \\ &+\frac{1}{2^3}4\pi(\frac{g^2}{4\pi})^3(N_c^2-1)^2\Big(\sum_a n_a(\beta C_{2a})^2\Big)(\sum_a n_{a'}\beta C_{2a}) \\ &-\frac{1}{2\cdot 3!}\beta^3(\frac{g^2}{4\pi})^3 4\pi\frac{q_3}{4}(\sum_a n_a)^2 E_1(3\kappa_a\sigma) \end{aligned} \tag{2.6.23}$$

Here $E_1(x)$ is the exponential integral($-Ei(-x) = E_1(x) = \int_x^\infty \frac{e^{-t}}{t}dt$), which is logarithmically divergent at short distance. It is made finite by the hard core potential.

2.6.3 Three Loop

A partial three loop analysis will be carried out in this section. There are in total 8 diagrammatic contributions at three loop that can be organized in terms of the particle density: 1 (one-particle density); 3 (two-particle density); 4 (three- and four-particle density). They will be considered sequentially.

The three loop contribution stemming from the one-particle density is shown in Fig. 2.3. It is

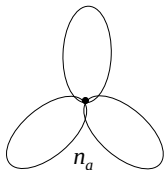

Figure 2.3: Three loop contribution from one particle (2.6.24)

$$-\frac{1}{3!}\frac{1}{2^3}\beta^3\sum_a n_a\int d\boldsymbol{r}G^3(\mathbf{0}){q_{2a}}^3 \tag{2.6.24}$$

The vertex involves 6 color charges which are integrated with the help of the identity (see Appendix 2.10.2)

$$\begin{aligned}\int dQQ^\alpha Q^\beta Q^\gamma Q^\delta Q^\epsilon Q^\zeta = A\Big(&d^{\alpha\beta\gamma}d^{\delta\epsilon\zeta}+d^{\alpha\beta\delta}d^{\gamma\epsilon\zeta}+d^{\alpha\beta\epsilon}d^{\gamma\delta\zeta}+d^{\alpha\beta\zeta}d^{\gamma\delta\epsilon}\\&+d^{\alpha\gamma\delta}d^{\beta\epsilon\zeta}+d^{\alpha\gamma\epsilon}d^{\beta\delta\zeta}+d^{\alpha\gamma\zeta}d^{\beta\delta\epsilon}+d^{\alpha\delta\epsilon}d^{\beta\gamma\zeta}+d^{\alpha\delta\zeta}d^{\beta\gamma\epsilon}+d^{\alpha\epsilon\zeta}d^{\beta\gamma\delta}\Big)\\&+B\Big(\delta^{\alpha\beta}\delta^{\gamma\delta}\delta^{\epsilon\zeta}+\delta^{\alpha\beta}\delta^{\gamma\epsilon}\delta^{\delta\zeta}+\delta^{\alpha\beta}\delta^{\gamma\zeta}\delta^{\delta\epsilon}+\delta^{\alpha\gamma}\delta^{\beta\delta}\delta^{\epsilon\zeta}+\delta^{\alpha\gamma}\delta^{\beta\epsilon}\delta^{\delta\zeta}\\&+\delta^{\alpha\gamma}\delta^{\beta\zeta}\delta^{\delta\epsilon}+\delta^{\alpha\delta}\delta^{\beta\gamma}\delta^{\epsilon\zeta}+\delta^{\alpha\delta}\delta^{\beta\epsilon}\delta^{\gamma\zeta}+\delta^{\alpha\delta}\delta^{\beta\zeta}\delta^{\gamma\epsilon}+\delta^{\alpha\epsilon}\delta^{\beta\gamma}\delta^{\delta\zeta}\\&+\delta^{\alpha\epsilon}\delta^{\beta\delta}\delta^{\gamma\zeta}+\delta^{\alpha\epsilon}\delta^{\beta\zeta}\delta^{\gamma\delta}+\delta^{\alpha\zeta}\delta^{\beta\gamma}\delta^{\delta\epsilon}+\delta^{\alpha\zeta}\delta^{\beta\delta}\delta^{\gamma\epsilon}+\delta^{\alpha\zeta}\delta^{\beta\epsilon}\delta^{\gamma\delta}\Big)\end{aligned} \tag{2.6.25}$$

with $A=0$, $B=\frac{1}{105}q_2^3$ for SU(2) and $A=-\frac{9}{8!}q_2^3+\frac{27}{2}\frac{1}{7!}q_3^2$, $B=\frac{85}{2}\frac{1}{8!}q_2^3-\frac{6}{8!}q_3^2$ for SU(3). Note that this contribution is similar to one-loop for both SU(2) and SU(3) despite the differences in the contributions and the color averaging.

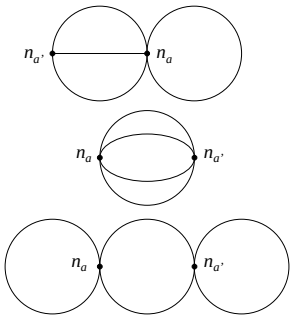

Figure 2.4: Three loop contribution from two particles (2.6.26)

The three loop contribution stemming from the two-particle density are shown in Fig 2.4. The top diagram vanishes for SU(2) as an odd number of color charges are brought to a single point which vanish by color averaging.

Their contribution is

$$\begin{aligned}
&\frac{1}{2}\frac{1}{3!}\beta^4\sum_a n_a q_{2a}\sum_{a'} n_{a'}\frac{q_3}{4}\int d\boldsymbol{r}d\boldsymbol{r}' G^3(\boldsymbol{r}-\boldsymbol{r}')G(\boldsymbol{0})\\
+&\frac{1}{2^3}\frac{1}{{N_c}^2-1}\beta^4\sum_a n_a {q_{2a}}^2\sum_{a'} n_{a'}{q_{2a'}}^2\int d\boldsymbol{r}d\boldsymbol{r}' G^2(\boldsymbol{r}'-\boldsymbol{r})G^2(\boldsymbol{0})\\
+&\frac{3}{({N_c}^2-1)({N_c}^2+1)}\frac{1}{4!}\beta^4\sum_a n_a {q_{2a}}^2\sum_{a'} n_{a'}{q_{2a'}}^2\int d\boldsymbol{r}d\boldsymbol{r}' G^4(\boldsymbol{r}'-\boldsymbol{r})
\end{aligned} \tag{2.6.26}$$

The three loop contribution stemming from three- and four-particle density is shown in Fig. 2.5. These contributions will not be quoted here. They only contribute for $N_c > 2$. They can be shown to arise from color magnetism, thus subleading in the electric cQGP under considerations.

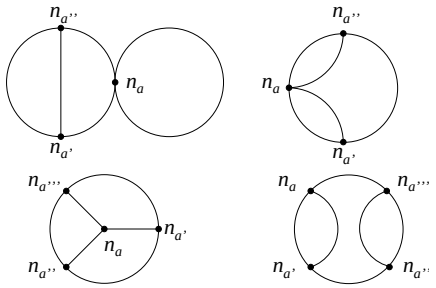

Figure 2.5: Three loop contribution from three and four particle interactions

2.6.4 Higher Loops

So far, the color averaging at one- two and three-loops have led to simple powers of Casimirs. This observation does not carry simply at higher orders as more complex combination of Casimirs appear. Indeed, consider the five loop contribution shown in Fig. 2.6. Its contribution can be found explicitly

as

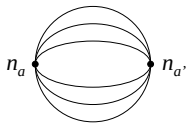

Figure 2.6: A typical five-loop contribution. See text.

$$\begin{cases} \frac{1}{2}\frac{1}{7!}\beta^6 \sum_a n_a {q_{2a}}^3 \sum_{a'} n_{a'} {q_{2a'}}^3 \int d\boldsymbol{r} d\boldsymbol{r}' G^6(\boldsymbol{r}' - \boldsymbol{r}) & SU(2) \\ \frac{1}{2}\frac{1}{7!}\beta^6 \sum_a n_a \sum_{a'} n_{a'} \left(\frac{3}{2^4} {q_3}^2 {q_3}^2 - \frac{1}{2^6} {q_3}^2 ({q_{2a}}^3 + {q_{2a'}}^3) + \frac{85}{2^8} {q_{2a}}^3 {q_{2a'}}^3 \right) & \\ \times \int d\boldsymbol{r} d\boldsymbol{r}' G^6(\boldsymbol{r}' - \boldsymbol{r}) & SU(3) \end{cases}$$

The color averaging leads a more complex combination of Casimirs for SU(3) in comparison to SU(2). The cubic Casimir for SU(3) is absent for SU(2). The way the color averaging occurs is by noting that each vertex involves 6 lines in Fig. 2.6. In SU(2) the averaging involves only the quadratic Casimir, and the result with 3 quadratic Casimirs follow. This observation explains why the SU(2) color averaging in (2.4.16) (low density expansion) can not be extended to SU(3) in closed form. The culpright is the occurence of the third Casimir.

2.6.5 Result

Now we combine the one, two and (partial) three loop results for the grand partition function, namely (2.6.23), (2.6.24) and (2.6.26) and use (2.6.12), to get

$$\frac{\ln Z}{V} = (\sum_a n_a) + \frac{1}{3}\sqrt{4\pi}(\frac{g^2}{4\pi})^{\frac{3}{2}}(N_c^2-1)(\sum_a n_a\beta C_{2a})^{\frac{3}{2}}$$
$$+\frac{1}{2^3}4\pi(\frac{g^2}{4\pi})^3(N_c^2-1)^2\Big(\sum_a n_a(\beta C_{2a})^2\Big)(\sum_a n_a\beta C_{2a})$$
$$+\frac{1}{3!}\frac{1}{2^3}(4\pi)^{\frac{3}{2}}(\frac{g^2}{4\pi})^{\frac{9}{2}}(N_c^2-1)^3\Big(\sum_a n_a(\beta C_{2a})^3\Big)(\sum_a n_a\beta C_{2a})^{\frac{3}{2}}$$
$$+\frac{1}{16}(4\pi)^{\frac{3}{2}}\Big(\frac{g^2}{4\pi}\Big)^{\frac{9}{2}}({N_c}^2-1)^3\Big(\sum_a n_a(\beta C_{2a})^2\Big)^2\Big(\sum_a n_a(\beta C_{2a})\Big)^{\frac{1}{2}}e^{-2\kappa_a\sigma}$$
$$-\frac{3}{{N_c}^2+1}\frac{1}{4!}4\pi\Big(\frac{g^2}{4\pi}\Big)^4({N_c}^2-1)^3\Big(\sum_a n_a(\beta C_{2a})^2\Big)^2$$
$$\times\frac{1}{\sigma}\Big(e^{-4\kappa_a\sigma}+4\kappa_a\sigma E_1(4\kappa_a\sigma)\Big) \tag{2.6.27}$$

for both SU(2) and SU(3), with in addition for SU(3) alone

$$-\frac{1}{2}\frac{1}{3!}(\frac{g^2}{4\pi})^3 4\pi(\sum_a n_a)^2\beta^3\frac{q_3}{4}E_1(3\kappa_a\sigma)$$
$$-\frac{1}{2}\frac{1}{3!}(4\pi)^{\frac{3}{2}}\Big(\frac{g^2}{4\pi}\Big)^{\frac{9}{2}}({N_c}^2-1)\Big(\sum_a n_a(\beta C_{2a})\Big)^{\frac{3}{2}}\sum_a n_a\beta^3\frac{q_3}{4}E_1(3\kappa_a\sigma) \tag{2.6.28}$$

To proceed further, we set all classical fugacities for the three species $a = 1, 2, 3$ (quark, antiquark, gluon) to be the same, $n_a = n_{a'} = \lambda$. We also rescale all dimensions to the core size σ to be reinstated by inspection as announced. Specifically $\tilde{\lambda} = \sigma^3\lambda$, with all radial integrations cutoff by the core. Using (2.6.27) and (2.6.28) with $\varepsilon_a = \frac{g^2}{4\pi}\beta C_{2a}/\sigma$, we have for both SU(2) and SU(3)

$$\begin{aligned}\frac{\sigma^3 \ln Z_{\tilde{\lambda}}}{V} &= \tilde{\lambda}\sum_a + \tilde{\lambda}^{\frac{3}{2}}\frac{1}{3}(4\pi)^{\frac{1}{2}}(N_c^2-1)(\sum_a \varepsilon_a)^{\frac{3}{2}} \\ &+\tilde{\lambda}^2\frac{1}{8}4\pi(N_c^2-1)^2(\sum_a {\varepsilon_a}^2)(\sum_a \varepsilon_a) \\ &-\tilde{\lambda}^2\frac{3}{{N_c}^2+1}\frac{1}{4!}4\pi(N_c^2-1)^3(\sum_a {\varepsilon_a}^2)^2\Big(e^{-4\kappa_a\sigma}+4\kappa_a\sigma E_1(4\kappa_a\sigma)\Big) \\ &+\tilde{\lambda}^{\frac{5}{2}}\frac{1}{3!}\frac{1}{8}(4\pi)^{\frac{3}{2}}(N_c^2-1)^3(\sum_a {\varepsilon_a}^3)(\sum_a \varepsilon_a)^{\frac{3}{2}} \\ &+\tilde{\lambda}^{\frac{5}{2}}\frac{1}{16}(4\pi)^{\frac{3}{2}}(N_c^2-1)^3(\sum_a {\varepsilon_a}^2)^2(\sum_a \varepsilon_a)^{\frac{1}{2}}e^{-2\kappa_a\sigma}\end{aligned} \tag{2.6.29}$$

while in addition for SU(3),

$$\begin{aligned}&-\tilde{\lambda}^2\frac{1}{2}\frac{1}{3!}4\pi\Big(\frac{g^2}{4\pi}\Big)^3(\sum_a)^2(\frac{\beta^3 q_3}{4\sigma^3})E_1(3\kappa_a\sigma) \\ &-\tilde{\lambda}^{\frac{5}{2}}\frac{1}{2}\frac{1}{3!}(4\pi)^{\frac{3}{2}}\Big(\frac{g^2}{4\pi}\Big)^3({N_c}^2-1)(\sum_a \varepsilon_a)^{\frac{3}{2}}\sum_a(\frac{\beta^3 q_3}{4\sigma^3})E_1(3\kappa_a\sigma)\end{aligned} \tag{2.6.30}$$

We note that the core integrations stemming from $\mid \boldsymbol{r}-\boldsymbol{r}' \mid < \sigma$ reduce to

$$\begin{aligned}\frac{\ln Z}{V}_{|\boldsymbol{r}-\boldsymbol{r}'|<\sigma} &= -\lambda^2\frac{1}{4}(N_c^2-1)\Big(\sum_a \beta C_{2a}\Big)^2\int d\boldsymbol{r}G^2(r) \\ &+\lambda^2\frac{1}{4}(N_c^2-1)^2\Big(\sum_a(\beta C_{2a})^2\Big)\Big(\sum_a \beta C_{2a}\Big)\int d\boldsymbol{r}G^2(r)G(0) \\ &-\lambda^2\frac{1}{8}(N_c^2-1)^3\Big(\sum_a(\beta C_{2a})^3\Big)\Big(\sum_a \beta C_{2a}\Big)\int d\boldsymbol{r}G^2(r)G^2(0)\end{aligned} \tag{2.6.31}$$

where the divergences are lumped in $G(0)$. Our final result for SU(2) and SU(3) is then

$$\begin{aligned}
\frac{\sigma^3 \ln Z_{\tilde{\lambda}}}{V} &= \tilde{\lambda} \sum_a + \tilde{\lambda}^{\frac{3}{2}} \frac{1}{3} (4\pi)^{\frac{1}{2}} (N_c^2 - 1) (\sum_a \varepsilon_a)^{\frac{3}{2}} \\
&- \tilde{\lambda}^{\frac{3}{2}} \frac{1}{8} (4\pi)^{\frac{1}{2}} (N_c^2 - 1) (\sum_a \varepsilon_a)^{\frac{3}{2}} (1 - e^{-2(4\pi)^{\frac{1}{2}} \tilde{\lambda}^{\frac{1}{2}} (\sum_a \varepsilon_a)^{\frac{1}{2}}}) \\
&- \tilde{\lambda}^2 \frac{1}{8} (4\pi) (N_c^2 - 1)^2 (\sum_a \varepsilon_a) (\sum_a {\varepsilon_a}^2) (1 - e^{-2(4\pi)^{\frac{1}{2}} \tilde{\lambda}^{\frac{1}{2}} (\sum_a \varepsilon_a)^{\frac{1}{2}}}) \\
&+ \tilde{\lambda}^2 \frac{1}{8} (4\pi) (N_c^2 - 1)^2 (\sum_a \varepsilon_a) (\sum_a {\varepsilon_a}^2) \\
&- \tilde{\lambda}^2 \frac{3}{{N_c}^2 + 1} \frac{1}{4!} (4\pi) (N_c^2 - 1)^3 (\sum_a {\varepsilon_a}^2)^2 \\
&\times \Big(e^{-4(4\pi)^{\frac{1}{2}} \tilde{\lambda}^{\frac{1}{2}} (\sum_a \varepsilon_a)^{\frac{1}{2}}} + 4(4\pi)^{\frac{1}{2}} \tilde{\lambda}^{\frac{1}{2}} (\sum_a \varepsilon_a)^{\frac{1}{2}} E_1 (4(4\pi)^{\frac{1}{2}} \tilde{\lambda}^{\frac{1}{2}} (\sum_a \varepsilon_a)^{\frac{1}{2}}) \Big) \\
&- \tilde{\lambda}^{\frac{3}{2}} \frac{1}{16} (4\pi)^{\frac{3}{2}} (N_c^2 - 1)^3 (\sum_a \varepsilon_a)^{\frac{3}{2}} (\sum_a {\varepsilon_a}^3) (1 - e^{-2(4\pi)^{\frac{1}{2}} \tilde{\lambda}^{\frac{1}{2}} (\sum_a \varepsilon_a)^{\frac{1}{2}}}) \\
&+ \tilde{\lambda}^{\frac{5}{2}} \frac{1}{3!} \frac{1}{8} (4\pi)^{\frac{3}{2}} (N_c^2 - 1)^3 (\sum_a \varepsilon_a)^{\frac{3}{2}} (\sum_a {\varepsilon_a}^3) \\
&+ \tilde{\lambda}^{\frac{5}{2}} \frac{1}{16} (4\pi)^{\frac{3}{2}} (N_c^2 - 1)^3 (\sum_a {\varepsilon_a}^2)^2 (\sum_a \varepsilon_a)^{\frac{1}{2}} e^{-2(4\pi)^{\frac{1}{2}} \tilde{\lambda}^{\frac{1}{2}} (\sum_a \varepsilon_a)^{\frac{1}{2}}}
\end{aligned} \tag{2.6.32}$$

with in addition for SU(3)

$$\begin{aligned}
&- \tilde{\lambda}^2 \frac{1}{2} \frac{1}{3!} 4\pi \Big(\frac{g^2}{4\pi} \Big)^3 (\sum_a)^2 (\frac{\beta^3 q_3}{4\sigma^3}) E1 \Big(3(4\pi)^{\frac{1}{2}} \tilde{\lambda}^{\frac{1}{2}} (\sum_a \varepsilon_a)^{\frac{1}{2}} \Big) \\
&- \tilde{\lambda}^{\frac{5}{2}} \frac{1}{2} \frac{1}{3!} (4\pi)^{\frac{3}{2}} \Big(\frac{g^2}{4\pi} \Big)^3 ({N_c}^2 - 1) (\sum_a \varepsilon_a)^{\frac{3}{2}} \sum_a (\frac{\beta^3 q_3}{4\sigma^3}) E1 \Big(3(4\pi)^{\frac{1}{2}} \tilde{\lambda}^{\frac{1}{2}} (\sum_a \varepsilon_a)^{\frac{1}{2}} \Big)
\end{aligned} \tag{2.6.33}$$

This is our final result for up to three loops ignoring the diagrams of

Fig. 2.5, which yields contributions that are of order $\tilde{\lambda}^3$ or higher.

2.6.6 High Temperature

The results of the high-temperature expansion can be recovered from the three loop results (2.6.32). For that we need to go back to the unintegrated contributions in r-space and expand in powers of β the exponentials. Up to order β^3 the result is

$$\begin{aligned}\frac{\ln Z}{V} &= \lambda\sum_a + \lambda^{\frac{3}{2}}\frac{1}{3}(4\pi)^{\frac{1}{2}}(N_c^2-1)(\sum_a\gamma_a)^{\frac{3}{2}} \\ &-\lambda^2\frac{1}{4}(N_c^2-1)(\sum_a\gamma_a)^2\int_{r<\sigma}d\boldsymbol{r}\frac{1}{r^2} \\ &+\lambda^{\frac{5}{2}}\frac{1}{2}(4\pi)^{\frac{1}{2}}(N_c^2-1)(\sum_a\gamma_a)^{\frac{5}{2}}\int_{r<\sigma}d\boldsymbol{r}\frac{1}{r} \\ &-\lambda^3\frac{1}{2}(4\pi)(N_c^2-1)(\sum_a\gamma_a)^3\int_{r<\sigma}d\boldsymbol{r}+\lambda^2\frac{1}{8}4\pi(N_c^2-1)^2(\sum_a{\gamma_a}^2)(\sum_a\gamma_a) \\ &-\lambda^2\frac{1}{2}\frac{1}{3!}\Big(\frac{g^2}{4\pi}\Big)^3(\sum_a)^2(\frac{\beta^3q_3}{4})\int_{\sigma<r<\infty}d\boldsymbol{r}\frac{1}{r^3}e^{-3(4\pi)^{\frac{1}{2}}\lambda^{\frac{1}{2}}(\sum_a\gamma_a)^{\frac{1}{2}}r}+\mathcal{O}(\beta^{\frac{7}{2}})\end{aligned} \tag{2.6.34}$$

where we used $\epsilon_a = \gamma/\sigma$ from (2.2.11). For SU(2) the latter contribution is absent. This result agrees with (2.5.4) to order $\beta^{5/2}$ for $h_0^{(2)}(r) = -\theta(\sigma - r)$. There is a difference to order β^3 which can be traced back to the handling of the core potential $h_0^{(2)}(r)$ and $w(r)$ in each of the two expansions. In the loop expansion we used an infinite core with $e^{-w(r)} = 1$ for $r > \sigma$. In reality $e^{-w(r)}$ is a function of r much like $h_0^{(2)}(r)$ when $r > \sigma$. A similar observation was made for hard sphere liquids in [9].

2.7 Free Energies of cQGP

The free energy follows from the grand partition function which we have now constructed for both the density (virial) expansion and the loop (high) temperature expansion. The latter is understood for a liquid of hard spheres with $h_0^{(2)}(r) = -\theta(\sigma - r)$ as in (2.6.34) up to order $\beta^{5/2}$. The former is given in (2.4.15) up to order λ^2.

Specializing to SU(2) one component plasma($\sum_a \gamma_a \to \gamma$) in (2.6.34) and carrying the r-integration with the hard core potential in mind as noted, we have

$$\begin{aligned}\frac{\ln Z}{V} \quad &= \lambda + \lambda^{\frac{3}{2}}\frac{1}{3}(4\pi)^{\frac{1}{2}}(N_c^2-1)\gamma^{\frac{3}{2}} - \lambda^2\pi(N_c^2-1)\gamma^2\sigma + 2\pi^{\frac{3}{2}}\lambda^{\frac{5}{2}}(N_c^2-1)\gamma^{\frac{5}{2}}\sigma^2 \\ &-\lambda^3\frac{8}{3}\pi^2(N_c^2-1)\gamma^3\sigma^3 + \lambda^2\frac{1}{2}\pi(N_c^2-1)^2\gamma^3 + \mathcal{O}(\beta^{\frac{7}{2}}) \qquad (2.7.1)\end{aligned}$$

The density $c(= \lambda\frac{\partial}{\partial\lambda}(\frac{\ln Z}{V}))$ is

$$c = \lambda + \triangle c = \lambda + \sqrt{\pi}(N_c^2-1)\gamma^{\frac{3}{2}}\lambda^{\frac{3}{2}} + \mathcal{O}(\beta^2) \qquad (2.7.2)$$

The corresponding shift induced in the chemical potential, $\beta\mu_c = \beta\mu_\lambda + \beta\triangle\mu_c$, due to the interactions can be extracted from

$$c = \frac{g}{\Lambda^3}e^{\beta\mu_c} = \frac{g}{\Lambda^3}e^{\beta\mu_\lambda+\beta\triangle\mu_c} \simeq \frac{g}{\Lambda^3}e^{\beta\mu_\lambda}(1+\beta\triangle\mu_c) = \lambda + \lambda\beta\triangle\mu_c = \lambda + \triangle c \qquad (2.7.3)$$

with

$$\beta\triangle\mu_c = \frac{\triangle c}{\lambda} = \sqrt{\pi}(N_c^2-1)\gamma^{\frac{3}{2}}\lambda^{\frac{1}{2}} + \mathcal{O}(\beta^2)\ . \tag{2.7.4}$$

Using this shift and defining the free energy through the legendre transform

$$\beta\frac{F(\beta,c)}{V} = -\frac{1}{V}\ln Z(\beta,\lambda) + c\beta\mu_c \tag{2.7.5}$$

we obtain for either the loop expansion or the high temperature expansion

$$\begin{aligned}
\beta\frac{F_{loop}(\beta,c)}{V} &= -c + \frac{2\sqrt{\pi}}{3}(N_c^2-1)\lambda^{\frac{3}{2}}\gamma^{\frac{3}{2}} + \pi(N_c^2-1)\lambda^2\gamma^2\sigma \\
&-2\pi^{\frac{3}{2}}(N_c^2-1)\lambda^{\frac{5}{2}}\gamma^{\frac{5}{2}}\sigma^2 - \frac{\pi}{2}(N_c^2-1)^2\lambda^2\gamma^3 + c\beta\mu_\lambda + \mathcal{O}(\beta^{\frac{7}{2}}) \\
&\simeq -\lambda\Big(1+\frac{\triangle c}{\lambda}\Big) - \frac{2\sqrt{\pi}}{3}(N_c^2-1)\gamma^{\frac{3}{2}}\lambda^{\frac{3}{2}}\Big(1+\frac{\triangle c}{\lambda}\Big)^{\frac{3}{2}} \\
&+\pi(N_c^2-1)\lambda^2\Big(1+\frac{\triangle c}{\lambda}\Big)^2\gamma^2\sigma - 2\pi^{\frac{3}{2}}(N_c^2-1)\lambda^{\frac{5}{2}}\Big(1+\frac{\triangle c}{\lambda}\Big)^{\frac{5}{2}}\gamma^{\frac{5}{2}}\sigma^2 \\
&+c(\beta\mu_\lambda + \beta\triangle\mu_c) + \mathcal{O}(\beta^3) \\
&= -c - \frac{2\sqrt{\pi}}{3}(N_c^2-1)\gamma^{\frac{3}{2}}c^{\frac{3}{2}} + \pi(N_c^2-1)c^2\gamma^2\sigma \\
&-2\pi^{\frac{3}{2}}(N_c^2-1)c^{\frac{5}{2}}\gamma^{\frac{5}{2}}\sigma^2 + c\beta\mu_c + \mathcal{O}(\beta^3)\ .
\end{aligned} \tag{2.7.6}$$

From (2.7.2), we note that $\triangle c \sim \beta^{\frac{3}{2}}$ so that λ can be substituted by the concentration c for terms that are of order β^2 or higher to accuracy $\beta^{5/2}$. For the free energy, the high temperature expansion deviates from the loop-expansion by such substitutions in higher order.

The free energy in the low density expansion can be extracted from (2.4.15) using a similar transform and substitution. For SU(2) the procedure of substitution of $\tilde{\lambda}$ by $\tilde{c}$ is detailed in [8]. For SU(2) $D_2 = B_2 + \frac{3}{8}B_{3/2}^2$ where the

B's are Bernoulli's numbers. For a one species SU(2) plasma $\epsilon = \sqrt{\epsilon_a \epsilon_a} = \epsilon_a$. Recalling that in [8] the normalizations were carried using the Wigner-Seitz radius instead of the core size with $\delta = \sigma/a_{WS}$, we have $\epsilon = \Gamma/\delta$. The SU(2) free energy of a one-species cQGP in the low density expansion is

$$\begin{aligned}\beta\frac{F_{low}(\beta,c)}{V} &= -c - 2\sqrt{\pi}\gamma^{\frac{3}{2}}c^{\frac{3}{2}} - 3\pi\gamma^3c^2 - \frac{9}{4}\pi\gamma^3c^2\int_0^{\frac{3}{\sigma}\gamma}\frac{\sinh t}{t}dt \\ &+ \frac{\pi}{12}\frac{\sigma^4}{\gamma}c^2\Big(2\sinh(\frac{3}{\sigma}\gamma) + 2\frac{\gamma}{\sigma}\cosh(\frac{3}{\sigma}\gamma) + 3\frac{\gamma^2}{\sigma^2}\sinh(\frac{3}{\sigma}\gamma) \\ &+ 9\frac{\gamma^3}{\sigma^3}\cosh(\frac{3}{\delta}\gamma)\Big) + c\beta\mu_c + \mathcal{O}(c^{\frac{5}{2}})\ . \end{aligned} \tag{2.7.7}$$

2.8 Excess Free Energies for cQGP

The free energies obtained above can be rewritten in terms of the plasma constant

$$\Gamma = \frac{g^2}{4\pi}\frac{C_2}{Ta_{WS}} \tag{2.8.1}$$

with $k_B = 1$ and a_{WS} the Wigner-Seitz radius satisfying $N/V(4\pi a_{WS}^3/3) = 1$. C_2 is the quadratic Casimir, $C_2 = q_2/(N_c^2 - 1)$ and g is the strength of the coupling. Since the Wigner-Seitz radius is related to the density, $N/V = c$, it is straightforward to rewrite the expanded free energies above in terms of Γ. For instance, the first two terms in the loop expansion (2.7.6) read

$$\begin{aligned}
\frac{F_{loop}(\Gamma)}{NT} &= -c\frac{V}{N} - c^{\frac{3}{2}}\frac{V}{N}\frac{2\sqrt{\pi}}{3}(\frac{g^2}{4\pi})^{\frac{3}{2}}(N_c^2-1)(\beta C_2)^{\frac{3}{2}} \\
&= -1 - c^{\frac{3}{2}}\frac{4\pi}{3}a_{WS}^3\frac{(4\pi)^{\frac{1}{2}}}{3}(\frac{g^2}{4\pi})^{\frac{3}{2}}(N_c^2-1)(\beta C_2)^{\frac{3}{2}} \\
&= -1 - \frac{1}{\sqrt{3}}c^{\frac{3}{2}}\left(\frac{4\pi a_{WS}^3}{3}\right)^{\frac{3}{2}}(N_c^2-1)(\frac{g^2}{4\pi}\beta\frac{C_2}{a_{WS}})^{\frac{3}{2}} \\
&= -1 - \frac{1}{\sqrt{3}}(N_c^2-1)\Gamma^{\frac{3}{2}} \qquad (2.8.2)
\end{aligned}$$

If we define the excess free energy F_{ex} as $F(\Gamma) = F(0) + F_{ex}(\Gamma)$, we get the excess free energies for (2.7.6) and (2.7.7) as

$$\begin{aligned}
\frac{F_{loop,ex}}{NT} &= -\frac{1}{\sqrt{3}}(N_c^2-1)\Gamma^{\frac{3}{2}} + \frac{3}{4}\delta(N_c^2-1)\Gamma^2 - 3\sqrt{3}\delta^2(N_c^2-1)\Gamma^{\frac{5}{2}} + \mathcal{O}(\Gamma^3) \\
\frac{F_{low,ex}}{NT} &= -\sqrt{3}\Gamma^{\frac{3}{2}} - \frac{9}{4}\Gamma^3 - \frac{27}{16}\Gamma^3\int_0^{\frac{3}{\delta}\Gamma}\frac{\sinh t}{t}dt \\
&+ \frac{1}{16}\frac{\delta^4}{\Gamma}\left(2\sinh(\frac{3}{\delta}\Gamma) + 2\frac{\Gamma}{\delta}\cosh(\frac{3}{\delta}\Gamma) + 3\frac{\Gamma^2}{\delta^2}\sinh(\frac{3}{\delta}\Gamma) + 9\frac{\Gamma^3}{\delta^3}\cosh(\frac{3}{\delta}\gamma)\right) \qquad (2.8.3)
\end{aligned}$$

To compare these expanded results with the full molecular dynamics simulations in [3], we may also write

$$\frac{F_{mol,ex}}{NT} = -4.9\int_{+0}^{\Gamma}\frac{d\Gamma'}{\Gamma'} - 2\Gamma + 3.2\cdot 4\Gamma^{\frac{1}{4}} - 2.2\cdot 4\Gamma^{-\frac{1}{4}} + \frac{F_{mol,ex}(+0)}{NT} \qquad (2.8.4)$$

$F_{mol,ex}$ was obtained from the potential energy (36) in [3] through the following relation

$$\frac{F_{ex}(\Gamma)}{NT} = \int_{+0}^{\Gamma} \frac{U_{ex}}{NT}\frac{d\Gamma'}{\Gamma'} + \frac{F_{ex}(+0)}{NT} \ . \tag{2.8.5}$$

For completeness we also quote the excess energy in the Debye-Huckel limit [8],

$$\frac{F_{DH,ex}}{NT} \ = \ -(N_c^2-1)\frac{3d}{2}\Big((A\Gamma)^{\frac{3}{2}}\tan^{-1}\Big(\frac{1}{\sqrt{A\Gamma}}\Big) - \frac{1}{2}\Big(\ln(1+A\Gamma) - A\Gamma\Big)\Big) \ . \tag{2.8.6}$$

with $A = 2/3(2/(\frac{\pi}{2}N_c(N_c-1))^2)^{1/3}$.

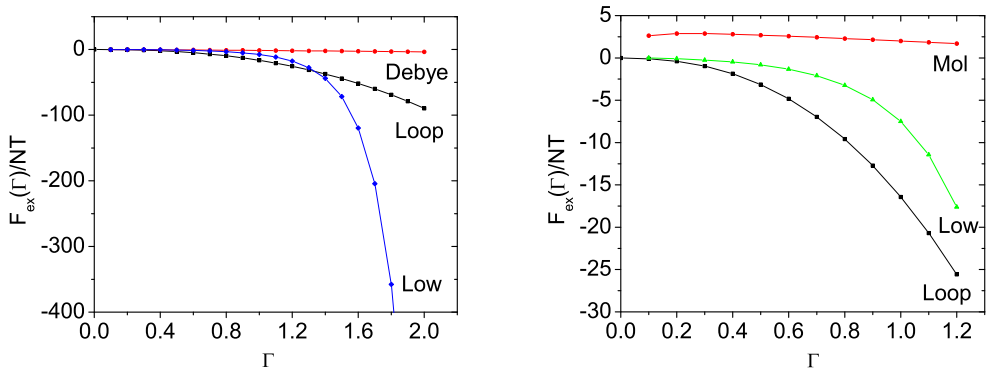

Figure 2.7: Excess free energies vs Debye-Huckel (a) and molecular dynamics (b). See text.

In Fig. 2.7a we show the behavior of the excess free energies for the low density and loop expansions in comparison to the Debye-Huckel result. By about $\Gamma \approx 1.5$ the three expansions deviate substantially and are no longer reliable for the free energy. The deviation occurs earlier in the energy density as we discussed in [11]. In Fig. 2.7b we compare the three expansions to the molecular dynamics simulations in [3] for $0.2 < \Gamma < 1.2$. We note that the $\ln(+0)$ contribution in (2.8.4) combines with $F(+0)$ to zero (infrared renor-

malization). The molecular dynamics simulations use a finite 3-box in space which at weak coupling does not accomodate the Debye cloud which lowers (attractive) the free energy. Thus the discrepancy occurs with the Debye-Huckel limit which is exact for a classical plasma. Simulations with larger 3-boxes are possible but numerically time consuming. At strong coupling, the molecular simulations readily accomodate the short range liquid and/or crystal correlations with the current finite 3-boxes. They are more reliable at large Γ.

2.9 Conclusions

We have explicitly analyzed the grand partition function of a cQGP defined by colored spheres with a hard core potential and a long range Coulomb field, borrowing on methods used for classical liquids [7]. The partition function was worked out explicitly for both SU(2) and SU(3) at low densities through a cumulant expansion, and at high temperature through a loop expansion. Both expansions are shown to be valid for low plasma coupling $\Gamma = V/K \approx 1$. This is the regime where the quantum QGP is expected to be dilute. Current interest in the quantum QGP is in the range of $\Gamma \approx 3$ were the Coulomb interactions are much stronger and the phase liquid-like. In the follow up paper [11] we construct an equation of state that interpolates smoothly between the expanded results of this paper at low Γ and the strongly coupled molecular dynamics results at large Γ [3].

2.10 Appendices

2.10.1 Color charges

The set of classical color charges form a Darboux's set

$$\boldsymbol{\phi} = (\phi_1, \cdots, \phi_{\frac{1}{2}N_c(N_c-1)}) \quad \boldsymbol{\pi} = (\pi_1, \cdots, \pi_{\frac{1}{2}N_c(N_c-1)}) \tag{2.10.1}$$

with canonical Poisson brackets

$$\{\phi_\alpha, \pi_\beta\} = \delta_{\alpha\beta} \quad \{Q^\alpha, Q^\beta\} = f^{\alpha\beta\gamma}Q^\gamma \tag{2.10.2}$$

where N_c is the number of colors and $f^{\alpha\beta\gamma}$ is the structure constant of SU(N_c). The explicit SU(2) and SU(3) representations of these sets can be found in [4, 12]. In this Appendix, we quote some formulas for completeness.

The Darboux's set for SU(2) is [12]

$$Q^1 = \cos\phi_1\sqrt{J^2 - \pi_1^2}, \quad Q^2 = \sin\phi_1\sqrt{J^2 - \pi_1^2}, \quad Q^3 = \pi \tag{2.10.3}$$

where J^2 is used to represent the quadratic Casimir with $q_2 = \sum_\alpha^{N_c^2-1} Q^\alpha Q^\alpha$. The phase space SU(2) measure used in the text is

$$dQ = c_R d\pi_1 d\phi_1 J dJ \delta(J^2 - q_2) \tag{2.10.4}$$

The representation dependent constant c_R is chosen so that $\int dQ = 1$.

The Darboux's set for SU(3) is more involved. Following [12] we define the canonical set as $(\pi_1, \pi_2, \pi_3, \phi_1, \phi_2, \phi_3, J_1, J_2)$ in terms of which the 8 color charges read

$$
\begin{aligned}
&Q^1 = \cos\phi_1\pi_+\pi_- \quad Q^2 = \sin\phi_1\pi_+\pi_- \quad Q^3 = \pi_1 \quad Q^8 = \pi_2 \\
&Q^4 = C_{++}\pi_+ A + C_{+-}\pi_- B \qquad Q^5 = S_{++}\pi_+ A + S_{+-}\pi_- B \\
&Q^6 = C_{--}\pi_- A - C_{--}\pi_+ B \qquad Q^7 = S_{--}\pi_- A - S_{--}\pi_+ B
\end{aligned} \tag{2.10.5}
$$

with

$$
\begin{aligned}
&\pi_+ = \sqrt{\pi_3 + \pi_1}, \qquad C_{\pm\pm} = \cos\left[\frac{1}{2}(\pm\phi_1 + \sqrt{3}\phi_2 \pm \phi_3)\right] \\
&\pi_- = \sqrt{\pi_3 - \pi_1}, \qquad S_{\pm\pm} = \sin\left[\frac{1}{2}(\pm\phi_1 + \sqrt{3}\phi_2 \pm \phi_3)\right]
\end{aligned} \tag{2.10.6}
$$

and

$$
\begin{aligned}
A &= \frac{1}{2\pi_3}\sqrt{(\frac{J_1 - J_2}{3} + \pi_3 + \frac{\pi_2}{\sqrt{3}})(\frac{J_1 + 2J_2}{3} + \pi_3 + \frac{\pi_2}{\sqrt{3}})(\frac{2J_1 + J_2}{3} - \pi_3 - \frac{\pi_2}{\sqrt{3}})} \\
B &= \frac{1}{2\pi_3}\sqrt{(\frac{J_1 - J_2}{3} + \pi_3 - \frac{\pi_2}{\sqrt{3}})(\frac{J_1 + 2J_2}{3} - \pi_3 + \frac{\pi_2}{\sqrt{3}})(\frac{2J_1 + J_2}{3} + \pi_3 - \frac{\pi_2}{\sqrt{3}})}
\end{aligned} \tag{2.10.7}
$$

J_1 and J_2 define the quadratic Casimir q_2 and cubic Casimir q_3. Specifically,

$$
\begin{aligned}
q_2 &= \sum_{\alpha}^{N_c^2-1} Q^\alpha Q^\alpha = \frac{1}{3}(J_1^2 + J_1 J_2 + J_2^2) \\
q_3 &= \sum_{\alpha,\beta,\gamma}^{N_c^2-1} d_{\alpha\beta\gamma} Q^\alpha Q^\beta Q^\gamma = \frac{1}{18}(J_1 - J_2)(J_1 + 2J_2)(2J_1 + J_2)
\end{aligned} \tag{2.10.8}
$$

with the help of the SU(2) symmetric tensor $d_{\alpha\beta\gamma}$. we recall that $d_{\alpha\beta\gamma} = d^{\alpha\beta\gamma}$ and $d^{\alpha\beta\gamma} = d^{\beta\gamma\alpha} = d^{\gamma\alpha\beta} = d^{\alpha\gamma\beta} = d^{\gamma\beta\alpha} = d^{\beta\alpha\gamma}$.

To carry some of the color integrations in the text, we quote some useful identities involving d's. For instance,

$$\begin{aligned} \sum_{\alpha,\beta,\gamma} d^{\alpha\beta\gamma} d^{\alpha\beta\gamma} &= 4q_3 \\ \sum_{\alpha,\beta,\gamma} d^{\alpha\alpha\gamma} d^{\beta\beta\gamma} &= 0 \end{aligned} \tag{2.10.9}$$

and

$$\begin{aligned} \sum_{\alpha,\beta,\gamma,\delta,\epsilon,\zeta} d^{\alpha\gamma\epsilon} d^{\beta\gamma\epsilon} d^{\alpha\delta\zeta} d^{\beta\delta\zeta} &= 2{q_3}^2 \\ \sum_{\alpha,\beta,\gamma,\delta,\epsilon,\zeta} d^{\alpha\beta\epsilon} d^{\gamma\delta\epsilon} d^{\alpha\gamma\zeta} d^{\beta\delta\zeta} &= -2q_3 \end{aligned} \tag{2.10.10}$$

The SU(3) phase space measure is

$$\begin{aligned} dQ = c_R d\phi_1 d\phi_2 d\phi_3 d\pi_1 d\pi_2 d\pi_3 dJ_1 dJ_2 \frac{\sqrt{3}}{48} J_1 J_2 (J_1 + J_2) \\ \times \delta(\tfrac{1}{3}(J_1^2 + J_1 J_2 + J_2^2) - q_2) \delta(\tfrac{1}{18}(J_1 - J_2)(J_1 + 2J_2)(2J_1 + J_2) - q_3) \end{aligned} \tag{2.10.11}$$

with again c_R set by the normalization of the color space volume to 1.

Table 2.1: Non-zero constants of $d^{\alpha\beta\gamma}$ for SU(3)

d^{118}	d^{228}	d^{338}	d^{448}	d^{558}	d^{668}	d^{778}	d^{888}
$\frac{1}{\sqrt{3}}$	$\frac{1}{\sqrt{3}}$	$\frac{1}{\sqrt{3}}$	$-\frac{1}{2\sqrt{3}}$	$-\frac{1}{2\sqrt{3}}$	$-\frac{1}{2\sqrt{3}}$	$-\frac{1}{2\sqrt{3}}$	$-\frac{1}{\sqrt{3}}$
d^{146}	d^{157}	d^{247}	d^{256}	d^{344}	d^{355}	d^{366}	d^{377}
$\frac{1}{2}$	$\frac{1}{2}$	$-\frac{1}{2}$	$\frac{1}{2}$	$\frac{1}{2}$	$\frac{1}{2}$	$-\frac{1}{2}$	$-\frac{1}{2}$

2.10.2 Color integrations

In this Appendix we explicit some of the color integrations. For SU(2) all color charge integrations can be done analytically. The representation dependent c_R is set to give the normalization of the colored space volume to be 1. For instance $c_R = 1/2\pi\sqrt{q_2}$[12] by using $\int dQ = 1$. The SU(3) integrations cannot be done analytically given the cubic nature of the constraint in the color measure. The quadratic and cubic Casimirs are fixed by

$$\begin{aligned}\int dQ q_2 &= \int dQ \frac{1}{3}(J_1^2 + J_1 J_2 + J_2^2) = q_2 \\ \int dQ q_3 &= \int dQ \frac{1}{18}(J_1 - J_2)(J_1 + 2J_2)(2J_1 + J_2) = q_3 \end{aligned} \quad (2.10.12)$$

One Color:

$$\int dQ Q^\alpha = 0 \ . \quad (2.10.13)$$

Two Colors:

$$\int dQQ^\alpha Q^\beta = C_2\delta^{\alpha\beta} = \frac{q_2}{N_c^2-1}\delta^{\alpha\beta} \tag{2.10.14}$$

with $C_2 = N_c$ for gluons and $C_2 = 1/2$ for quarks. For SU(3), the cubic Casimir $q_3 = 0$ for gluons and $q_3 = (N_c^2-1)(N_c^2-4)/4N_c$ for quarks. It is zero for SU(2).

Three Colors:

$$\begin{aligned}\sum_{\alpha,\beta,\gamma} d_{\alpha\beta\gamma}Q^\alpha Q^\beta Q^\gamma = q_3 = \frac{1}{4}\sum_{\alpha,\beta,\gamma} d_{\alpha\beta\gamma}d^{\alpha\beta\gamma} \\ = \int dQ q_3 = \sum_{\alpha,\beta,\gamma} d_{\alpha\beta\gamma}\int dQQ^\alpha Q^\beta Q^\gamma\end{aligned} \tag{2.10.15}$$

where we used (2.10.8) and (2.10.12) and the identity

$$\sum_{\alpha,\beta,\gamma} d^{\alpha\beta\gamma}d_{\alpha\beta\gamma} = \frac{1}{N_c}(N_c^2-1)(N_c^2-4) = 4q_3 \tag{2.10.16}$$

Thus

$$\int dQQ^\alpha Q^\beta Q^\gamma = \frac{1}{4}d^{\alpha\beta\gamma} \tag{2.10.17}$$

Four Colors:

$$\begin{aligned}\int dQQ^\alpha Q^\beta Q^\gamma Q^\delta &= A(\sum_n d^{\alpha\beta n}d^{\gamma\delta n} + \sum_n d^{\alpha\gamma n}d^{\beta\delta n} + \sum_n d^{\alpha\delta n}d^{\beta\gamma n}) \\ &+ B(\delta^{\alpha\beta}\delta^{\gamma\delta} + \delta^{\alpha\gamma}\delta^{\beta\delta} + \delta^{\alpha\delta}\delta^{\beta\gamma})\end{aligned} \tag{2.10.18}$$

For SU(2) $A = 0$ and $B = q_2^2/15$. For SU(3) this integral is more involved. However, for certain arrangements of charges, say Q^1, Q^2, Q^3, Q^8 the integrations can be done and thus the constants A, B fixed. For that we need to undo integrals involving $\pi' s$ since $Q^8 = \pi^2$.

The π integrations are bounded [4, 13]. To carry them, it is best to change variables

$$x = \pi_3 + \frac{\pi_2}{\sqrt{3}}, \quad y = \pi_3 - \frac{\pi_2}{\sqrt{3}} \tag{2.10.19}$$

so that

$$d\pi_2 d\pi_3 = \frac{\sqrt{3}}{2} dx dy \tag{2.10.20}$$

It is also useful to define

$$K_1 = \frac{1}{3}(2J_1 + J_2), \quad K_2 = \frac{1}{3}(J_1 + 2J_2) \tag{2.10.21}$$

so that

$$K_2 - K_1 < x < K_1, \quad K_1 - K_2 < y < K_2 \tag{2.10.22}$$

With these definitions, we can esily unwind some π integrations. For instance

$$\int d\pi_1 d\pi_2 d\pi_3 = \frac{\sqrt{3}}{2} \int_{K_2-K_1}^{K_1} dx \int_{K_1-K_2}^{K_2} dy \int_{-\frac{1}{2}(x+y)}^{\frac{1}{2}(x+y)} d\pi_1 = \frac{\sqrt{3}}{4} J_1 J_2 (J_1 + J_2) \tag{2.10.23}$$

and

$$\int d\pi_1 {\pi_2}^2 d\pi_2 d\pi_3 \quad = \frac{\sqrt{3}}{2}\int_{K_2-K_1}^{K_1} dx \int_{K_1-K_2}^{K_2} dy \Big(\frac{\sqrt{3}}{2}(x-y)\Big)^2 \int_{-\frac{1}{2}(x+y)}^{\frac{1}{2}(x+y)} d\pi_1$$
$$= \frac{1}{8}\frac{\sqrt{3}}{4} J_1 J_2 (J_1+J_2)\frac{1}{3}(J_1^2+J_1J_2+J_2^2)\ . \qquad (2.10.24)$$

This latter integral is directly related to

$$\int dQ Q^8 Q^8 \quad = c_R \int d\phi_1 d\phi_2 d\phi_3 \int d\pi_1 {\pi_2}^2 d\pi_2 d\pi_3 \int dJ_1 dJ_2 \frac{\sqrt{3}}{48} J_1 J_2 (J_1+J_2)$$
$$\times\delta(\frac{1}{3}(J_1^2+J_1J_2+J_2^2)-q_2)$$
$$\times\delta(\frac{1}{18}(J_1-J_2)(J_1+2J_2)(2J_1+J_2)-q_3)$$
$$= \int dQ \frac{1}{8}\frac{1}{3}(J_1^2+J_1J_2+J_2^2) = \int dQ \frac{1}{8} q_2 = \frac{1}{N_c^2-1} q_2 \qquad (2.10.25)$$

after using (2.10.11) and (2.10.12). The result agrees with (2.10.14). Similarly,

$$\int d\pi_1 {\pi_2}^3 d\pi_2 d\pi_3 \quad = \frac{\sqrt{3}}{2}\int_{K_2-K_1}^{K_1} dx \int_{K_1-K_2}^{K_2} dy \Big(\frac{\sqrt{3}}{2}(x-y)\Big)^3 \int_{-\frac{1}{2}(x+y)}^{\frac{1}{2}(x+y)} d\pi_1$$
$$= -\frac{\sqrt{3}}{40}\frac{\sqrt{3}}{4} J_1 J_2 (J_1+J_2)\frac{1}{18}(J_1-J_2)(J_1+2J_2)(2J_1+J_2) \qquad (2.10.26)$$

is related to

$$\begin{aligned}\int dQQ^8Q^8Q^8 \quad &= c_R \int d\phi_1 d\phi_2 d\phi_3 \int d\pi_1 {\pi_2}^3 d\pi_2 d\pi_3 \int dJ_1 dJ_2 \frac{\sqrt{3}}{48} J_1 J_2 (J_1 + J_2) \\ &\times \delta(\frac{1}{3}(J_1^2 + J_1 J_2 + J_2^2) - q_2) \\ &\times \delta(\frac{1}{18}(J_1 - J_2)(J_1 + 2J_2)(2J_1 + J_2) - q_3) \\ &= -\frac{\sqrt{3}}{40} \int dQ \frac{1}{18}(J_1 - J_2)(J_1 + 2J_2)(2J_1 + J_2) \\ &= -\frac{\sqrt{3}}{40} \int dQ q_3 = -\frac{1}{4}\frac{1}{\sqrt{3}}\frac{3}{10} q_3 = \frac{1}{4} d^{888} \end{aligned} \tag{2.10.27}$$

after using $q_3 = (N_c^2 - 1)(N_c^2 - 4)/4N_c = 10/3$ for SU(3). This result is in agreement with (2.10.17). A similirar reasoning, yields

$$A + 3B = \frac{3}{80} q_2^2 \tag{2.10.28}$$

for the A, B constants in (2.10.18).

Five Colors:

$$\begin{aligned}\int dQQ^\alpha Q^\beta Q^\gamma Q^\delta Q^\epsilon = \frac{3}{560} q_2 q_3 \Big(&\delta^{\alpha\beta} d^{\gamma\delta\epsilon} + \delta^{\alpha\gamma} d^{\beta\delta\epsilon} + \delta^{\alpha\delta} d^{\beta\gamma\epsilon} + \delta^{\alpha\epsilon} d^{\beta\gamma\delta} \\ &+ \delta^{\beta\gamma} d^{\alpha\delta\epsilon} + \delta^{\beta\delta} d^{\alpha\gamma\epsilon} + \delta^{\beta\epsilon} d^{\alpha\gamma\delta} + \delta^{\gamma\delta} d^{\alpha\beta\epsilon} + \delta^{\gamma\epsilon} d^{\alpha\beta\delta} + \delta^{\delta\epsilon} d^{\alpha\beta\gamma} \Big) \end{aligned} \tag{2.10.29}$$

with

$$\frac{3}{560} q_2 q_3 = \frac{1}{7}\frac{1}{8} q_2 \frac{3}{10} q_3 = \frac{1}{7} C_2 \tag{2.10.30}$$

Six Colors:

$$
\begin{aligned}
&\int dQQ^\alpha Q^\beta Q^\gamma Q^\delta Q^\epsilon Q^\zeta \\
&= A\Big(d^{\alpha\beta\gamma}d^{\delta\epsilon\zeta} + d^{\alpha\beta\delta}d^{\gamma\epsilon\zeta} + d^{\alpha\beta\epsilon}d^{\gamma\delta\zeta} + d^{\alpha\beta\zeta}d^{\gamma\delta\epsilon} + d^{\alpha\gamma\delta}d^{\beta\epsilon\zeta} \\
&+d^{\alpha\gamma\epsilon}d^{\beta\delta\zeta} + d^{\alpha\gamma\zeta}d^{\beta\delta\epsilon} + d^{\alpha\delta\epsilon}d^{\beta\gamma\zeta} + d^{\alpha\delta\zeta}d^{\beta\gamma\epsilon} + d^{\alpha\epsilon\zeta}d^{\beta\gamma\delta}\Big) \\
&+B\Big(\delta^{\alpha\beta}\delta^{\gamma\delta}\delta^{\epsilon\zeta} + \delta^{\alpha\beta}\delta^{\gamma\epsilon}\delta^{\delta\zeta} + \delta^{\alpha\beta}\delta^{\gamma\zeta}\delta^{\delta\epsilon} + \delta^{\alpha\gamma}\delta^{\beta\delta}\delta^{\epsilon\zeta} + \delta^{\alpha\gamma}\delta^{\beta\epsilon}\delta^{\delta\zeta} \\
&+\delta^{\alpha\gamma}\delta^{\beta\zeta}\delta^{\delta\epsilon} + \delta^{\alpha\delta}\delta^{\beta\gamma}\delta^{\epsilon\zeta} + \delta^{\alpha\delta}\delta^{\beta\epsilon}\delta^{\gamma\zeta} + \delta^{\alpha\delta}\delta^{\beta\zeta}\delta^{\gamma\epsilon} + \delta^{\alpha\epsilon}\delta^{\beta\gamma}\delta^{\delta\zeta} \\
&+\delta^{\alpha\epsilon}\delta^{\beta\delta}\delta^{\gamma\zeta} + \delta^{\alpha\epsilon}\delta^{\beta\zeta}\delta^{\gamma\delta} + \delta^{\alpha\zeta}\delta^{\beta\gamma}\delta^{\delta\epsilon} + \delta^{\alpha\zeta}\delta^{\beta\delta}\delta^{\gamma\epsilon} + \delta^{\alpha\zeta}\delta^{\beta\epsilon}\delta^{\gamma\delta}\Big)
\end{aligned}
\tag{2.10.31}
$$

with the A, B constants tabulated below.

Table 2.2: Constants A and B in the integration of six color charges

	A	B
$SU(2)$		$\frac{1}{105}q_2^3$
$SU(3)$	$-\frac{9}{8!}q_2^3 + \frac{27}{2}\frac{1}{7!}q_3^2$	$\frac{85}{2}\frac{1}{8!}q_2^3 - \frac{6}{8!}q_3^2$

Chapter 3

Thermodynamics

3.1 Introduction

Classical plasmas are statistical systems with constituents that are locally charged but globally neutral. An example is the electromagnetic one component plasma (OCP) also referred to as Jelium. A number of many-body theories have been devised to analyze the OCP in the regime of small $\Gamma = V/K$, the ratio of the average Coulomb energy to kinetic energy [14]. Most of the extensions to larger values of Γ are based on higher order transport equations [1] or classical molecular dynamics [15].

The classical quark-gluon plasma (cQGP) as developed by Gelman, Shuryak and Zahed [3] can be regarded as an extension of the OCP plasma to many components with non-Abelian color charges. Stability against core collapse is enforced classically through a phenomenological core potential. The origin of the core is quantum mechanical. Detailed molecular dynamics simulations of the cQGP [3] have shown a strongly coupled plasma for $\Gamma = V/K \approx 1$ or larger. The cQGP maybe in a liquid state at moderate values of Γ. In a recent

analysis [16] we have used analytical methods of classical liquids to construct the free energy for small Γ both in the dilute case and at high temperature after resummation of the screening effects.

In this chapter we combine the results in [3] obtained from molecular dynamics with the one-loop analytical results in [16] to construct the equation of state of the cQGP for all values of Γ. We show that the strongly coupled component of the cQGP contributes significantly to the thermodynamics across the transition whether in the energy density, pressure or entropy density. In section 3.2, we derive the excess energy of the cQGP for small Γ in the one-loop approximation. In section 3.3, we use ideas from classical electromagnetic plasmas to interpolate between the one-loop result at low Γ and the molecular dynamics results at large Γ for the SU(2) cQGP. Particular attention will be given to the core parameter using Debye-Hückel plus Hole (DHH) theory. In the quantum QCD plasma, Γ runs with T. In section 3.4, we use the interpolated excess energy density together with the Gibbs relations to derive the pressure and entropy of the cQGP. In section 3.5, we compare the results for the SU(2) cQGP with SU(2) lattice simulations in two ways: (1) by fitting the bulk energy density to extract Γ and (2) by using a lattice extracted running coupling constant to set Γ. Our conclusions are in section 3.6. In Appendix 3.7.1 we show that the interaction corrections to the concentration do not affect the one-loop result to order $\Gamma^{\frac{5}{2}}$ with the bare particle concentration. In Appendix 3.7.2 we summarize the Debye-Hückel plus Hole theory to assess the range of the core in terms of the Debye length. In Appendix 3.7.3 we explicitly describe the effects of changing the core parameter on the bulk energy density.

3.2 Excess energy: One-Loop

In classical plasmas the key expansion parameter at zero chemical potential is $\Gamma = V/K$ the ratio of the mean Coulomb to kinetic energy. For an Abelian or QED plasma,

$$\Gamma = \frac{(Ze)^2}{ak_BT} \tag{3.2.1}$$

while for a non-Abelian or QCD plasma [3]

$$\Gamma = \frac{g^2}{4\pi}\frac{C_2}{Ta_{WS}} \tag{3.2.2}$$

with $k_B = 1$ and a_{WS} the Wigner-Seitz radius satisfying $N/V(4\pi a_{WS}^3/3) = 1$. C_2 is the quadratic Casimir ($C_2 = q_2/(N_c^2 - 1)$) and g is the strength of the coupling. In the cQGP g is fixed, whereas in the QGP g runs with temperature. The running is quantum mechanical and beyond the present classical analysis. In sections 4,5 it is addressed phenomenologically.

Since the Wigner-Seitz radius a_{WS} is tied with the density or concentration (the bare concentration is $c_0 = N/V$), it is straightforward to express the free energy in terms of Γ. After resumming the screening effects and to one-loop, the free energy reads [16]

$$\begin{aligned}\beta\frac{F_{loop}(\beta,c)}{V} &= -c - \frac{2\sqrt{\pi}}{3}(N_c^2-1)\gamma^{\frac{3}{2}}c^{\frac{3}{2}} + \pi(N_c^2-1)c^2\gamma^2\sigma \\ &\quad -2\pi^{\frac{3}{2}}(N_c^2-1)c^{\frac{5}{2}}\gamma^{\frac{5}{2}}\sigma^2 + c\beta\mu_c + \mathcal{O}(\beta^3)\end{aligned} \tag{3.2.3}$$

with $\gamma = g^2/4\pi\beta C_2$, c being the concentration and σ being the core radius. The concentration is determined by the chemical equation [16] and to leading order

is $c_0 = N/V$ as detailed in Appendix 3.7.1. The core σ is a parameter in the cQGP much like in normal classical liquids. Its origin is quantum mechanical. In Appendix B, we use the classical Debye-Hückel plus Hole (DHH) theory to assess the size of the core in terms of the Debye screening length.

To see how the expansion in the concentration c in (3.2.3) converts to an expansion in Γ, we note that the Debye-Hückel contributions (first two terms) can be rewritten as

$$\begin{aligned}
\frac{F_{DH}(\Gamma)}{NT} &= -c\frac{V}{N} - c^{\frac{3}{2}}\frac{V}{N}\frac{2\sqrt{\pi}}{3}(\frac{g^2}{4\pi})^{\frac{3}{2}}(N_c^2-1)(\beta C_2)^{\frac{3}{2}} \\
&= -1 - c^{\frac{3}{2}}\frac{4\pi}{3}a_{WS}^3\frac{(4\pi)^{\frac{1}{2}}}{3}(\frac{g^2}{4\pi})^{\frac{3}{2}}(N_c^2-1)(\beta C_2)^{\frac{3}{2}} \\
&= -1 - \frac{1}{\sqrt{3}}c^{\frac{3}{2}}\Big(\frac{4\pi a_{WS}^3}{3}\Big)^{\frac{3}{2}}(N_c^2-1)(\frac{g^2}{4\pi}\beta\frac{C_2}{a_{WS}})^{\frac{3}{2}} \\
&= -1 - \frac{1}{\sqrt{3}}(N_c^2-1)\Gamma^{\frac{3}{2}} \qquad (3.2.4)
\end{aligned}$$

By defining the excess free energy F_{ex} as $F_{ex}(\Gamma) = F(\Gamma) - F(0)$ we obtain the one-loop excess energy density,

$$\frac{F_{loop,ex}}{NT} = -\frac{1}{\sqrt{3}}(N_c^2-1)\Gamma^{\frac{3}{2}} + \frac{3}{4}\delta(N_c^2-1)\Gamma^2 - 3\sqrt{3}\delta^2(N_c^2-1)\Gamma^{\frac{5}{2}} + \mathcal{O}(\Gamma^3) \quad (3.2.5)$$

with $\delta = \sigma/a_{WS}$. $F(0)$ will be identified with the free gas or Stephan-Boltzman contribution.

The excess energy U_{ex} of the cQGP follows from the excess free energy F_{ex} as

$$\frac{F_{ex}(\Gamma)}{NT} = \int_0^\Gamma \frac{U_{ex}}{NT}\frac{d\Gamma'}{\Gamma'} \qquad (3.2.6)$$

For instance, the Debye-Hückel contribution in (3.2.3) yields through (3.2.6) the excess energy

$$\frac{U_{DH,ex}}{NT} = -\frac{\sqrt{3}}{2}(N_c^2 - 1)\Gamma^{\frac{3}{2}} \tag{3.2.7}$$

in agreement with the Debye-Hückel excess energy for the cQGP initially discussed in [8] using different methods. In general, the energy density splits into the free contributiom plus excess contribution,

$$\epsilon(\Gamma) = \frac{U(\Gamma)}{V} = \frac{U_0}{V} + \frac{U_{ex}(\Gamma)}{V} = \epsilon_0 + \epsilon(\Gamma) \tag{3.2.8}$$

with the free contribution $\epsilon_0 = \epsilon_{SB}$ identified with the Stefan-Boltzmann energy density ϵ_{SB}. In relative notations,

$$\frac{\epsilon(\Gamma)}{\epsilon_{SB}} = 1 + \frac{1}{\epsilon_{SB}}\frac{U_{ex}(\Gamma)}{V} \tag{3.2.9}$$

Using (3.2.6) together with (3.2.5), we obtain the one-loop excess energy density

$$\frac{U_{loop,ex}}{NT} = -\frac{\sqrt{3}}{2}(N_c^2 - 1)\Gamma^{\frac{3}{2}} + \frac{3}{2}\delta(N_c^2 - 1)\Gamma^2 - \frac{15}{2}\sqrt{3}\delta^2(N_c^2 - 1)\Gamma^{\frac{5}{2}} + \mathcal{O}(\Gamma^3) \tag{3.2.10}$$

which is valid for small Γ. In Appendix 3.7.1, we show that although the concentration c in Γ is not c_0 because of interactions, to order $\Gamma^{5/2}$ we may set $c = c_0$.

3.3 Excess Energy: Full

In [16] the one-loop expansion was shown to converge up to $\Gamma \approx 1$ for the free energy. The range is even smaller for the energy with $\Gamma \approx 1/2$ (see below). Larger values of Γ have been covered by molecular dynamics simulations in [3]. For an SU(2) plasma (say a constituent gluonic plasma) the numerical results for the excess energy were found to follow the parametric form [3]

$$u_{mol}(\Gamma) = \frac{U_{mol}}{NT} \simeq -4.9 - 2\Gamma + 3.2\Gamma^{\frac{1}{4}} + \frac{2.2}{\Gamma^{\frac{1}{4}}} \ . \tag{3.3.1}$$

For $N_c = 2$ the one-loop result (3.2.10) reads

$$u_{anal}(\Gamma) = \frac{U_{anal}}{NT} = -\frac{3}{2}\sqrt{3}\Gamma^{\frac{3}{2}} + \frac{9}{2}\delta\Gamma^2 - \frac{45}{2}\sqrt{3}\delta^2\Gamma^{\frac{5}{2}} \tag{3.3.2}$$

To construct the full excess energy valid for all Γ we proceed phenomenologically by seeking an interpolating formula between (3.3.1) and (3.3.2) borrowing from ideas in classical plasma physics [17]. A similar approach was also advocated in [18] using different limits.

In the Abelian or QED plasma, the excess energy based on Debye-Hückel theory is evaluated for $\Gamma < 0.1$. Molecular dynamics simulations are generated for $1 < \Gamma < 180$. The two are combined numerically through a power function in the form [17]

$$u_{full}(\Gamma) = \frac{u_{\Gamma<0.1}(\Gamma) + f(\Gamma)u_{\Gamma>1}(\Gamma)}{1 + f(\Gamma)} \tag{3.3.3}$$

with $f(\Gamma)$ being a fitting power function of the type $a\Gamma^b (= 3.0 \times 10^3\Gamma^{5.7})$. (3.3.3) interpolates smoothly between the exact analytical results at low Γ and the simulations at large Γ as shown in Fig. 3.1(a). In the insert we show

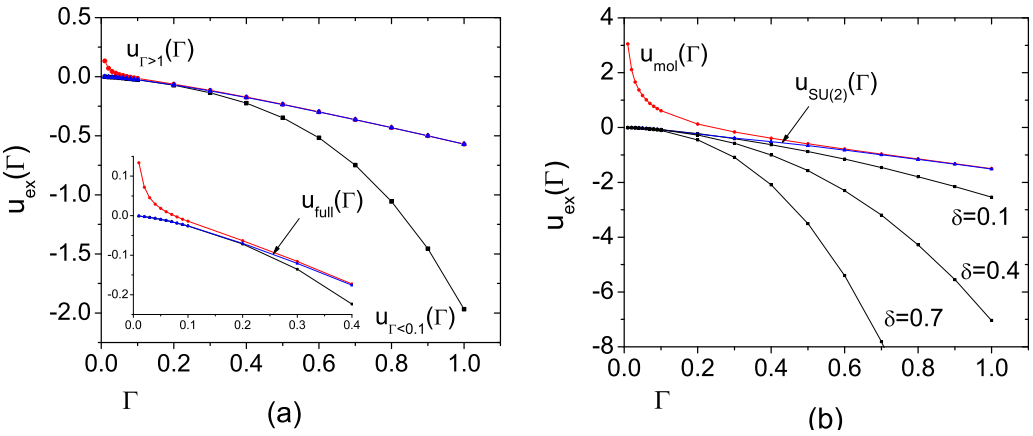

Figure 3.1: Excess energy for QED and $N_c = 2$ QCD

the nature of the size of the gap in the range $0.1 < \Gamma < 1$ for the Abelian plasma.

In Fig. 3.1(b) we show our $N_c = 2$ results at low values of Γ (one-loop) and large values of Γ (simulations). The one-loop results depend on the size of the hard core σ. Recall that the simulations in [3] are carried with a fixed higher power law repulsion to mock up the core. So the simulations seem to favor a small hard core in the Wigner-Seitz units. In fact, σ can be set by the Debye radius in the DHH theory [19] detailed in Appendix 3.7.2. It changes with Γ. Specifically,

$$\delta = \frac{\sigma}{a_{WS}} = \frac{1}{a_{WS}\kappa_D}\Big((1+(3\Gamma)^{\frac{3}{2}})^{\frac{1}{3}} - 1\Big) = \frac{1}{(3\Gamma)^{\frac{1}{2}}}\Big((1+(3\Gamma)^{\frac{3}{2}})^{\frac{1}{3}} - 1\Big) \quad (3.3.4)$$

which is shown in Fig. 3.2. The core size δ varies in the range $0.2-0.5$ for Γ in the range $0.1-1$. We fix $\delta = 0.4$ in the range $0.1-1$. With this in mind and following the Abelian plasma construction, we find the excess energies shown in Fig. 3.1(b) to be fit by

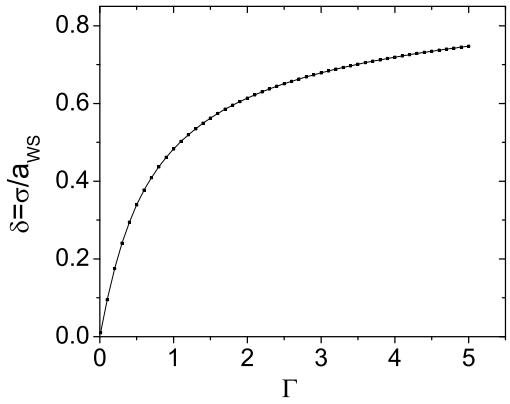

Figure 3.2: Core parameter $\delta = \sigma/a_{WS}$. See text.

$$u_{SU(2)}(\Gamma) = \frac{u_{anal}(\Gamma) + 2.0 \times 10^3 \Gamma^{6.3} u_{mol}(\Gamma)}{1 + 2.0 \times 10^3 \Gamma^{6.3}} \tag{3.3.5}$$

The power function is numerically adopted to yield a small deviation (less than 0.1%) for $\Gamma < 0.1$ and $\Gamma > 1$. The precise choice of the core parameter is actually not very important, because small changes in core size can be compensated by small changes in the power function for the same overall accuracy. This point is discussed further in Appendix 3.7.3.

3.4 Thermodynamics

Knowledge of the energy density for all values of Γ can be used to extract all extensive thermodynamical quantities in the cQGP with the help of the Gibbs relations. Indeed, the pressure and entropy follow from the Gibbs relations

$$\begin{aligned}\epsilon &= T\frac{\partial P}{\partial T} - P \\ s &= \frac{S}{V} = \frac{1}{V}\frac{\partial P}{\partial T}\ .\end{aligned} \tag{3.4.1}$$

In so far the classical plasma parameter Γ as defined (4.2.2) is a fixed parameter. However, in QCD it runs through α_s. It is only a function of temperature. Specifically,

$$\Gamma = \frac{\alpha_s C_2}{T a_{WS}} = \left(\frac{4\pi}{3}c_0\right)^{\frac{1}{3}}\beta C_2 \alpha_s(T) = \left(0.244(N_c^2-1)\frac{4\pi}{3}\right)^{\frac{1}{3}} C_2\alpha_s(T) \tag{3.4.2}$$

where $0.244(N_c^2-1)$ is the black-body concentration for adjoint gluons. The exact running of $\alpha_s(T)$ is fixed below.

Using (3.4.1) together with (3.4.2) yields the pressure and the entropy density directly in terms of the energy density

$$\begin{aligned}\frac{P}{P_{SB}} &= 3\frac{1}{T^3}\int_{T_c}^{T} dT' T'^2 \frac{\epsilon}{\epsilon_{SB}}(T') \\ \frac{s}{s_{SB}} &= \frac{3}{4}\frac{\epsilon}{\epsilon_{SB}}(T) + \frac{3}{4}\frac{1}{T^3}\int_{T_c}^{T} dT' T'^2 \frac{\epsilon}{\epsilon_{SB}}(T')\ .\end{aligned} \tag{3.4.3}$$

Here T_c is identified with the SU(2) transition with $P_c = 0$. For a constituent gluonic plasma $T_c = 215$ MeV. All bulk thermodynamics is tied to the energy density by the Gibbs relations.

3.5 SU(2) Lattice Comparison

To proceed further we need to know how $\alpha_s(T)$ runs with T in pure YM and QCD, to determine the behavior of the extensive thermodynamical quantities. The loop expansion allows a specific determination of the running $\alpha_s(T)$ that is unfortunately valid at high temperature or weak coupling. How $\alpha_s(T)$ runs at strong coupling is unknown. Here we suggest two ways to *extract* $\alpha_s(T)$: (1) by fitting the energy density (3.2.9) to lattice data and deducing $\Gamma(T)$ and (2) by using a lattice extracted running coupling constant to set $\Gamma(T)$ directly.

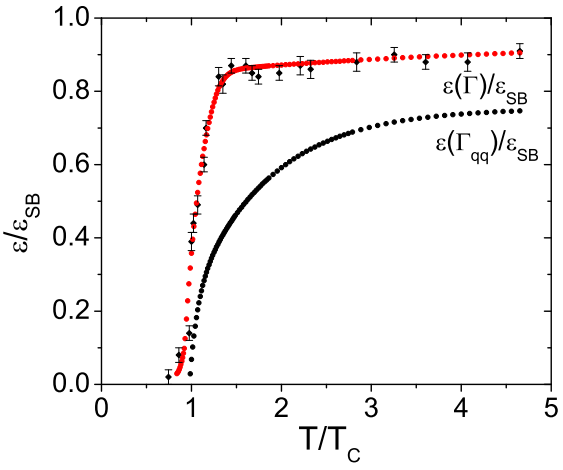

Figure 3.3: Energy densities vs SU(2) lattice data. See text.

In Fig. 3.3 we show the fit (upper line) of the normalized energy density in the cQGP to the SU(2) lattice data in [20] (method 1). The lattice results are used with $\Lambda_L = 5$ MeV and $T_c = 215$ MeV as suggested in [20]. Alternatively, we can use the lattice extracted running coupling constant in [21] to predict the behavior of the bulk energy density of the cQGP (method 2). This is also shown in Fig. 3.3 (lower line). The corresponding running couplings are shown in Fig. 3.4(a) and their corresponding Γ in Fig. 3.4(b). In method 1, we used

(3.2.9), (3.3.5) and (3.4.2) for the extraction and note that the lattice data [20] are for $N_c = 2$. In method 2, we used the running coupling constant α_{qq} determined from the short distance fit to the free energy in [21] for $N_c = 3$ and a screening length of about 1/2 fm. The conversion to $N_c = 2$ follows from (3.4.2) with $C_2 = N_c = 2$. The solid curve through the lattice data is our best fit including the error bars. We note that in [21] the long distance fit to the free energy yields a larger running coupling.

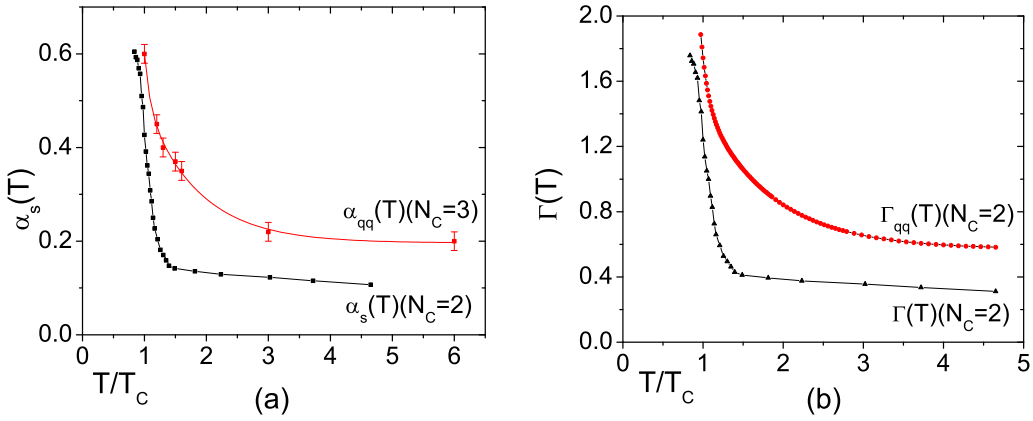

Figure 3.4: $\alpha_s(T)$ and $\Gamma(T)$. See text.

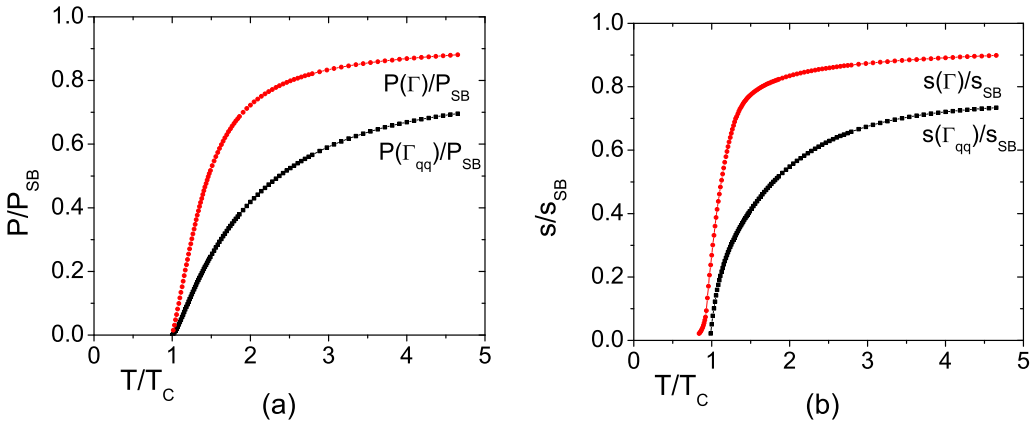

Figure 3.5: Bulk thermodynamics from the SU(2) cQGP. See text.

In Fig. 3.5 we show the results originating from both fitting methods: (1) by fitting the energy density to extract Γ and (2) by predicting the energy density from the extracted lattice Γ. The fit to the energy density (method 1) produces a running coupling constant weaker than the $N_c = 2$ adjusted running coupling constant from the lattice and it produces better bulk thermodynamics in the cQGP thanks to the Gibbs relations. The lattice extracted running coupling constant (method 2) shows a rapid rise in the bulk thermodynamics in the cQGP reminiscent of a phase-like change. However the transition takes place in the region of Γ where the numerical interpolation of section 3 is taking place.

Finally in Fig. 3.6 we detail the various contributions to the bulk thermodynamics in the cQGP using method 1 and (3.3.5) and the Gibbs relations (3.4.1) to assess the role of the strongly coupled component of the cQGP. For instance, the contributions to the energy density are separated as follows

$$\begin{aligned} u_{SU(2),anal}(\Gamma) &= \frac{u_{anal}(\Gamma)}{1 + 2.0 \times 10^3 \Gamma^{6.3}} \\ u_{SU(2),mol}(\Gamma) &= \frac{2.0 \times 10^3 \Gamma^{6.3} u_{mol}(\Gamma)}{1 + 2.0 \times 10^3 \Gamma^{6.3}} \end{aligned} \tag{3.5.1}$$

The strongly coupled component of the cQGP generated by the molecular dynamics simulations contributes significantly across the transition temperature, say in the range $(1 - 2.5)\, T_c$.

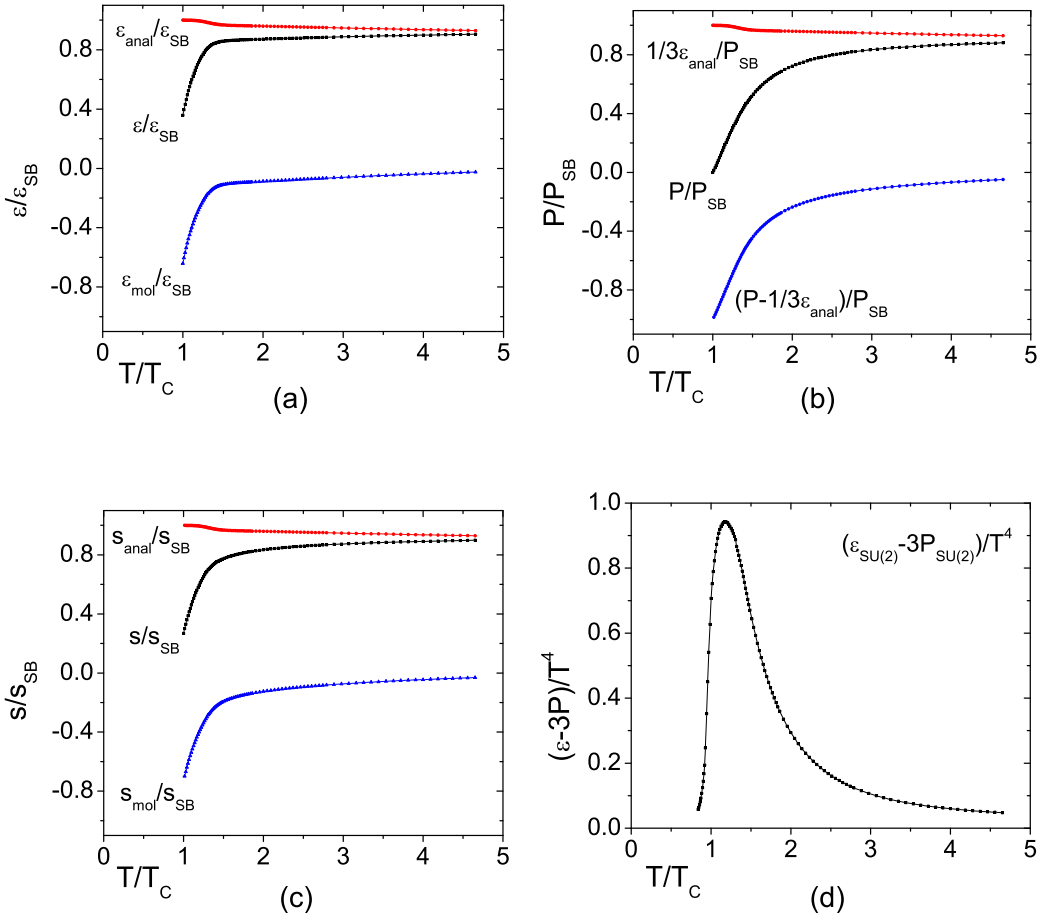

Figure 3.6: Relative contributions in the cQGP bulk thermodynamics. See text.

3.6 Conclusion

We have constructed the energy density of the cQGP valid for all values of the plasma parameter Γ, which interpolates between the one-loop result at small Γ and the molecular dynamics simulations at large Γ. We have used it in conjunction with the Gibbs relations to derive the pressure and entropy of the cQGP.

In quantum QCD Γ runs through the QCD coupling constant at weak coupling. The running at strong coupling is unknown in general except for

some recent lattice simulations [21]. We have suggested that a fit of our energy density to the lattice energy density [20] allows an extraction of the running coupling that is smaller than the one suggested by direct lattice simulations [21].

We have used the extracted running coupling constant to predict the entropy density and pressure of the cQGP. The latter compares well to direct lattice SU(2) simulations. We have shown that the strongly coupled component of the cQGP contributes significantly to the bulk thermodynamics across the transition temperature.

Alternatively, a direct use of the lattice extracted running coupling constant yields bulk energy, pressure and entropy densities for the cQGP that are softer than the directly measured lattice counterparts. However, the bulk thermodynamics show a rapid rise across the transition temperature in the cQGP following the rapid drop in the Coulomb coupling, a behavior usually assigned to a phase change.

We expect transport properties such as diffusion and viscosity, as well as energy loss to be significantly affected in the transition region from strong to weak coupling in the cQGP as we discuss next [22].

3.7 Appendices

3.7.1 Concentration

The bare concentration $c_0 = N/V$ which is identified with the black-body radiation in the cQGP is in general modified to $c = c_0 + \Delta c$ because of interactions. As a result, the plasma parameter Γ (3.4.2) is in principle different from the one used in the text. The corrected plasma constant is

$$\begin{aligned}\Gamma_c &= \Big(\frac{4\pi}{3}c\Big)^{\frac{1}{3}}\beta C_2\alpha_s(T) = \Big(\frac{4\pi}{3}(c_0+\triangle c)\Big)^{\frac{1}{3}}\beta C_2\alpha_s(T)\\ &= \Big(\frac{4\pi}{3}c_0\Big)^{\frac{1}{3}}(1+\frac{\triangle c}{c_0})^{\frac{1}{3}}\beta C_2\alpha_s(T)\\ &\simeq \Big(\frac{4\pi}{3}c_0\Big)^{\frac{1}{3}}\beta C_2\alpha_s(T) + \Big(\frac{4\pi}{3}c_0\Big)^{\frac{1}{3}}\frac{1}{3}\frac{\triangle c}{c_0}\beta C_2\alpha_s(T) + \mathcal{O}((\frac{\triangle c}{c_0})^2)\end{aligned} \tag{3.7.1}$$

From [16], the shift in the concentration reads

$$c = c_0 + \triangle c = c_0 + c_0^{\frac{3}{2}}\pi^{\frac{1}{2}}(N_c^2-1)(\beta C_2)^{\frac{3}{2}}\alpha_s^{\frac{3}{2}}(T) + \mathcal{O}(\beta^2) \tag{3.7.2}$$

The corrected plasma constant becomes

$$\begin{aligned}\Gamma_c &\simeq \Big(\frac{4\pi}{3}c_0\Big)^{\frac{1}{3}}\beta C_2\alpha_s(T) + \Big(\frac{4\pi}{3}c_0\Big)^{\frac{1}{3}}\frac{1}{3}c_0^{\frac{1}{2}}\pi^{\frac{1}{2}}(N_c^2-1)(\beta C_2)^{\frac{5}{2}}\alpha_s^{\frac{5}{2}}(T)\\ &= \Gamma + \frac{\sqrt{3}}{6}(N_c^2-1)\Gamma^{\frac{5}{2}}\\ &= \Big(0.244(N_c^2-1)\frac{4\pi}{3}\Big)^{\frac{1}{3}}C_2\alpha_s(T)\\ &+\frac{\sqrt{3}}{6}(N_c^2-1)\Big(0.244(N_c^2-1)\frac{4\pi}{3}\Big)^{\frac{1}{3}\cdot\frac{5}{2}}C_2^{\frac{5}{2}}\alpha_s^{\frac{5}{2}}(T)\end{aligned} \tag{3.7.3}$$

Inserting (3.7.3) in the excess energy density yields

$$\begin{aligned}\frac{U_{loop,ex}(\Gamma)}{\epsilon_{SB}} &= -\frac{\sqrt{3}}{2}(N_c^2-1)\Gamma_c^{\frac{3}{2}} + \frac{3}{2}\delta(N_c^2-1)\Gamma_c^2 - \frac{15}{2}\sqrt{3}\delta^2(N_c^2-1)\Gamma_c^{\frac{5}{2}} + \mathcal{O}(\Gamma_c^3)\\ &\simeq -\frac{\sqrt{3}}{2}(N_c^2-1)\Gamma^{\frac{3}{2}} + \frac{3}{2}\delta(N_c^2-1)\Gamma^2 - \frac{15}{2}\sqrt{3}\delta^2(N_c^2-1)\Gamma^{\frac{5}{2}} + \mathcal{O}(\Gamma^3)\end{aligned} \tag{3.7.4}$$

which shows that to order $\Gamma^{\frac{5}{2}}$ the replacement $\Gamma_c = \Gamma$ is allowed.

3.7.2 Debye-Hückel plus hole (DHH) theory

At strong coupling the Debye-Hückel (DH) theory, which is essentially a classical screening theory, fails. The Debye-Hückel plus Hole (DHH) theory is a way to address DH shortcomings at strong coupling by building a hole around each charge to account for the non-penetrability or core in classical liquids [19] at higher density or larger Γ. As a result, in the DHH theory of the cQGP a color charge density around a test charge is

$$\rho^{\alpha}(r) = \begin{cases} -c\frac{g}{\sqrt{4\pi}}Q^{\alpha} & (r < \sigma) \\ -c\frac{g}{\sqrt{4\pi}}Q^{\alpha}\frac{\sigma}{r}e^{(-\kappa_D(r-\sigma))} & (r \geq \sigma) \end{cases}$$

σ is the size of the hole, α is a classical color index $(1, .., N_c^2 - 1)$, $\beta = 1/T$ and κ_D is the Debye momentum

$$\kappa_D^2 = \frac{g^2}{N_c^2 - 1} c\beta \sum_{\alpha}^{N_c^2-1} Q^{\alpha 2} \ . \tag{3.7.5}$$

The negative sign in (3.7.5) reflects on the screening, with the Debye cloud left unchanged outside σ. The hole size σ is fixed by demanding that each test particle is completely screened through

$$\int_0^{\infty} dr 4\pi r^2 \rho^{\alpha}(r) = -\frac{g}{\sqrt{4\pi}}Q^{\alpha} \tag{3.7.6}$$

This condition, fixes the size of the hole

$$\sigma = \frac{1}{\kappa_D}\Big((1 + \frac{3\kappa_D^3}{4\pi c})^{\frac{1}{3}} - 1\Big) \tag{3.7.7}$$

In terms of

$$\Gamma = \frac{g^2}{4\pi}\frac{C_2}{T a_{WS}} \tag{3.7.8}$$

the hole radius is

$$\sigma = \frac{1}{\kappa_D}\Big((1+(3\Gamma)^{\frac{3}{2}})^{\frac{1}{3}} - 1\Big) \tag{3.7.9}$$

after fixing the Wigner-Seitz radius a_{WS} through $c_0(4\pi a_{WS}^3/3) = 1$. Again we have set $c = c_0$. From (3.7.9) it follows that the hole size is smaller the higher the density or temperature.

3.7.3 Role of the core δ

The fits in Fig . 3.2 depend on the value of the dimensionless core parameter $\delta = \sigma/a_{WS}$. In the DHH model detailed in the previous Appendix 3.7.2, this parameter is tied to Γ. As a result, the excess free energy density reads

$$\begin{aligned} u_\delta(\Gamma) &= -\frac{3}{2}\sqrt{3}\Gamma^{\frac{3}{2}} + \frac{9}{2}\delta\Gamma^2 - \frac{45}{2}\sqrt{3}\delta^2\Gamma^{\frac{5}{2}} \\ &= -\frac{3}{2}\sqrt{3}\Gamma^{\frac{3}{2}} + \frac{3}{2}\sqrt{3}\Gamma^{\frac{3}{2}}\Big((1+(3\Gamma)^{\frac{3}{2}})^{\frac{1}{3}} - 1\Big) - \frac{9}{2}\sqrt{3}\Gamma^{\frac{3}{2}}\Big((1+(3\Gamma)^{\frac{3}{2}})^{\frac{1}{3}} - 1\Big)^2 \end{aligned} \tag{3.7.10}$$

after using (5.5.3) and (3.3.2).

In Fig. 3.7, we display $u_\delta(\Gamma)$ and $u_{mol}(\Gamma)$ from the molecular simulations. The curves for $\delta = 0.3, 0.4$ and 0.5 follow from the first relation in (3.7.10) which is set by the DHH core (3.7.9) in the range $0 < \Gamma < 0.5$. Thus our choice of the core parameter should be in the range $0.3 < \delta < 0.5$. In Table I

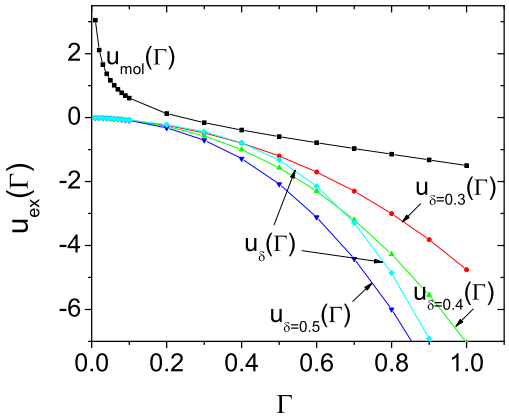

Figure 3.7: Excess energy density with varying core sizes δ

Table 3.1: $a\Gamma^b$ for different cores δ

δ	δ	0.3	0.4	0.5
$a(\times 10^3)$	4.4	1.8	2.0	3.4
b	7.7	6.6	6.3	6.4

we show four best fit interpolations using $f(\Gamma) = a\Gamma^b$ for different cores δ. All fits are subject to the same requirement that the deviation is less than 0.1% for $\Gamma < 0.1$ and $\Gamma > 1$. In the text we have used $\delta = 0.4$.

Chapter 4

Structure factor

4.1 Introduction

High temperature QCD is expected to asymptote a weakly coupled Coulomb plasma albeit with still strong infrared divergences. The latters cause its magnetic sector to be non-perturbative at all temperatures. At intermediate temperatures of relevance to heavy-ion collider experiments, the electric sector is believed to be strongly coupled.

Recently, Shuryak and Zahed [23] have suggested that certain aspects of the quark-gluon plasma in range of temperatures $(1-3)\,T_c$ can be understood by a stronger Coulomb interaction causing persistent correlations in singlet and colored channels. As a result the quark and gluon plasma is more a liquid than a gas at intermediate temperatures. A liquid plasma should exhibit shorter mean-free paths and stronger color dissipation, both of which are supported by the current experiments at RHIC [24].

To help understand transport and dissipation in the strongly coupled quark gluon plasma, a classical model of the colored plasma was suggested in [3]. The

model consists of massive quarks and gluons interacting via classical colored Coulomb interactions. The color is assumed classical with all equations of motion following from Poisson brackets. For the SU(2) version both molecular dynamics simulations [3] and bulk thermodynamics were recently presented [11] including simulations of the energy loss of heavy quarks [25].

In this chapter we follow up on our recent equilibrium analysis of the bulk thermodynamics [11] to the static structure factors. In section 4.2 we define the energy functional for the cQGP. In section 4.3 we derive generalized Ornstein-Zernicke equations for the pair correlation functions. In section 4.4 we show that the cQGP supports multiple structure factors that measure a variety of colored correlations. Each structure factor obeys a generalized Ornstein-Zernicke equation. In section 4.5 we introduce the Debye-Huckel-hole potential for the cQGP. In section 4.6, we use Debye charging process to derive analytical expressions for the lowest two structure factors in the cQGP for arbitrary Γ. In section 4.7, we construct numerically the lowest two structure factors using molecular dynamics simulations and compare them with our analytical results for values of Γ in the liquid phase. Our conclusions are in section 4.8. Appendix 4.9 is added to streamline our conventions for the SU(2) color charges.

4.2 Free Energy Functional

We consider the canonical partition function of a single species, either quarks and gluons, at finite temperature $1/\beta = T$ and in the presence of an external scalar source ψ

$$\mathcal{Z}_N[\psi] = \frac{1}{N!}\int \prod_i \frac{d\boldsymbol{r}_i dQ_i}{\lambda^3} \exp\Big(\beta \int d\boldsymbol{r} dQ n(\boldsymbol{r},\boldsymbol{Q})\psi(\boldsymbol{r},\boldsymbol{Q})\Big)$$
$$\times \exp\Big(-\frac{\beta}{2}\frac{g^2}{4\pi}\int d\boldsymbol{r}d\boldsymbol{r}' dQ dQ' n(\boldsymbol{r},\boldsymbol{Q})\frac{\boldsymbol{Q}\cdot\boldsymbol{Q}'}{|\boldsymbol{r}-\boldsymbol{r}'|}n(\boldsymbol{r}',\boldsymbol{Q}')\Big) \quad (4.2.1)$$

The color charges are treated classically and we refer to [4, 12, 16] for further details regarding the nature of the measure. Here, we have defined

$$n(\boldsymbol{r},\boldsymbol{Q}) = \sum_i^N \delta(\boldsymbol{r}-\boldsymbol{r}_i)\delta(\boldsymbol{Q}-\boldsymbol{Q}_i) \quad (4.2.2)$$

The generalization to many species is straightforward. The associated Coulomb parameter is

$$\Gamma = \frac{g^2}{4\pi}\frac{\beta\, C_2}{a_{WS}} \quad (4.2.3)$$

where C_2 is the quadratic Casimir ($= \sum_i Q_i^2/(N_c^2-1)$) and a_{WS} is the Wigner-Seitz radius $4\pi a_{WS}^3/3 = 1/n$. For small Γ, Eq. (4.2.1) behaves as a screened but weakly coupled gas, while for intermediate values of Γ, Eq. (4.2.1) describes a liquid [3, 8]. At large values of Γ Eq. (4.2.1) yields a solid as a ground state. From now on, the canonical charge of $g^2/4\pi$ will be set to 1 for simplicity, and will be restored in the final parameters by inspection.

The static correlations both in space and in phase space associated with Eq. (4.2.1) are involved and will be the subject of most of this paper. For that, we note that Eq. (4.2.1) yields the free energy generating functional

$$\begin{aligned}\mathcal{F}_N[\psi] \quad &= \frac{1}{\beta}\int d\boldsymbol{r}dQn^{(1)}(\boldsymbol{r},\boldsymbol{Q})\Big(\ln\left(\lambda^3 n^{(1)}(\boldsymbol{r},\boldsymbol{Q})\right)-1\Big)\\ &-\int d\boldsymbol{r}\psi(\boldsymbol{r},\boldsymbol{Q})n^{(1)}(\boldsymbol{r},\boldsymbol{Q})+\mathcal{F}_c(n^{(1)}(\boldsymbol{r},\boldsymbol{Q}))\\ &+\frac{1}{2}\int d\boldsymbol{r}\boldsymbol{r}'dQdQ'n^{(1)}(\boldsymbol{r},\boldsymbol{Q})\frac{\boldsymbol{Q}\cdot\boldsymbol{Q}'}{|\boldsymbol{r}-\boldsymbol{r}'|}n^{(1)}(\boldsymbol{r}',\boldsymbol{Q}') \qquad (4.2.4)\end{aligned}$$

Here we have set

$$n^{(1)}(\boldsymbol{r},\boldsymbol{Q})=\langle n(\boldsymbol{r},\boldsymbol{Q})\rangle=\langle\sum_i^N\delta(\boldsymbol{r}-\boldsymbol{r}_i)\delta(\boldsymbol{Q}-\boldsymbol{Q}_i)\rangle \qquad (4.2.5)$$

as the expectation value with the averaging carried using Eq. (4.2.1). The second contribution in Eq. (4.2.4) is the ideal classical contribution following from the measure in Eq. (4.2.1) using the asymptotic Stirling formulae. The third contribution is the excess free energy functional. $\mathcal{F}_c$ is the connected free energy that sums up the second and higher cumulants of $n(\boldsymbol{r},\boldsymbol{Q})$ from Eq. (4.2.1). We note that for zero scalar source $\psi=0$,

$$\mathcal{F}_N[0]=\mathcal{F}_{id}+\mathcal{F}_{ex} \qquad (4.2.6)$$

where the first contribution is the classical ideal part and the second contribution the excess part.

4.3 Ornstein-Zernicke Equations

To quantify the static interactions between pairs of particles in (4.2.1) we define

$$
\begin{aligned}
-\frac{1}{\beta}\frac{\delta^2\mathcal{F}_N}{\delta\psi\delta\psi} &= \Big\langle \sum_{i,j} \delta(\boldsymbol{r}-\boldsymbol{r}_i)\delta(\boldsymbol{r}'-\boldsymbol{r}_j)\delta(\boldsymbol{Q}-\boldsymbol{Q}_i)\delta(\boldsymbol{Q}'-\boldsymbol{Q}_j)\Big\rangle \\
&= \Big(n^{(1)}(\boldsymbol{r},\boldsymbol{Q})n^{(1)}(\boldsymbol{r}',\boldsymbol{Q}')\mathbf{h}(\boldsymbol{r}-\boldsymbol{r}',\boldsymbol{Q}\cdot\boldsymbol{Q}') \\
&\quad +n^{(1)}(\boldsymbol{r},\boldsymbol{Q})\delta(\boldsymbol{r}-\boldsymbol{r}')\delta(\boldsymbol{Q}-\boldsymbol{Q}')\Big)
\end{aligned} \tag{4.3.1}
$$

with $\mathbf{h}$ the pair correlation function for $\psi = 0$. The pair correlation function is invariant under space translation and color rotation. Generically

$$
\mathbf{h}(\boldsymbol{r}-\boldsymbol{r}',\boldsymbol{Q}\cdot\boldsymbol{Q}') = \frac{1}{n^2}\Big\langle \sum_{i\neq j} \delta(\boldsymbol{r}-\boldsymbol{r}_i)\delta(\boldsymbol{r}'-\boldsymbol{r}_j)\delta(\boldsymbol{Q}-\boldsymbol{Q}_i)\delta(\boldsymbol{Q}'-\boldsymbol{Q}_j)\Big\rangle \tag{4.3.2}
$$

The direct correlation function $\mathbf{c}_D$ follows from the excess free energy (4.2.6) through

$$
-\frac{1}{\beta}\mathbf{c}_D(\boldsymbol{r}-\boldsymbol{r}',\boldsymbol{Q}\cdot\boldsymbol{Q}') = \frac{\delta^2\mathcal{F}^{ex}}{\delta n^{(1)}\delta n^{(1)}} = \left(\frac{\boldsymbol{Q}\cdot\boldsymbol{Q}'}{|\boldsymbol{r}-\boldsymbol{r}'|} + \frac{\delta^2\mathcal{F}_c}{\delta n^{(1)}\delta n^{(1)}}\right) \tag{4.3.3}
$$

which plays the role of a correlated potential. $\mathbf{c}_D$ will be used below as a renormalized Coulomb potential in the liquid phase. It also obeys the identity

$$
\frac{\delta^2\mathcal{F}_N}{\delta n^{(1)}\delta n^{(1)}} = -\frac{\delta\psi}{\delta n^{(1)}} = \frac{1}{\beta}\left(\frac{1}{n}\delta(\boldsymbol{r}-\boldsymbol{r}')\delta(\boldsymbol{Q}-\boldsymbol{Q}') - \mathbf{c}_D(\boldsymbol{r}-\boldsymbol{r}',\boldsymbol{Q}\cdot\boldsymbol{Q}')\right) \tag{4.3.4}
$$

Using the chain rule,

$$\int d\boldsymbol{r}''dQ'' \frac{\delta\psi(\boldsymbol{r},\boldsymbol{Q})}{\delta n^{(1)}(\boldsymbol{r}'',\boldsymbol{Q}'')}\frac{\delta n^{(1)}(\boldsymbol{r}'',\boldsymbol{Q}'')}{\delta\psi(\boldsymbol{r}',\boldsymbol{Q}')} = \delta(\boldsymbol{r}-\boldsymbol{r}')\delta(\boldsymbol{Q}-\boldsymbol{Q}') \tag{4.3.5}$$

we obtain

$$\mathbf{h}(\boldsymbol{r}-\boldsymbol{r}',\boldsymbol{Q}\cdot\boldsymbol{Q}') = \mathbf{c}_D(\boldsymbol{r}-\boldsymbol{r}',\boldsymbol{Q}\cdot\boldsymbol{Q}')+n\int d\boldsymbol{r}''dQ''\mathbf{h}(\boldsymbol{r}-\boldsymbol{r}'',\boldsymbol{Q}\cdot\boldsymbol{Q}'')\mathbf{c}_D(\boldsymbol{r}''-\boldsymbol{r}',\boldsymbol{Q}'\cdot\boldsymbol{Q}'') \tag{4.3.6}$$

which is the Orstein-Zernicke equation that ties the pair correlation $\mathbf{h}$ to the direct correlation or the pair potential $\mathbf{c}_D$. For a uniform plasma (4.3.6) unfolds agebraically in momentum and color space using

$$\begin{aligned}\mathbf{h}(\boldsymbol{r}-\boldsymbol{r}',\boldsymbol{Q}\cdot\boldsymbol{Q}') &= \int d\boldsymbol{k}e^{i\boldsymbol{k}\cdot(\boldsymbol{r}-\boldsymbol{r}')}\sum_l \frac{2l+1}{4\pi}\mathbf{h}_l(\boldsymbol{k})P_l(\boldsymbol{Q}\cdot\boldsymbol{Q}') \\ \mathbf{c}_D(\boldsymbol{r}-\boldsymbol{r}',\boldsymbol{Q}\cdot\boldsymbol{Q}') &= \int d\boldsymbol{k}e^{i\boldsymbol{k}\cdot(\boldsymbol{r}-\boldsymbol{r}')}\sum_l \frac{2l+1}{4\pi}\mathbf{c}_{Dl}(\boldsymbol{k})P_l(\boldsymbol{Q}\cdot\boldsymbol{Q}')\end{aligned} \tag{4.3.7}$$

Thus

$$\mathbf{h}_l(\boldsymbol{k}) = \mathbf{c}_{Dl}(\boldsymbol{k}) + n\mathbf{h}_l(\boldsymbol{k})\,\mathbf{c}_{Dl}(\boldsymbol{k}) \tag{4.3.8}$$

which holds for each partial waves. (4.3.8) are the generalized Orstein-Zernicke equations for each color partial wave of the SU(2) colored Coulomb plasma.

4.4 Static Structure Factors

The statistical aspects of the colored charged particles are best captured by correlations in the phase space distributions. The static structure factor is defined as

$$\mathbf{S}_0(\boldsymbol{r}-\boldsymbol{r}',\boldsymbol{p}\boldsymbol{p}',\boldsymbol{Q}\cdot\boldsymbol{Q}') = \langle \delta f(\boldsymbol{r}\boldsymbol{p}\boldsymbol{Q})\delta f(\boldsymbol{r}'\boldsymbol{p}'\boldsymbol{Q}')\rangle \tag{4.4.1}$$

with formally

$$f(\boldsymbol{r}\boldsymbol{p}\boldsymbol{Q}) = \sum_i \delta(\boldsymbol{r}-\boldsymbol{x}_i)\delta(\boldsymbol{p}-\boldsymbol{p}_i)\delta(\boldsymbol{Q}-\boldsymbol{Q}_i) \tag{4.4.2}$$

and $\delta f = f - \langle f\rangle$. The averaging in (4.4.1) is carried using the canonical partition function (4.2.1). Color and translational invariance imply

$$\langle f(\boldsymbol{r}\boldsymbol{p}\boldsymbol{Q})\rangle = n f_0(\boldsymbol{p}) = n\Big(\frac{\beta}{2\pi m}\Big)^{3/2} e^{-\beta \boldsymbol{p}^2/2m} \tag{4.4.3}$$

which is the Maxwellian distribution for massive constituent quarks or gluons. It is readily shown that

$$\begin{aligned}\mathbf{S}_0(\boldsymbol{r}-\boldsymbol{r}',\boldsymbol{p}\boldsymbol{p}',\boldsymbol{Q}\cdot\boldsymbol{Q}') &= n f_0(\boldsymbol{p})\delta(\boldsymbol{r}-\boldsymbol{r}')\delta(\boldsymbol{p}-\boldsymbol{p}')\delta(\boldsymbol{Q}-\boldsymbol{Q}')\\ &+n^2 f_0(\boldsymbol{p}) f_0(\boldsymbol{p}')\mathbf{h}(\boldsymbol{r}-\boldsymbol{r}',\boldsymbol{Q}\cdot\boldsymbol{Q}')\end{aligned} \tag{4.4.4}$$

The reduced static structure factor

$$\mathbf{S}_0(\boldsymbol{k},\boldsymbol{Q}\cdot\boldsymbol{Q}') = \frac{1}{n}\int d\boldsymbol{p}d\boldsymbol{p}' \int d\boldsymbol{k} e^{i\boldsymbol{k}\cdot(\boldsymbol{r}-\boldsymbol{r}')}\mathbf{S}_0(\boldsymbol{r}-\boldsymbol{r}',\boldsymbol{p}\boldsymbol{p}',\boldsymbol{Q}\cdot\boldsymbol{Q}') \tag{4.4.5}$$

ties with the pair correlation function (4.3.2) through

$$\mathbf{S}_0(\boldsymbol{k}, \boldsymbol{Q}\cdot\boldsymbol{Q}') = \delta(\boldsymbol{Q}-\boldsymbol{Q}') + n\mathbf{h}(\boldsymbol{k}, \boldsymbol{Q}\cdot\boldsymbol{Q}') \tag{4.4.6}$$

Its Legendre transform in the color charge reads

$$\mathbf{S}_{0l}(\boldsymbol{k}) = 1 + n\mathbf{h}_l(\boldsymbol{k}) \tag{4.4.7}$$

So the knowledge of the partial-wave structure factor $S_l(k)$ yields the pair correlation $\mathbf{c}_{Dl}$ through (4.3.7) and (4.4.7)

$$1 = \mathbf{S}_{0l}(\boldsymbol{k})^{-1} + n\mathbf{c}_{Dl}(\boldsymbol{k}) \tag{4.4.8}$$

We note that in configuration space the lth partial wave of the static structure factor is

$$\mathbf{S}_{0l}(\boldsymbol{r}-\boldsymbol{r}') = \frac{1}{n}\int d\boldsymbol{p}\, d\boldsymbol{p}' \int dQ\, P_l(\boldsymbol{Q}\cdot\boldsymbol{Q}')\, \mathbf{S}_0(\boldsymbol{r}-\boldsymbol{r}', \boldsymbol{p}\boldsymbol{p}', \boldsymbol{Q}\cdot\boldsymbol{Q}') \tag{4.4.9}$$

Using (4.3.2) and (4.4.4) and enforcing space translational and color rotational invariance in the averaging process yields

$$\mathbf{S}_{0l}(\boldsymbol{r}) = \delta(\boldsymbol{r}) + \frac{1}{N}\Big\langle \sum_{i\neq j} \delta(\boldsymbol{r}-\boldsymbol{r}_{ij})\, P_l(\boldsymbol{Q}_i\cdot\boldsymbol{Q}_j)\Big\rangle \tag{4.4.10}$$

In particular, the two lowest static structure factors are the density structure factor

$$\mathbf{S}_{00}(\boldsymbol{r}) = \delta(\boldsymbol{r}) + \frac{1}{N}\Big\langle \sum_{i\neq j} \delta(\boldsymbol{r} - \boldsymbol{r}_{ij})\Big\rangle = \delta(\boldsymbol{r}) + n\mathbf{h}_0(\boldsymbol{r}) \tag{4.4.11}$$

and the charge structure factor

$$\mathbf{S}_{01}(\boldsymbol{r}) = \delta(\boldsymbol{r}) + \frac{1}{N}\Big\langle \sum_{i\neq j} \delta(\boldsymbol{r} - \boldsymbol{r}_{ij})\, \boldsymbol{Q}_i \cdot \boldsymbol{Q}_j\Big\rangle \tag{4.4.12}$$

Higher structure factors are given by (4.4.10) as they measure the various color correlation content of the SU(2) strongly coupled QGP. Below, we propose both an analytical and numerical derivation of the two lowest structure factors (4.4.11) and (4.4.12).

4.5 Debye-Huckel-Hole Potential

To derive the static structure factors we will use the Debye charging procedure for a fixed color charge. For that, we need the Poisson-Boltzman equation for the 1-species SU(2) colored plasma in the presence of a colored test charge $\boldsymbol{q}$ [3]

$$\nabla^2\boldsymbol{\phi}(\boldsymbol{r},\boldsymbol{r}',\boldsymbol{q}) = -4\pi\left(\boldsymbol{q}\delta(\boldsymbol{r}-\boldsymbol{r}') + \int dQ'\boldsymbol{Q}' n(\boldsymbol{r},\boldsymbol{q}) e^{-\beta\boldsymbol{Q}'\cdot(\boldsymbol{\phi}(\boldsymbol{r},\boldsymbol{r}',\boldsymbol{q})-\boldsymbol{\Phi}(\boldsymbol{r},\boldsymbol{q}))}\right) \tag{4.5.1}$$

with the *fixed* external density profile

$$n(\boldsymbol{r},\boldsymbol{q}) = n + n(\triangle_0 + \boldsymbol{\Delta}_1\cdot\boldsymbol{q})\cos(\boldsymbol{k}\cdot\boldsymbol{r}) \tag{4.5.2}$$

We note that (4.5.2) is a scalar under rigid and orthogonal color rotations $\mathbf{R}Q$ if the external parameters Δ_l transform unitarily as $D(\mathbf{R})\Delta$ with $D(\mathbf{R})$ the Wigner rotation in the adjoint representation. This fixed density causes an imposed potential

$$\nabla^2\mathbf{\Phi}(\boldsymbol{r},\boldsymbol{q}) = -4\pi\,\boldsymbol{q}\,(n(\boldsymbol{r},\boldsymbol{q}) - n) \tag{4.5.3}$$

which is used to normalize the Poisson-Boltzman equation in (4.5.1). We solve (4.5.1) in the linear approximation. For that we define the shifted potential $\delta\boldsymbol{\phi} = \boldsymbol{\phi} - \mathbf{\Phi}$,

$$\Big(\nabla^2 - \kappa_D^2 n(\boldsymbol{r},\boldsymbol{q})/n\Big)\delta\boldsymbol{\phi}(\boldsymbol{r},\boldsymbol{r}',\boldsymbol{q}) \approx -4\pi\boldsymbol{q}\Big(\delta(\boldsymbol{r}-\boldsymbol{r}') - (n(\boldsymbol{r},\boldsymbol{q}) - n)\Big) \tag{4.5.4}$$

with $\kappa_D^2 \equiv 4\pi\beta n C_2$ the squared Debye constant. (4.5.4) is the linearized Poisson-Boltzman or Debye-Huckel equation for the classical colored plasma. At short separations (4.5.4) is known to misrepresent the hole caused by the strong Coulomb correlations. To fix that we use the Debye-Huckel plus hole approximation[19]

$$\Big(\nabla^2 - \kappa_D^2 n(\boldsymbol{r},\boldsymbol{q})/n\Theta\Big)\delta\boldsymbol{\phi}(\boldsymbol{r},\boldsymbol{r}',\boldsymbol{q}) \approx -4\pi\boldsymbol{q}\Big(\delta(\boldsymbol{r}-\boldsymbol{r}') - (n(\boldsymbol{r},\boldsymbol{q}) - n)\Big)(1-\Theta) \tag{4.5.5}$$

with $\Theta = \theta(|\boldsymbol{r}-\boldsymbol{r}'| - \sigma)$ the spherical hole insertion of radius σ. The mean-induced potential is

$$\mathbf{\Psi}(\boldsymbol{r},\boldsymbol{q}) = \lim_{\boldsymbol{r}\to\boldsymbol{r}'}\left(\delta\boldsymbol{\phi}(\boldsymbol{r},\boldsymbol{r}',\boldsymbol{q}) - \frac{\boldsymbol{q}}{|\boldsymbol{r}-\boldsymbol{r}'|}\right) \tag{4.5.6}$$

4.6 Debye Charging Process

To assess the static structure factors for the classical and strongly coupled colored plasma, we note that the excess free energy (4.2.6) can be readily rewritten in terms of the pair correlations

$$-\beta\mathcal{F}^{ex} = \frac{1}{2}\int d\boldsymbol{r}d\boldsymbol{r}'dQdQ'n^{(1)}(\boldsymbol{r},\boldsymbol{Q})c_D(\boldsymbol{r}-\boldsymbol{r}',\boldsymbol{Q}\cdot\boldsymbol{Q}')n^{(1)}(\boldsymbol{r}',\boldsymbol{Q}') \quad (4.6.1)$$

In Fourier (space) and Legendre (color) space (4.6.1) reads

$$-\beta\mathcal{F}^{ex} = \frac{1}{2}\int d\boldsymbol{k}\,dQ\,dQ'\sum_{l,m} n^{(1)}_{lm}(\boldsymbol{k},\boldsymbol{Q})\,\mathbf{c}_{Dl}(\boldsymbol{k})\,n^{(1)}_{lm}(-\boldsymbol{k},\boldsymbol{Q}') \quad (4.6.2)$$

with

$$n^{(1)}_{lm}(\boldsymbol{k},\boldsymbol{Q}) = \int d\boldsymbol{r}e^{-i\boldsymbol{k}\cdot\boldsymbol{r}}Y^m_l(\boldsymbol{Q})n^{(1)}(\boldsymbol{r},\boldsymbol{Q}) \quad (4.6.3)$$

and Y^m_l a spherical harmonic for an SU(2) colored plasma. Using the partial wave form of the Orstein-Zernicke equations (4.4.8), (4.6.2) becomes

$$-\beta\mathcal{F}^{ex} = \frac{1}{2n}\int d\boldsymbol{k}\,dQ\,dQ'\sum_{l,m} n^{(1)}_{lm}(\boldsymbol{k},\boldsymbol{Q})\Big(1-\mathbf{S}^{-1}_{0l}(\boldsymbol{k})\Big)n^{(1)}_{lm}(-\boldsymbol{k},\boldsymbol{Q}') \quad (4.6.4)$$

This shows that the quadratic change in the excess free energy caused by an external density profile $n_{lm}(k)$ is directly proportional to the lth partial wave of the inverse of the static structure factor.

The external density profile (4.5.2) changes the color Coulomb potential

locally through (4.5.4), thereby affecting the free energy. To assess the change in the latter we use the Debye charging procedure [26]. For that, we note that by dialing (4.5.2) the free energy shifts. The shift can be decomposed into three parts,

$$\mathcal{F} = \mathcal{F}_{\text{ideal}} + \mathcal{F}_{\text{imposed}} + \mathcal{F}_{\text{induced}} \tag{4.6.5}$$

The shift in the ideal part is set by the first term in (4.2.4) after inserting (4.5.2). The imposed contribution is

$$\mathcal{F}_{\text{imposed}} = \int d\boldsymbol{r} dQ (n(\boldsymbol{r}, \boldsymbol{q}) - n)\boldsymbol{q} \cdot \int_0^1 d\lambda \boldsymbol{\Phi}(\boldsymbol{r}, \lambda \boldsymbol{q}) \tag{4.6.6}$$

and follows from the imposed charge. Specifically,

$$\mathcal{F}_{\text{imposed}} = \frac{n^2}{2} q^2 (3\Delta_0^2 + |\boldsymbol{\Delta}_1|^2) \int d\boldsymbol{r} d\boldsymbol{r}' \frac{\cos(\boldsymbol{k} \cdot \boldsymbol{r}) \cos(\boldsymbol{k} \cdot \boldsymbol{r}')}{|\boldsymbol{r} - \boldsymbol{r}'|} \tag{4.6.7}$$

The induced free energy is

$$\mathcal{F}_{\text{induced}} = \int d\boldsymbol{r} dQ n(\boldsymbol{r}, \boldsymbol{q}) \boldsymbol{q} \cdot \int_0^1 d\lambda \boldsymbol{\Psi}(\boldsymbol{r}, \lambda \boldsymbol{q}) \tag{4.6.8}$$

and follows from the induced but shifted screening potential (4.5.6).

The integrand can be obtained by solving (4.5.5) for $\delta\boldsymbol{\phi}(\boldsymbol{r}, \boldsymbol{r}', \boldsymbol{q})$ with the help of the Green function,

$$\left[\nabla^2 - \kappa_D^2 \Theta(|\boldsymbol{r} - \boldsymbol{r}'| - \sigma)\right] G(\boldsymbol{r}'', \boldsymbol{r} - \boldsymbol{r}') = -4\pi\delta^3(\boldsymbol{r}'' - (\boldsymbol{r} - \boldsymbol{r}')) \tag{4.6.9}$$

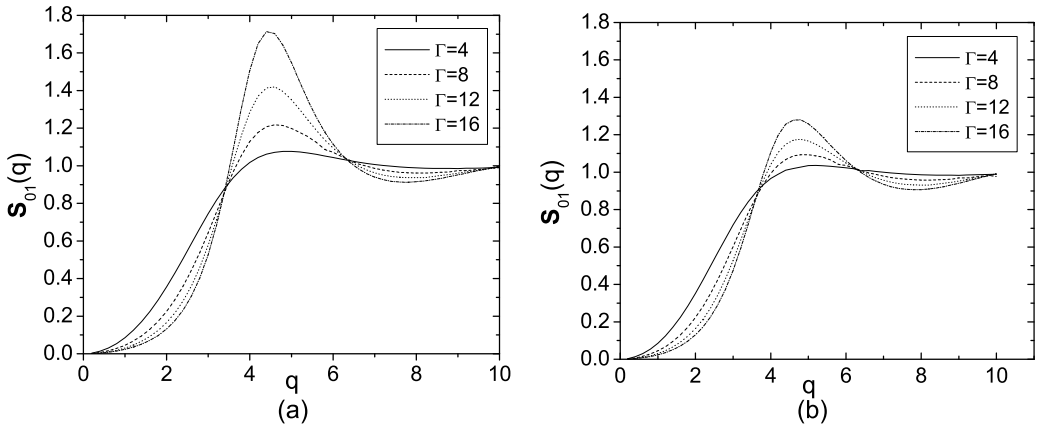

Figure 4.1: $\mathbf{S}_{01}(q)$ for $\Gamma = 4, 8, 12, 16$ summed up to $l = 1$ (a) and $l = 2$ (b). See text.

The method has been developed in [27–29] for the one-component plasma and readily extends to our colored plasma. For that we evaluate the reduced free energy $f = \beta\mathcal{F}/V$ to quadratic order in Δ^2. By comparing the terms with (4.6.4), we can extract S_{00}^{-1} as the coefficient of Δ_0^2 and S_{01}^{-1} as the coefficient of $\mathbf{\Delta}_1^2$. We find that both static structure factors are finite and identical in this approximation,

$$
\begin{aligned}
\mathbf{S}_{00}^{-1}(\boldsymbol{k}) = \mathbf{S}_{01}^{-1}(\boldsymbol{k}) &= 1 + 2(\frac{\kappa_D}{k})^2 \int_0^1 d\lambda \frac{\lambda}{w_\lambda} \cos\left(\frac{1}{\lambda}\frac{k}{\kappa_D}(w_\lambda - 1)\right) \\
&+ 2(\frac{\kappa_D}{k})^3 \int_0^1 d\lambda \frac{\lambda^2}{w_\lambda} \sin\left(\frac{1}{\lambda}\frac{k}{\kappa_D}(w_\lambda - 1)\right) \\
&- 2\int_0^1 \frac{d\lambda}{\lambda}\frac{w_\lambda - 1}{w_\lambda} \mathcal{I}_0^+(w_\lambda - 1, \frac{1}{\lambda}\frac{k}{\kappa_D}) \\
&+ \sum_{l=0}^{\infty}(2l+1)\Bigg(2\frac{\kappa_D}{k}\int_0^1 d\lambda \frac{(w_\lambda - 1)^{l+2}}{w_\lambda g_{l+1}(w_\lambda - 1)} \\
&\times j_{l+1}(\frac{1}{\lambda}\frac{\kappa_D}{k}(w_\lambda - 1))\mathcal{I}_l^+(w_\lambda - 1, \frac{1}{\lambda}\frac{k}{\kappa_D}) \\
&+ (-1)^{l+1}\int_0^1 \frac{d\lambda}{\lambda}\frac{w_\lambda - 1}{w_\lambda}\Big(\frac{g_{l+1}(-w_\lambda + 1)}{g_{l+1}(w_\lambda - 1)}(\mathcal{I}_l^+(w_\lambda - 1, \frac{1}{\lambda}\frac{k}{\kappa_D}))^2 \\
&+ 2\mathcal{I}_l^+(w_\lambda - 1, \frac{1}{\lambda}\frac{k}{\kappa_D})\mathcal{I}_l^-(w_\lambda - 1, \frac{1}{\lambda}\frac{k}{\kappa_D}) - 2\mathcal{I}_l^0(w_\lambda - 1, \frac{1}{\lambda}\frac{k}{\kappa_D})\Big)\Bigg)
\end{aligned}
\tag{4.6.10}
$$

The three integral contributions are

$$
\begin{aligned}
\mathcal{I}_l^-(z, y) &= \int_0^z dw w^{-l} g_l(-w) j_l(yw) \\
\mathcal{I}_l^0(x, y) &= \int_x^\infty dz z^{-l} g_l(z) j_l(yz) \mathcal{I}_l^-(z, y) e^{(2(x-z))} \\
\mathcal{I}_l^+(x, y) &= \int_x^\infty dz z^{-l} g_l(z) j_l(yz) e^{(2(x-z))}
\end{aligned}
\tag{4.6.11}
$$

with $g_l(z) = e^z z^{l+1} k_l(z)$. Here $j_l(yz)$ is a spherical Bessel function, and $k_l(z)$ a modified spherical Bessel function. The parameter w_λ is defined as

$$
w_\lambda = \left(1 + \lambda^3 (3\Gamma)^{\frac{3}{2}}\right)^{\frac{1}{3}} \tag{4.6.12}
$$

The static structure factors in (4.6.10) involve summations over multiple par-

tial waves. The sums are rapidly converging as we show in Fig. 1 with $l = 1$ retained (a) and $l = 2$ retained (b). Here $q = ka_{WS}$ is a dimensionless wave-vector. To assess the accuracy of the analytical method developed above for the static correlation functions in the colored Coulomb plasma, we now carry numerical simulations for the same structure factors using molecular dynamics simulations.

4.7 Structure Factors from Molecular Dynamics

For an SU(2) plasma, the details of the molecular dynamics simulations can be found in [3]. Color motion is treated as a point coordinate on a 3-sphere with a fixed radius that is equal to the quadratic Casimir for SU(2). Classical stability of the colored Coulomb gas at short distances is achieved by using a scalar core potential of the type

$$V_{core} = \frac{1}{n} \frac{1}{|\boldsymbol{r}_i - \boldsymbol{r}_j|^n} \tag{4.7. 1}$$

with $n = 9$. The two-body interparticle colored potential is [3, 30],

$$V(r, \boldsymbol{Q} \cdot \boldsymbol{Q}') = \frac{g^2}{\lambda} \Big[\frac{1}{9} \Big(\frac{\lambda}{r} \Big)^9 + \boldsymbol{Q} \cdot \boldsymbol{Q}' \Big(\frac{\lambda}{r} \Big) \Big] \tag{4.7. 2}$$

with λ setting the unit of length scale. At close packing the density is $n_{\rm cp} = 1/\lambda^3$. We choose the unit of length λ so that $n_{\rm cp} = 1$. The unit of time is set by the inverse plasma frequency $\tau = \omega_p^{-1}$. In these units, the strength of the colored Coulomb potential is $\frac{1}{4\pi} \frac{1}{n\lambda^3}$ [3].

We have adopted the Verlet algorithm in [1] to integrate the equations of

motion for a system composed of 108 particles. The particles are confined in a box and surrounded by images via periodic boundary conditions. The simulations are carried in a fixed volume $1/(n\lambda^3) = V/(N\lambda^3) = 2.72$ as in [30]. The Wigner-Seitz radius $a_{WS} = (4\pi n/3)^{-1/3}$ is 0.866λ. With these parameters, the interparticle interaction strength is set by the Coulomb constant Γ.

We first measure the particle radial distribution function $\mathbf{g}(r) = \mathbf{h}_0(r)$ as a function of Γ. $\mathbf{g}(r)$ measures the probability of finding two particles between r and $r + \Delta r$,

$$\mathbf{g}(r) \equiv \mathbf{h}_0(r) = \frac{1}{nN}\Big\langle \sum_{i\neq j}^{N} \delta(\boldsymbol{r} - \boldsymbol{r}_{ij})\Big\rangle \tag{4.7. 3}$$

In Fig. 4.2 we show $\mathbf{g}(r)$ versus r for different Coulomb couplings $\Gamma = 2.2, 6.6, 12.8$. The larger Γ the larger the size of the Coulomb hole surrounding each colored Coulomb particle. Also, the larger Γ, the higher the peak, the tighter the Coulomb packing.

The radial distribution function in Fig. 4.2 for the SU(2) colored Coulomb plasma appears overall similar to the one observed for the one component plasma (OCP). Although our colored particles attract for color antiparallell charges, they overall statistically repel due to the larger color repulsive orientations. The difference with the OCP is best seen by taking the Fourier transform of (4.7. 3) which is the $l = 0$ density structure factor $\mathbf{S}_{00}(q)$

$$\mathbf{S}_{00}(\boldsymbol{k}) = \frac{1}{N}\langle|\mathbf{n}_{\boldsymbol{k}}|^2\rangle \tag{4.7. 4}$$

with

$$\mathbf{n}_{\boldsymbol{k}} = \sum_{i=1}^{N} e^{i\boldsymbol{k}\cdot\boldsymbol{r}_i} \tag{4.7. 5}$$

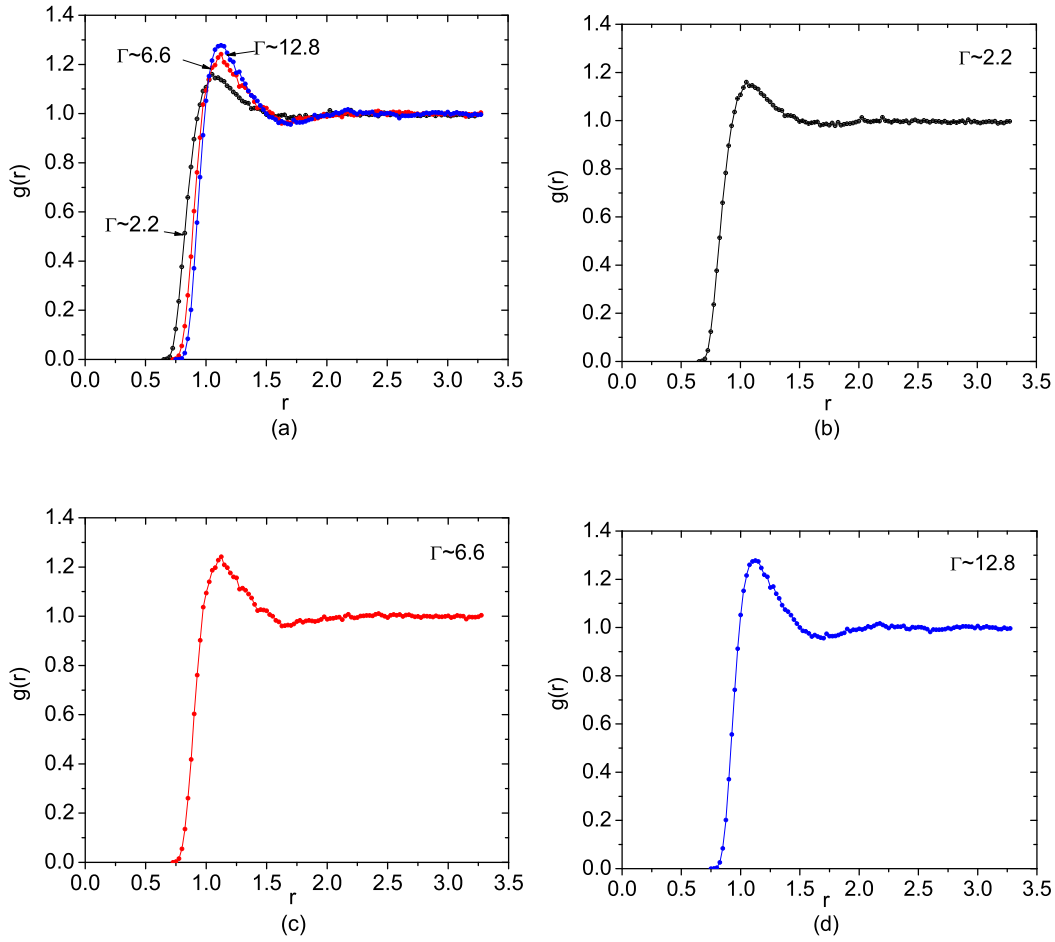

Figure 4.2: Radial distribution function for Γ =2.2(b) , 6.6(c) and 12.8(d). See text.

Fig. 4.3 shows the behavior of $\mathbf{S}_{00}(q)$ versus the dimensionless wave-vector $q = a_{WS}k$. The nonvanishing of $\mathbf{S}_{00}$ at the origin reflects on the coupling to the sound mode. In the static and long-wavelength approximation it is just

$$\mathbf{S}_{00}(\boldsymbol{k}) \approx \frac{\boldsymbol{k}^2}{c_S^2 \boldsymbol{k}^2} = \frac{1}{c_S^2} \tag{4.7. 6}$$

with $c_S^2 = (\partial P/\partial\rho)_T$ the isothermal squared speed of sound, with P the pressure and ρ the mass density. Since k is a multiple of $2\pi/L$ because of the finite cubic box $L \times L \times L$, only about a dozen points were accessible numerically.

Since $L \approx N^{1/3}$, we need to increase the number of particles in the box to smoothen out the structure factor in momentum space.

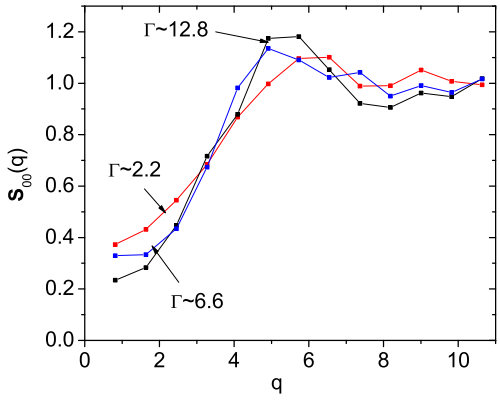

Figure 4.3: Static Structure factor $\mathbf{S}_{00}(q)$ versus q for $\Gamma = 2.2, 6.6, 12.8$. See text.

In Fig. 6.2, we show the $l = 1$ or charge structure factor

$$\mathbf{S}_{01}(k) = \frac{1}{N}\langle|\boldsymbol{\rho}_{\boldsymbol{k}}|^2\rangle \tag{4.7. 7}$$

with

$$\boldsymbol{\rho}_{\boldsymbol{k}} = \sum_{i=1}^{N} \boldsymbol{Q}_i \, e^{i\boldsymbol{k}\cdot\boldsymbol{r}_i} \tag{4.7. 8}$$

Unlike $\mathbf{S}_{00}$ which correlates a pair of scalar densities, $\mathbf{S}_{01}$ correlates a pair of charge densities. In the OCP plasma both correlators are identical. They are not in the SU(2) colored Coulomb plasma. In the long wavelength approximation, the static density structure factor is saturated by the plasmon mode

$$\mathbf{S}_{01}(\boldsymbol{k}) \approx \frac{\boldsymbol{k}^2}{k_D^2} \tag{4.7. 9}$$

which is seen to vanish at zero momentum.

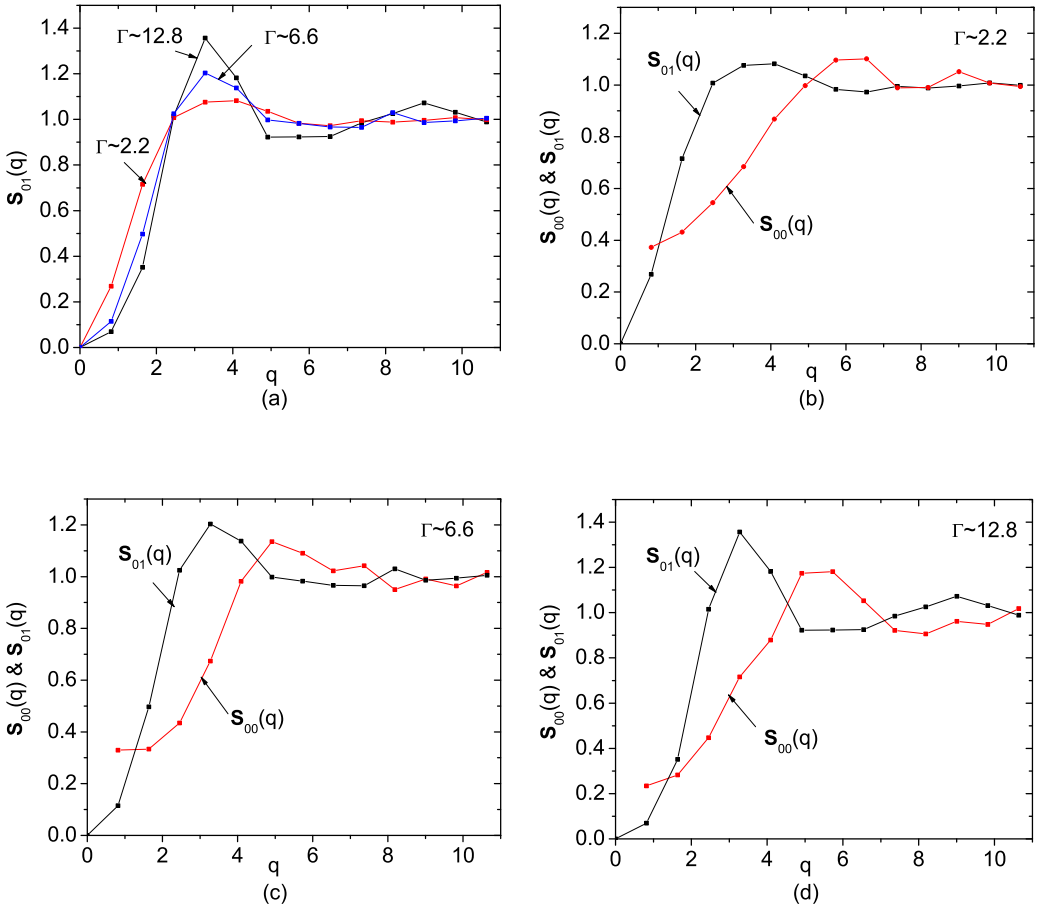

Figure 4.4: The static structure factor $\mathbf{S}_{01}(q)$ for $\Gamma = 2.2, 6.6, 12.8$. See text.

Our analytical result for $\mathbf{S}_{01}(k)$ in (4.6.10) is in agreement with the molecular dynamics simulations for the charged correlator (4.7. 7). Our analytical result for $\mathbf{S}_{00}(k)$ is identical with $\mathbf{S}_{01}(k)$. It differs from the molecular dynamics simulation results for small momenta since the sound mode drops out of the Debye-Huckel colored potential on which our charging process was based.

The contribution of the sound mode is additive at small momenta, and drops out at large momentum due to damping through the shear viscosity.

4.8 Conclusions

The strongly coupled SU(2) QGP is characterized by a number of static correlators in phase space with color treated as a classical 3-vector on S^3 with a radius fixed by the second Casimir. Space translational invariance and color rotational invariance yields multiple structure factors characterizing color correlations with color charges sourced by Legendre polynomials. Each structure factor obeys a generalized Ornstein-Zernicke equation.

To evaluate analytically these multiple structure factors, we have made use of the Debye charging process and the linearized Poisson-Boltzman equation in line with linear response theory. We have derived explicit relations for the two lowest structure factors, ie $l = 0, 1$ which corresponds to the density and charge structure factors.

To check the validity of the linear response analysis, we have numerically extracted the density and charge static structure factors using SU(2) molecular dynamics simulations. Modulo the sound mode, both analytical structure factors compare favorably with the numerical results. The current analysis extends to higher multipoles, ie $l = 2, 3, ...$ and generalizes to higher color SU(N $>$ 2) groups.

The static structure factors play an important role in characterizing the correlations in the colored SU(2) QGP at intermediate and large values of the coupling coupling Γ. They also enter in the assessment of transport parameters at strong coupling. The results will be presented elsewhere.

The current classical and strongly coupled SU(2) colored Coulomb plasma can be extended to several species to account for gluons, quarks and anti-quarks [3]. The effects of quantum mechanics being a renormalization of the constituent parameters such as the mass and charge. It will be interesting to see whether a quantum phase space formulation of QCD is achievable through the background field formulation in a way that allows for the introduction of colored static structure factors.

4.9 Appendix

4.9.1 SU(2) Color charges

The explicit representation of the classical color charges is [4, 12]

$$Q^1 = \cos\phi_1\sqrt{J^2-\pi_1^2}, \quad Q^2 = \sin\phi_1\sqrt{J^2-\pi_1^2}, \quad Q^3 = \pi_1 \tag{4.9.1}$$

with J^2 the quadratic Casimir $q_2 = \sum_\alpha^{N_c^2-1} Q^\alpha Q^\alpha$. The measure in the SU(2) phase space can be set to

$$dQ = c_R d\pi_1 d\phi_1 J dJ \delta(J^2 - q_2) \tag{4.9.2}$$

where c_R is a representation dependent constant. These SU(2) color charges satisfy

$$\int dQQ^\alpha = 0$$
$$\int dQQ^\alpha Q^\beta = C_2\delta^{\alpha\beta} \tag{4.9.3}$$

For fixed Casimir $\sum_\alpha Q^\alpha Q^\alpha = (N_c^2 - 1)C_2$, we can chose the spherical representation for (5.11.1)

$$Q^1 = \sin\theta\cos\phi, \quad Q^2 = \sin\theta\sin\phi, \quad Q^3 = \cos\theta \tag{4.9.4}$$

for which the measure (5.11.2) reads

$$dQ = \sin\theta d\theta d\phi \tag{4.9.5}$$

Equivalently,

$$Q^1 = -\sqrt{\frac{2\pi}{3}}\Big(Y_1^{-1}(\theta,\phi) - Y_1^1(\theta,\phi)\Big)$$
$$Q^2 = i\sqrt{\frac{2\pi}{3}}\Big(Y_1^{-1}(\theta,\phi) + Y_1^1(\theta,\phi)\Big)$$
$$Q^3 = \sqrt{\frac{4\pi}{3}}Y_1^0(\theta,\phi) \tag{4.9.6}$$

in terms of spherical harmonics. In the spherical representation, we have $\int dQ = 4\pi$, $\sum_\alpha Q^\alpha Q^\alpha = 1$ and $\int dQ\boldsymbol{Q}\cdot\boldsymbol{Q} = 4\pi$.

Chapter 5

Shear viscosity and self diffusion

5.1 Introduction

High temperature QCD is expected to asymptote a weakly coupled Coulomb plasma albeit with still strong infrared divergences. The latters cause its magnetic sector to be non-perturbative at all temperatures. At intermediate temperatures of relevance to heavy-ion collider experiments, the electric sector is believed to be strongly coupled.

Recently, Shuryak and Zahed [23] have suggested that certain aspects of the quak-gluon plasma in range of temperatures $(1-3)\,T_c$ can be understood by a stronger Coulomb interaction causing persistent correlations in singlet and colored channels. As a result the quark and gluon plasma is more a liquid than a gas at intermediate temperatures. A liquid plasma should exhibit shorter mean-free paths and stronger color dissipation, both of which are supported by the current experiments at RHIC [24].

To help understand transport and dissipation in the strongly coupled quark gluon plasma, a classical model of the colored plasma was suggested in [3]. The

model consists of massive quarks and gluons interacting via classical colored Coulomb interactions. The color is assumed classical with all equations of motion following from Poisson brackets. For the SU(2) version both molecular dynamics simulations [3] and bulk thermodynamics [11, 16] were recently presented including simulations of the energy loss of heavy quarks [25].

In this chapter we extend our recent equilibrium analysis of the static properties of the colored Coulomb plasma, to transport. In section 5.2 we discuss the classical equations of motion in the SU(2) colored phase space and derive the pertinent Liouville operator. In section 5.3, we show that the resolvent of the Liouville operator obeys a hierarchy of equations in the SU(2) phase space. In section 5.4 we derive an integral equation for the time-dependent structure factor by introducing a non-local self-energy kernel in phase space. In section 5.5, we close the Liouville hierarchy through a free streaming approximation on the 4-point resolvent and derive the self-energy kernel in closed form. In section 5.6, we project the self-energy kernel and the non-static structure factor onto the colorless hydrodynamical phase space. In section 5.7, we show that the sound and plasmon mode are the leading hydrodynamical modes in the SU(2) colored Coulomb plasma. In section 5.8, we analyze the shear viscosity for the transverse sound mode for arbitrary values of Γ. We show that a minimum forms at $\Gamma \approx 5$ at the cross-over between the hydrodynamical and single-particle regimes. In section 5.9, we analyze self-diffusion in phase space, and derive an explicit expression for the diffusion constant at strong coupling. Our conclusions and prospects are in section 5.10. In appendix 5.11.1 we briefly summarize our variables in the SU(2) phase space. In appendix 5.11.2 we detail the projection method for the self-energy kernel used in the text. In appendix 5.11.3 we show that

the collisional color contribution to the Liouville operator drops in the self-energy kernel. In appendix 5.11.4 some useful aspects of the hydrodynamical projection method are outlined.

5.2 Colored Liouville Operator

The canonical approach to the colored Coulomb plasma was discussed in [3]. In brief, the Hamiltonian for a single species of constituent quarks or gluons in the SU(2) representation is defined as

$$H = \sum_{i}^{N} \frac{\boldsymbol{p}_i^2}{2m_i} + \sum_{i>j=1}^{N} \frac{\boldsymbol{Q}_i \cdot \boldsymbol{Q}_j}{|\boldsymbol{r}_i - \boldsymbol{r}_j|} \tag{5.2.1}$$

The charge $g^2/4\pi$ has been omitted for simplicity of the notation flow and will be reinserted in the pertinent physical quantities by inspection.

The equations of motion in phase space follows from the classical Poisson brackets. In particular

$$\frac{d\boldsymbol{r}_i}{dt} = -\{H, \boldsymbol{r}_i\} = \frac{\partial H}{\partial \boldsymbol{p}_j}\frac{\partial \boldsymbol{r}_i}{\partial \boldsymbol{r}_j} = \frac{\boldsymbol{p}_i}{m} \tag{5.2.2}$$

The Newtonian equation of motion is just the colored electric Lorentz force

$$\frac{d\boldsymbol{p}_i}{dt} = -\{H, \boldsymbol{p}_i\} = -\frac{\partial H}{\partial \boldsymbol{r}_j}\frac{\partial \boldsymbol{p}_i}{\partial \boldsymbol{p}_j} = Q_i^a \, \boldsymbol{E}_i^a = \boldsymbol{F}_i \tag{5.2.3}$$

with the colored electric field and potentials defined as ($a = 1, 2, 3$)

$$\boldsymbol{E}_i^a = -\boldsymbol{\nabla}_i \Phi_i^a = -\boldsymbol{\nabla}_i \sum_{j \neq i} \frac{Q_j^a}{|\boldsymbol{r}_i - \boldsymbol{r}_j|} \tag{5.2.4}$$

Our strongly coupled colored plasma is mostly electric following the original

assumptions in [3, 8]. The equation of motion of the color charges is

$$\frac{dQ_i^a}{dt} = -\{H, Q_i^a\} = -\sum_{j,b} \frac{\partial H}{\partial Q_i^b}\frac{\partial Q_i^a}{\partial Q_j^c}\{Q_j^b, Q_j^c\} = \sum_{j\neq i} \frac{Q_i T^a Q_j}{|\boldsymbol{r}_i - \boldsymbol{r}_j|} \tag{5.2.5}$$

for arbitrary color representation. For SU(2) the classical color charge (5.2.5) precesses around the net colored potential Φ determined by the other particles as defined in (5.2.4),

$$\frac{d\boldsymbol{Q}_i}{dt} = (\boldsymbol{\Phi}_i \times \boldsymbol{Q}_i) \tag{5.2.6}$$

This equation was initially derived by Wong [5]. Some aspects of the SU(2) phase space are briefly recalled in appendix 5.11.1.

The set (5.2.2), (5.2.3) and (5.2.5) define the canonical evolution in phase space. The time-dependent phase distribution is formally given by

$$f(t, \boldsymbol{r}\boldsymbol{p}\boldsymbol{Q}) = \sum_{i=1}^{N} \delta(\boldsymbol{r}-\boldsymbol{r}_i(t))\delta(\boldsymbol{p}-\boldsymbol{p}_i(t))\delta(\boldsymbol{Q}-\boldsymbol{Q}_i(t)) \equiv \sum_i \delta(\boldsymbol{q}-\boldsymbol{q}_i(t)) \tag{5.2.7}$$

For simplicity $\boldsymbol{q}$ is generic for $\boldsymbol{r}, \boldsymbol{p}, \boldsymbol{Q}$. Using the chain rule, the time-evolution operator on (5.2.7) obeys

$$\frac{d}{dt} = \frac{\partial}{\partial t} + \frac{d\boldsymbol{r}_i}{dt}\frac{\partial}{\partial \boldsymbol{r}_i} + \frac{d\boldsymbol{p}_i}{dt}\frac{\partial}{\partial \boldsymbol{p}_i} + \frac{d\boldsymbol{Q}_i}{dt}\frac{\partial}{\partial \boldsymbol{Q}_i} \equiv \partial_t + i\mathcal{L} \tag{5.2.8}$$

The last relation defines the Liouville operator

$$\mathcal{L} = \mathcal{L}_0 + \mathcal{L}_I + \mathcal{L}_Q = -i\boldsymbol{v}_i \cdot \nabla_{\boldsymbol{r}_i} - i\,\boldsymbol{F}_i \cdot \boldsymbol{\nabla}_{\boldsymbol{p}_i} - i\boldsymbol{\Phi}_i \cdot (\boldsymbol{Q}_i \times \boldsymbol{\nabla}_{\boldsymbol{Q}_i}) \tag{5.2.9}$$

The last contribution in (5.2.9) is genuily a 3-body force because of the cross product (orbital color operator). It requires 3 distinct colors to not vanish. This observation will be important in simplifying the color dynamics below. Also (5.2.9) is hermitean.

Since (5.2.7) depends implicitly on time, we can write formally

$$\frac{d}{dt} f(t, \boldsymbol{rpQ}) = i\mathfrak{L} f(t, \boldsymbol{rpQ}) \tag{5.2.10}$$

with a solution $f(t) = e^{i\mathfrak{L}t} f(0)$. The formal relation (5.2.10) should be considered with care since the action of the Liouville operator on the 1-body phase space distribution (5.2.7) generates also a 2-body phase space distribution. Indeed, while $\mathfrak{L}_0$ is local in phase space

$$\mathfrak{L}_0 \sum_i \delta(\boldsymbol{q} - \boldsymbol{q}_i) = -i\boldsymbol{v} \cdot \nabla_{\boldsymbol{r}} \sum_i \delta(\boldsymbol{q} - \boldsymbol{q}_i) = L_0(\boldsymbol{q}) \sum_i \delta(\boldsymbol{q} - \boldsymbol{q}_i) \tag{5.2.11}$$

the 2 other contributions are not. Specifically

$$\begin{aligned} \mathfrak{L}_I \sum_m \delta(\boldsymbol{q} - \boldsymbol{q}_m) &= i \sum_{i \neq j} \nabla_{\boldsymbol{r}_i} \frac{\boldsymbol{Q}_i \cdot \boldsymbol{Q}_j}{|\boldsymbol{r}_i - \boldsymbol{r}_j|} \cdot \nabla_{\boldsymbol{p}_i} \sum_m \delta(\boldsymbol{q} - \boldsymbol{q}_m) \\ &= i \int d\boldsymbol{q}' \sum_{i \neq j, mn} \nabla_{\boldsymbol{r}_i} \frac{\boldsymbol{Q}_i \cdot \boldsymbol{Q}_j}{|\boldsymbol{r}_i - \boldsymbol{r}_j|} \cdot \nabla_{\boldsymbol{p}_i} \, \delta(\boldsymbol{q} - \boldsymbol{q}_m) \delta(\boldsymbol{q}' - \boldsymbol{q}_n) \\ &= - \int d\boldsymbol{q}' L_I(\boldsymbol{q}, \boldsymbol{q}') \sum_{mn} \delta(\boldsymbol{q} - \boldsymbol{q}_m) \delta(\boldsymbol{q}' - \boldsymbol{q}_n) \end{aligned} \tag{5.2.12}$$

with

$$L_I(\boldsymbol{q}, \boldsymbol{q}') = i \nabla_{\boldsymbol{r}} \frac{\boldsymbol{Q} \cdot \boldsymbol{Q}'}{|\boldsymbol{r} - \boldsymbol{r}'|} \cdot (\nabla_{\boldsymbol{p}} - \nabla_{\boldsymbol{p}'}) \tag{5.2.13}$$

Similarly

$$\begin{aligned}\mathcal{L}_Q \sum_m \delta(\boldsymbol{q}-\boldsymbol{q}_m) &= -i \sum_{j\neq i,m} \frac{\boldsymbol{Q}_i \times \boldsymbol{Q}_j}{|\boldsymbol{r}_i - \boldsymbol{r}_j|} \cdot \nabla_{\boldsymbol{Q}_i} \delta(\boldsymbol{q}-\boldsymbol{q}_m) \\ &= -i \int d\boldsymbol{q}' \sum_{j\neq i,mn} \frac{\boldsymbol{Q}_i \times \boldsymbol{Q}_j}{|\boldsymbol{r}_i - \boldsymbol{r}_j|} \cdot \nabla_{\boldsymbol{Q}_i} \delta(\boldsymbol{q}-\boldsymbol{q}_m)\delta(\boldsymbol{q}'-\boldsymbol{q}_n) \\ &= -\int d\boldsymbol{q}' L_Q(\boldsymbol{q},\boldsymbol{q}') \sum_{mn} \delta(\boldsymbol{q}-\boldsymbol{q}_m)\delta(\boldsymbol{q}'-\boldsymbol{q}_n) \qquad (5.2.14)\end{aligned}$$

with

$$L_Q(\boldsymbol{q},\boldsymbol{q}') = -i\frac{\boldsymbol{Q}\times\boldsymbol{Q}'}{|\boldsymbol{r}-\boldsymbol{r}'|}\cdot(\nabla_{\boldsymbol{Q}} - \nabla_{\boldsymbol{Q}'}) \qquad (5.2.15)$$

Clearly (5.2.14) drops from 2-body and symmetric phase space distributions. It does not for 3-body and higher.

5.3 Liouville Hierarchy

An important correlation function in the analysis of the colored Coulomb plasma is the time dependent structure factor or 2-body correlation in the color phase space

$$\mathbf{S}(t-t', \boldsymbol{r}-\boldsymbol{r}', \boldsymbol{p}\boldsymbol{p}', \boldsymbol{Q}\cdot\boldsymbol{Q}') = \langle \delta f(t,\boldsymbol{r}\boldsymbol{p}\boldsymbol{Q})\, \delta f(t',\boldsymbol{r}'\boldsymbol{p}'\boldsymbol{Q}')\rangle \qquad (5.3.1)$$

with $\delta f = f - \langle f\rangle$ the shifted 1-body phase space distribution. The averaging in (5.3.1) is carried over the initial conditions with fixed number of particles N and average energy or temperature $\beta = 1/T$. Thus $\langle f\rangle = n f_0(p)$ which is the

Maxwellian distribution for constituent quarks or gluons. In equilibrium, the averaging in (5.3.1) is time and space translational invariant as well as color rotational invariant.

Using the ket notation with $\mathbf{1} \equiv \boldsymbol{q} \equiv \boldsymbol{rpQ}$

$$|\delta f(t,\mathbf{1})\rangle = \Big| \sum_m \delta(\boldsymbol{q} - \boldsymbol{q}_m(t)) - \langle \sum_m \delta(\boldsymbol{q} - \boldsymbol{q}_m(t)) \Big\rangle \equiv |\delta f(t,\mathbf{1}) - \langle f(t,\mathbf{1})\rangle > \tag{5.3.2}$$

with also $\mathbf{2} = \boldsymbol{q}'$, $\mathbf{3} = \boldsymbol{q}''$, $\mathbf{4} = \boldsymbol{q}'''$ and so on and the formal Liouville solution $\delta f(t,\mathbf{1}) = e^{i\mathcal{L}t}\delta f(\mathbf{1})$ we can write (5.3.1) as

$$\mathbf{S}(t-t',\boldsymbol{q},\boldsymbol{q}') = \langle \delta f(t,\mathbf{1})|\delta f(t',\mathbf{2})\rangle = \langle \delta f(\mathbf{1})|e^{i\mathcal{L}(t'-t)}|\delta f(\mathbf{2})\rangle \tag{5.3.3}$$

The bra-ket notation is short for the initial or equilibrium average. Its Laplace or causal transform reads

$$\mathbf{S}(z,\boldsymbol{q},\boldsymbol{q}') = -i\int_{-\infty}^{+\infty} dt\ \theta(t-t')\ e^{izt}\ \mathbf{S}(t-t',\boldsymbol{q},\boldsymbol{q}') = \langle \delta f(\mathbf{1})|\frac{1}{z+\mathcal{L}}|\delta f(\mathbf{2})\rangle \tag{5.3.4}$$

with $z = \omega + i0$. Clearly

$$z\mathbf{S}(z,\boldsymbol{q},\boldsymbol{q}') + \langle \delta f(\mathbf{1})|\mathcal{L}\frac{1}{z+\mathcal{L}}|\delta f(\mathbf{2})\rangle = \langle \delta f(\mathbf{1})|\delta f(\mathbf{2})\rangle \tag{5.3.5}$$

Since $\mathcal{L}^\dagger = \mathcal{L}$ is hermitian and using (5.2.11), (5.2.12) and (5.2.14) it follows that

$$\langle \delta f(\mathbf{1})|\mathfrak{L} = \langle \delta f(\mathbf{1})|L_0(\boldsymbol{q}) - \int d\boldsymbol{q}"\, L_{I+Q}(\boldsymbol{q},\boldsymbol{q}'')\, \langle \delta f(\mathbf{1})\delta f(\mathbf{3})| \tag{5.3.6}$$

Thus

$$\Big(z - L_0(\boldsymbol{q})\Big)\mathbf{S}(z,\boldsymbol{q},\boldsymbol{q}') - \int d\boldsymbol{q}'' L_{I+Q}(\boldsymbol{q}',\boldsymbol{q}'')\mathbf{S}(z,\boldsymbol{q}\boldsymbol{q}'',\boldsymbol{q}') = \mathbf{S}_0(\boldsymbol{q},\boldsymbol{q}') \tag{5.3.7}$$

where we have defined the 3-body phase space resolvent

$$\mathbf{S}(z,\boldsymbol{q}\boldsymbol{q}'',\boldsymbol{q}') = \langle \delta f(\mathbf{1})\delta f(\mathbf{3})|\frac{1}{z+\mathfrak{L}}|\delta f(\mathbf{2})> \tag{5.3.8}$$

$\mathbf{S}_0(\boldsymbol{q},\boldsymbol{q}')$ is the static colored structure factor discussed by us in [31]. Since $L_{I+Q}(\boldsymbol{q}',\boldsymbol{q})$ is odd under the switch $\boldsymbol{q} \leftrightarrow \boldsymbol{q}'$, and since $\mathbf{S}(z,\boldsymbol{q}\boldsymbol{q}'',\boldsymbol{q}') = \mathbf{S}(-z,\boldsymbol{q},\boldsymbol{q}'\boldsymbol{q}'')$ owing to the $t \leftrightarrow t'$ in (5.3.4), then

$$\Big(z + L_0(\boldsymbol{q}')\Big)\mathbf{S}(z,\boldsymbol{q},\boldsymbol{q}') - \int d\boldsymbol{q}'' L_{I+Q}(\boldsymbol{q}',\boldsymbol{q}'')\mathbf{S}(z,\boldsymbol{q},\boldsymbol{q}'\boldsymbol{q}'') = \mathbf{S}_0(\boldsymbol{q},\boldsymbol{q}') \tag{5.3.9}$$

(5.3.7) or equivalently (5.3.9) define the Liouville hierarchy, whereby the 2-body phase space distribution ties to the 3-body phase space distribution and so on. Indeed, (5.3.9) for instance implies

$$\Big(z + L_0(\boldsymbol{q}'')\Big)\mathbf{S}(z,\boldsymbol{q}\boldsymbol{q}',\boldsymbol{q}'') - \int d\boldsymbol{q}''' L_{I+Q}(\boldsymbol{q}'',\boldsymbol{q}''')\mathbf{S}(z,\boldsymbol{q}\boldsymbol{q}',\boldsymbol{q}''\boldsymbol{q}''') = \mathbf{S}_0(\boldsymbol{q}\boldsymbol{q}',\boldsymbol{q}'') \tag{5.3.10}$$

with the 4-point resolvent function

$$\mathbf{S}(z, \boldsymbol{q}\boldsymbol{q}', \boldsymbol{q}''\boldsymbol{q}''') = \langle \delta f(\mathbf{1})\delta f(\mathbf{2})| \frac{1}{z+\mathcal{L}} |\delta f(\mathbf{3})\delta f(\mathbf{4}) > \tag{5.3.11}$$

These are the microscopic kinetic equations for the color phase space distributions. They are only useful when closed, that is by a truncation as we discuss below. These formal equations where initially discussed in [32–35] in the context of the one component Abelian Coulomb plasma. We have now generalized them to the multi-component and non-Abelian colored Coulomb plasma.

5.4 Self-Energy Kernel

In (5.3.7) the non-local part of the Liouville operator plays the role of a non-local self-energy kernel Σ on the 2-body resolvent. Indeed, we can rewrite (5.3.7) as

$$(z - L_0(\boldsymbol{q}))\mathbf{S}(z, \boldsymbol{q}, \boldsymbol{q}') - \int dq''\Sigma(z, \boldsymbol{q}, \boldsymbol{q}'')\mathbf{S}(z, \boldsymbol{q}'', \boldsymbol{q}') = \mathbf{S}_0(\boldsymbol{q}, \boldsymbol{q}') \tag{5.4.1}$$

with the non-local self-energy kernel defined formally as

$$\int d\boldsymbol{q}''\Sigma(z, \boldsymbol{q}, \boldsymbol{q}'')\, \mathbf{S}(z, \boldsymbol{q}'', \boldsymbol{q}') = \int d\boldsymbol{q}'' L_{I+Q}(\boldsymbol{q}, \boldsymbol{q}'')\, \mathbf{S}(z, \boldsymbol{q}\boldsymbol{q}'', \boldsymbol{q}') \tag{5.4.2}$$

The self-energy kernel Σ can be regarded as the sum of a static or z-independent contribution Σ_S ans a non-static or collisional contribution Σ_C,

$$\Sigma(z, \boldsymbol{q}, \boldsymbol{q}'') = \Sigma_S(\boldsymbol{q}, \boldsymbol{q}'') + \Sigma_C(z, \boldsymbol{q}, \boldsymbol{q}'') \tag{5.4.3}$$

The stationary part Σ_S satisfies

$$\int d\boldsymbol{q}''\Sigma_S(\boldsymbol{q},\boldsymbol{q}'')\,\mathbf{S}_0(\boldsymbol{q}'',\boldsymbol{q}') = \int d\boldsymbol{q}''L_{I+Q}(\boldsymbol{q},\boldsymbol{q}'')\,\mathbf{S}_0(\boldsymbol{q},\boldsymbol{q}',\boldsymbol{q}'') \tag{5.4.4}$$

which identifies it with the sum of the 2- and 3-body part of the Liouville operator L_{I+Q}.

The collisional part Σ_C is more involved. To unwind it, we operate with $(z+L_0(\boldsymbol{q}'))$ on both sides of (5.4.2), and then reduce the left hand side contribution using (5.3.9) and the right hand side contribution using (5.3.10). The outcome reduces to

$$\begin{aligned}\Sigma_C(z,\boldsymbol{q},\boldsymbol{q}'')\,\mathbf{S}_0(\boldsymbol{q}'',\boldsymbol{q}') = \quad & -\int d\boldsymbol{q}'''\,L_{I+Q}(\boldsymbol{q},\boldsymbol{q}'')L_{I+Q}(\boldsymbol{q}',\boldsymbol{q}'')\,\mathbf{S}(z,\boldsymbol{q}\boldsymbol{q}'',\boldsymbol{q}'\boldsymbol{q}''') \\ & +\int dq'''\,\Sigma(z,\boldsymbol{q},\boldsymbol{q}'')\,L_{I+Q}(\boldsymbol{q}',\boldsymbol{q}'')\,\mathbf{S}(z,\boldsymbol{q}'',\boldsymbol{q}'\boldsymbol{q}''')\end{aligned} \tag{5.4.5}$$

after using (5.4.4). From (5.4.2) it follows formally that

$$\Sigma(z,\boldsymbol{q},\boldsymbol{q}'') = \int d\boldsymbol{q}'''\,L_{I+Q}(\boldsymbol{q},\boldsymbol{q}''')\,\mathbf{S}^{-1}(z,\boldsymbol{q}',\boldsymbol{q}'')\,\mathbf{S}(z,\boldsymbol{q}\boldsymbol{q}''',\boldsymbol{q}') \tag{5.4.6}$$

Inserting (5.4.6) into the right hand side of (5.4.5) and taking the $\boldsymbol{q}'$ integration on both sides yield

$$nf_0(p'')\,\Sigma_C(z,\boldsymbol{q},\boldsymbol{q}'') = -\int d\boldsymbol{q}''d\boldsymbol{q}'''\,L_{I+Q}(\boldsymbol{q},\boldsymbol{q}'')L_{I+Q}(\boldsymbol{q}',\boldsymbol{q}'''')\,\mathbf{G}(z,\boldsymbol{q}\boldsymbol{q}'',\boldsymbol{q}'\boldsymbol{q}'''') \tag{5.4.7}$$

with $\mathbf{G}$ a 4-point phase space correlation function

$$\begin{aligned}\mathbf{G}(z,\boldsymbol{q}\boldsymbol{q}_1',\boldsymbol{q}'\boldsymbol{q}_2') &= \mathbf{S}(z,\boldsymbol{q}\boldsymbol{q}_1',\boldsymbol{q}'\boldsymbol{q}_2')\\ &- \int d\boldsymbol{q}_3 d\boldsymbol{q}_4 \mathbf{S}(z,\boldsymbol{q}\boldsymbol{q}_1',\boldsymbol{q}_3)\mathbf{S}^{-1}(z,\boldsymbol{q}_3,\boldsymbol{q}_4)\mathbf{S}(z,\boldsymbol{q}_4,\boldsymbol{q}'\boldsymbol{q}_2')\end{aligned} \tag{5.4.8}$$

The collisional character of the self-energy Σ_C is manifest in (5.4.7). The formal relation for the collisional self-energy (5.4.7) was initially derived in [34, 35] for the one-component and Abelian Coulomb plasma. We now have shown that it holds for any non-Abelian SU(N) Coulomb plasma.

Eq. (5.4.7) shows that the connected part of the self-energy kernel is actually tied to a 4-point correlator in the colored phase space. In terms of (5.4.7), the original kinetic equation (5.3.7) now reads

$$\begin{aligned}&\Big(z - L_0(\boldsymbol{q})\Big)\mathbf{S}(z,\boldsymbol{q},\boldsymbol{q}') - \int d\boldsymbol{q}''\Sigma_S(\boldsymbol{q},\boldsymbol{q}'')\mathbf{S}(z,\boldsymbol{q}'',\boldsymbol{q}') = \mathbf{S}_0(\boldsymbol{q},\boldsymbol{q}')\\ &- \int d\boldsymbol{q}''\,d\boldsymbol{q}_1 d\boldsymbol{q}_2\,L_{I+Q}(\boldsymbol{q},\boldsymbol{q}_1)L_{I+Q}(\boldsymbol{q}'',\boldsymbol{q}_2)\,\mathbf{G}(z,\boldsymbol{q}\boldsymbol{q}_1,\boldsymbol{q}''\boldsymbol{q}_2)\,\mathbf{S}(z,\boldsymbol{q}'',\boldsymbol{q}')\end{aligned} \tag{5.4.9}$$

which is a Boltzman-like equation. The key difference is that it involves correlation functions and the Boltzman-like kernel in the right-hand side is **not** a scattering amplitude but rather a reduced 4-point correlation function. (5.4.9)

reduces to the Boltzman equation for weak coupling. An alternative derivation of (5.4.9) can be found in Appendix 5.11.2 through a direct projection of (5.4.2) in phase space.

5.5 Free Streaming Approximation

The formal kinetic equation (5.4.7) can be closed by approximating the 4-point correlation function in the color phase space by a product of 2-point correlation function [35],

$$\mathbf{G}(t, \boldsymbol{q}\boldsymbol{q}_1, \boldsymbol{q}'\boldsymbol{q}_2) \approx \Big(\mathbf{S}(t, \boldsymbol{q}, \boldsymbol{q}')\mathbf{S}(t, \boldsymbol{q}_1, \boldsymbol{q}_2) + \mathbf{S}(t, \boldsymbol{q}, \boldsymbol{q}_2)\mathbf{S}(t, \boldsymbol{q}', \boldsymbol{q}_1)\Big)$$

This reduction will be referred to as the free steaming approximation. Next we substitue the colored Coulomb potentials in the double Liouville operator $L_{1+Q} \times L_{1+Q}$ with a bare Coulomb $\mathbf{V}(\boldsymbol{r} - \boldsymbol{r}', \boldsymbol{Q} \cdot \boldsymbol{Q}') = \boldsymbol{Q} \cdot \boldsymbol{Q}'/|\boldsymbol{r} - \boldsymbol{r}'|$.

$$\begin{aligned} L_{I+Q}(\boldsymbol{q}, \boldsymbol{q}_1) &= i\nabla_{\boldsymbol{r}}\mathbf{V}(\boldsymbol{r} - \boldsymbol{r}_1, \boldsymbol{Q} \cdot \boldsymbol{Q}_1) \cdot (\nabla_{\boldsymbol{p}} - \nabla_{\boldsymbol{p}_1}) \\ &\quad -i\Big(\boldsymbol{Q} \times \nabla_{\boldsymbol{Q}}\mathbf{V}(\boldsymbol{r} - \boldsymbol{r}_1, \boldsymbol{Q} \cdot \boldsymbol{Q}_1) \cdot \nabla_{\boldsymbol{Q}} + \boldsymbol{Q}_1 \times \nabla_{\boldsymbol{Q}_1}\mathbf{V}(\boldsymbol{r} - \boldsymbol{r}_1, \boldsymbol{Q} \cdot \boldsymbol{Q}_1) \cdot \nabla_{Q_1}\Big) \end{aligned} \tag{5.5.1}$$

times a dressed colored Coulomb potential $\mathbf{c}_D$ defined in [31]

$$L^R_{I+Q}(\boldsymbol{q},\boldsymbol{q}_1) = -i\frac{1}{\beta}\nabla_{\boldsymbol{r}}\mathbf{c}_D(\boldsymbol{r}-\boldsymbol{r}_1,\boldsymbol{Q}\cdot\boldsymbol{Q}_1)\cdot(\nabla_{\boldsymbol{p}}-\nabla_{\boldsymbol{p}_1})$$
$$+i\frac{1}{\beta}\Big(\boldsymbol{Q}\times\nabla_{\boldsymbol{Q}}\mathbf{c}_D(\boldsymbol{r}-\boldsymbol{r}_1,\boldsymbol{Q}\cdot\boldsymbol{Q}_1)\cdot\nabla_{\boldsymbol{Q}}+\boldsymbol{Q}_1\times\nabla_{\boldsymbol{Q}_1}\mathbf{c}_D(\boldsymbol{r}-\boldsymbol{r}_1,\boldsymbol{Q}\cdot\boldsymbol{Q}_1)\cdot\nabla_{Q_1}\Big) \tag{5.5.2}$$

This bare-dressed or half renormalization was initially suggested [36] in the context of the one-component Coulomb plasma to overcome the shortcomings of a full or dressed-dressed renormalization initially suggested in [34, 35]. The latter was shown to upset the initial conditions. Thus

$$L_{I+Q}(\boldsymbol{q},\boldsymbol{q}_1)L_{I+Q}(\boldsymbol{q}',\boldsymbol{q}_2)$$
$$\to\frac{1}{2}\Big(L_{I+Q}(\boldsymbol{q},\boldsymbol{q}_1)L^R_{I+Q}(\boldsymbol{q}',\boldsymbol{q}_2)+L^R_{I+Q}(\boldsymbol{q},\boldsymbol{q}_1)L_{I+Q}(\boldsymbol{q}',\boldsymbol{q}_2)\Big) \tag{5.5.3}$$

Combining (5.5.1) and (5.5.3) in (5.4.7) yields

$$n\,f_0(\boldsymbol{p}')\,\Sigma_C(t,\boldsymbol{q},\boldsymbol{q}')\approx-\frac{1}{2}\int d\boldsymbol{q}_1\,d\boldsymbol{q}_2\,\Big(L_{I+Q}(\boldsymbol{q},\boldsymbol{q}_1)L^R_{I+Q}(\boldsymbol{q}',\boldsymbol{q}_2)$$
$$\times\mathbf{S}(t,\boldsymbol{q},\boldsymbol{q}')\mathbf{S}(t,\boldsymbol{q}_1,\boldsymbol{q}_2)+L_{I+Q}(\boldsymbol{q},\boldsymbol{q}_1)L^R_{I+Q}(\boldsymbol{q}',\boldsymbol{q}_2)\mathbf{S}(t,\boldsymbol{q},\boldsymbol{q}_2)\mathbf{S}(t,\boldsymbol{q}',\boldsymbol{q}_1)$$
$$+(\boldsymbol{q}_1\leftrightarrow\boldsymbol{q}_2,\boldsymbol{q}\leftrightarrow\boldsymbol{q}')\Big) \tag{5.5.4}$$

This is the half dressed but free streaming approximation for the connected part of the self-energy for the colored Coulomb plasma. Translational invariance in space and rotational invariance in color space allows a further reduction of (5.5.4) by Fourier and Legendre transforms respectively. Indeed, Eq. (5.5.4)

yields

$$
\begin{aligned}
& n\, f_0(\boldsymbol{p}')\, \Sigma_C(t, \boldsymbol{q}, \boldsymbol{q}') \\
& \quad \approx -\frac{1}{2} \int d\boldsymbol{q}_1\, d\boldsymbol{q}_2 \Big(L_I(\boldsymbol{q}, \boldsymbol{q}_1) L_I^R(\boldsymbol{q}', \boldsymbol{q}_2) \mathbf{S}(t, \boldsymbol{q}, \boldsymbol{q}') \mathbf{S}(t, \boldsymbol{q}_1, \boldsymbol{q}_2) \\
& \quad + L_I(\boldsymbol{q}, \boldsymbol{q}_1) L_I^R(\boldsymbol{q}', \boldsymbol{q}_2) \mathbf{S}(t, \boldsymbol{q}, \boldsymbol{q}_2) \mathbf{S}(t, \boldsymbol{q}', \boldsymbol{q}_1) + (\boldsymbol{q}_1 \leftrightarrow \boldsymbol{q}_2, \boldsymbol{q} \leftrightarrow \boldsymbol{q}') \Big) \\
& \quad = -\frac{1}{2\beta} \int d\boldsymbol{q}_1\, d\boldsymbol{q}_2 \Big(\nabla_{\boldsymbol{r}} \mathbf{c}_D(\boldsymbol{r} - \boldsymbol{r}_1, \boldsymbol{Q} \cdot \boldsymbol{Q}_1) \cdot \nabla_{\boldsymbol{p}} \\
& \quad \times \nabla_{\boldsymbol{r}'} \mathbf{V}(\boldsymbol{r}' - \boldsymbol{r}_2, \boldsymbol{Q}' \cdot \boldsymbol{Q}_2) \cdot \nabla_{\boldsymbol{p}'} \mathbf{S}(t, \boldsymbol{q}, \boldsymbol{q}') \mathbf{S}(t, \boldsymbol{q}_1, \boldsymbol{q}_2) \\
& \quad + \nabla_{\boldsymbol{r}} \mathbf{c}_D(\boldsymbol{r} - \boldsymbol{r}_1, \boldsymbol{Q} \cdot \boldsymbol{Q}_1) \cdot \nabla_{\boldsymbol{p}} \nabla_{\boldsymbol{r}'} \mathbf{V}(\boldsymbol{r}' - \boldsymbol{r}_2, \boldsymbol{Q}' \cdot \boldsymbol{Q}_2) \cdot \nabla_{\boldsymbol{p}'} \\
& \quad \times \mathbf{S}(t, \boldsymbol{q}, \boldsymbol{q}_2) \mathbf{S}(t, \boldsymbol{q}', \boldsymbol{q}_1) + (\boldsymbol{q}_1 \leftrightarrow \boldsymbol{q}_2, \boldsymbol{q} \leftrightarrow \boldsymbol{q}') \Big)
\end{aligned}
\tag{5.5.5}
$$

where we note that the colored part of the Liouville operator dropped from the collision kernel in the free streaming approximation as we detail in Appendix 5.11.3. Both sides of (5.11.9) can be now Legendre transformed in color to give

$$
\begin{aligned}
n\, f_0(\boldsymbol{p}') \sum_l \Sigma_{Cl}(t, \boldsymbol{r}\boldsymbol{r}', \boldsymbol{p}\boldsymbol{p}') \frac{2l+1}{4\pi} P_l(\boldsymbol{Q}\cdot\boldsymbol{Q}') \approx -\frac{1}{2\beta} \int d\boldsymbol{r}_1 d\boldsymbol{p}_1 d\boldsymbol{r}_2 d\boldsymbol{p}_2 \\
\times \sum_l \frac{2l+1}{4\pi} \left(\frac{l+1}{2l+1} P_{l+1}(\boldsymbol{Q}\cdot\boldsymbol{Q}') + \frac{l}{2l+1} P_{l-1}(\boldsymbol{Q}\cdot\boldsymbol{Q}') \right) \\
\times \Bigg(\nabla_{\boldsymbol{r}} \mathbf{c}_{D1}(\boldsymbol{r}-\boldsymbol{r}_1) \cdot \nabla_{\boldsymbol{p}} \nabla_{\boldsymbol{r}'} \frac{1}{|\boldsymbol{r}'-\boldsymbol{r}_2|} \cdot \nabla_{\boldsymbol{p}'} \mathbf{S}_l(t, \boldsymbol{r}\boldsymbol{r}', \boldsymbol{p}\boldsymbol{p}') \mathbf{S}_1(t, \boldsymbol{r}_1\boldsymbol{r}_2, \boldsymbol{p}_1\boldsymbol{p}_2) \\
+ \nabla_{\boldsymbol{r}} \mathbf{c}_{Dl}(\boldsymbol{r}-\boldsymbol{r}_1) \cdot \nabla_{\boldsymbol{p}} \nabla_{\boldsymbol{r}'} \frac{1}{|\boldsymbol{r}'-\boldsymbol{r}_2|} \cdot \nabla_{\boldsymbol{p}'} \mathbf{S}_1(t, \boldsymbol{r}\boldsymbol{r}_2, \boldsymbol{p}\boldsymbol{p}_2) \mathbf{S}_l(t, \boldsymbol{r}'\boldsymbol{r}_1, \boldsymbol{p}'\boldsymbol{p}_1) \\
+ \nabla_{\boldsymbol{r}'} \mathbf{c}_{Dl}(\boldsymbol{r}'-\boldsymbol{r}_2) \cdot \nabla_{\boldsymbol{p}'} \nabla_{\boldsymbol{r}} \frac{1}{|\boldsymbol{r}-\boldsymbol{r}_1|} \cdot \nabla_{\boldsymbol{p}} \mathbf{S}_l(t, \boldsymbol{r}\boldsymbol{r}_2, \boldsymbol{p}\boldsymbol{p}_2) \mathbf{S}_1(t, \boldsymbol{r}'\boldsymbol{r}_1, \boldsymbol{p}'\boldsymbol{p}_1) \\
\nabla_{\boldsymbol{r}'} \mathbf{c}_{D1}(\boldsymbol{r}'-\boldsymbol{r}_2) \cdot \nabla_{\boldsymbol{p}'} \nabla_{\boldsymbol{r}} \frac{1}{|\boldsymbol{r}-\boldsymbol{r}_1|} \cdot \nabla_{\boldsymbol{p}} \mathbf{S}_l(t, \boldsymbol{r}\boldsymbol{r}', \boldsymbol{p}\boldsymbol{p}') \mathbf{S}_1(t, \boldsymbol{r}_1\boldsymbol{r}_2, \boldsymbol{p}_1\boldsymbol{p}_2) \Bigg)
\end{aligned}
\tag{5.5.6}
$$

Thus

$$
\begin{aligned}
n\, f_0(\boldsymbol{p}')\, \Sigma_{Cl}(t, \boldsymbol{r}\boldsymbol{r}', \boldsymbol{p}\boldsymbol{p}') \approx -\frac{1}{2\beta} \int d\boldsymbol{r}_1 d\boldsymbol{p}_1 d\boldsymbol{r}_2 d\boldsymbol{p}_2 \\
\times \Bigg(\nabla_{\boldsymbol{r}} \mathbf{c}_{D1}(\boldsymbol{r} - \boldsymbol{r}_1) \cdot \nabla_{\boldsymbol{p}} \nabla_{\boldsymbol{r}'} \frac{1}{|\boldsymbol{r}' - \boldsymbol{r}_2|} \cdot \nabla_{\boldsymbol{p}'} \\
\times \Big(\frac{l}{2l+1} \mathbf{S}_{l-1}(t, \boldsymbol{r}\boldsymbol{r}', \boldsymbol{p}\boldsymbol{p}') \mathbf{S}_1(t, \boldsymbol{r}_1\boldsymbol{r}_2, \boldsymbol{p}_1\boldsymbol{p}_2) + \frac{l+1}{2l+1} \mathbf{S}_{l+1}(t, \boldsymbol{r}\boldsymbol{r}', \boldsymbol{p}\boldsymbol{p}') \mathbf{S}_1(t, \boldsymbol{r}_1\boldsymbol{r}_2, \boldsymbol{p}_1\boldsymbol{p}_2) \Big) \\
+ \nabla_{\boldsymbol{r}} \mathbf{c}_{D1}(\boldsymbol{r} - \boldsymbol{r}_1) \cdot \nabla_{\boldsymbol{p}} \nabla_{\boldsymbol{r}'} \frac{1}{|\boldsymbol{r}' - \boldsymbol{r}_2|} \cdot \nabla_{\boldsymbol{p}'} \\
\times \Big(\frac{l}{2l+1} \mathbf{S}_1(t, \boldsymbol{r}\boldsymbol{r}_2, \boldsymbol{p}\boldsymbol{p}_2) \mathbf{S}_{l-1}(t, \boldsymbol{r}'\boldsymbol{r}_1, \boldsymbol{p}'\boldsymbol{p}_1) + \frac{l+1}{2l+1} \mathbf{S}_1(t, \boldsymbol{r}\boldsymbol{r}_2, \boldsymbol{p}\boldsymbol{p}_2) \mathbf{S}_{l+1}(t, \boldsymbol{r}'\boldsymbol{r}_1, \boldsymbol{p}'\boldsymbol{p}_1) \Big) \\
+ \nabla_{\boldsymbol{r}'} \mathbf{c}_{Dl}(\boldsymbol{r}' - \boldsymbol{r}_2) \cdot \nabla_{\boldsymbol{p}'} \nabla_{\boldsymbol{r}} \frac{1}{|\boldsymbol{r} - \boldsymbol{r}_1|} \cdot \nabla_{\boldsymbol{p}} \\
\times \Big(\frac{l}{2l+1} \mathbf{S}_{l-1}(t, \boldsymbol{r}\boldsymbol{r}_2, \boldsymbol{p}\boldsymbol{p}_2) \mathbf{S}_1(t, \boldsymbol{r}'\boldsymbol{r}_1, \boldsymbol{p}'\boldsymbol{p}_1) + \frac{l+1}{2l+1} \mathbf{S}_{l+1}(t, \boldsymbol{r}\boldsymbol{r}_2, \boldsymbol{p}\boldsymbol{p}_2) \mathbf{S}_1(t, \boldsymbol{r}'\boldsymbol{r}_1, \boldsymbol{p}'\boldsymbol{p}_1) \Big) \\
+ \nabla_{\boldsymbol{r}'} \mathbf{c}_{D1}(\boldsymbol{r}' - \boldsymbol{r}_2) \cdot \nabla_{\boldsymbol{p}'} \nabla_{\boldsymbol{r}} \frac{1}{|\boldsymbol{r} - \boldsymbol{r}_1|} \cdot \nabla_{\boldsymbol{p}} \\
\times \Big(\frac{l}{2l+1} \mathbf{S}_{l-1}(t, \boldsymbol{r}\boldsymbol{r}', \boldsymbol{p}\boldsymbol{p}') \mathbf{S}_1(t, \boldsymbol{r}_1\boldsymbol{r}_2, \boldsymbol{p}_1\boldsymbol{p}_2) + \frac{l+1}{2l+1} \mathbf{S}_{l+1}(t, \boldsymbol{r}\boldsymbol{r}', \boldsymbol{p}\boldsymbol{p}') \mathbf{S}_1(t, \boldsymbol{r}_1\boldsymbol{r}_2, \boldsymbol{p}_1\boldsymbol{p}_2) \Big) \Bigg)
\end{aligned}
\tag{5.5.7}
$$

with $\mathbf{S}_{l-1} \equiv 0$ by definition. In the colored Coulomb plasma the collisional contributions diagonalize in the color projected channels labelled by l, with $l = 0$ being the density channel, $l = 1$ the plasmon channel and so on. In momentum space (5.5.7) reads

$$
\begin{aligned}
& n\, f_0(\boldsymbol{p}')\, \Sigma_{Cl}(t, \boldsymbol{k}, \boldsymbol{p}\boldsymbol{p}') \\
& = -\frac{1}{2\beta} \int d\boldsymbol{p}_1 d\boldsymbol{p}_2 \int \frac{d\boldsymbol{l}}{(2\pi)^3} \Big(\boldsymbol{l} \cdot \nabla_{\boldsymbol{p}} \boldsymbol{l} \cdot \nabla_{\boldsymbol{p}'} \mathbf{c}_{D1}(l) V_{\boldsymbol{l}} \\
& \times \Big(\frac{l}{2l+1} \mathbf{S}_{l-1}(t, \boldsymbol{k}-\boldsymbol{l}, \boldsymbol{p}\boldsymbol{p}') \mathbf{S}_1(t, \boldsymbol{l}, \boldsymbol{p}_1\boldsymbol{p}_2) + \frac{l+1}{2l+1} \mathbf{S}_{l+1}(t, \boldsymbol{k}-\boldsymbol{l}, \boldsymbol{p}\boldsymbol{p}') \mathbf{S}_1(t, \boldsymbol{l}, \boldsymbol{p}_1\boldsymbol{p}_2) \Big) \\
& + \boldsymbol{l} \cdot \nabla_{\boldsymbol{p}} (\boldsymbol{k}-\boldsymbol{l}) \cdot \nabla_{\boldsymbol{p}'} \mathbf{c}_{Dl}(l) V_{\boldsymbol{k}-\boldsymbol{l}} \\
& \times \Big(\frac{l}{2l+1} \mathbf{S}_1(t, \boldsymbol{k}-\boldsymbol{l}, \boldsymbol{p}\boldsymbol{p}_2) \mathbf{S}_{l-1}(t, \boldsymbol{l}, \boldsymbol{p}'\boldsymbol{p}_1) + \frac{l+1}{2l+1} \mathbf{S}_1(t, \boldsymbol{k}-\boldsymbol{l}, \boldsymbol{p}\boldsymbol{p}_2) \mathbf{S}_{1+1}(t, \boldsymbol{l}, \boldsymbol{p}'\boldsymbol{p}_1) \Big) \\
& + (\boldsymbol{k}-\boldsymbol{l}) \cdot \nabla_{\boldsymbol{p}} \boldsymbol{l} \cdot \nabla_{\boldsymbol{p}'} \mathbf{c}_{Dl}(l) V_{\boldsymbol{k}-\boldsymbol{l}} \\
& \times \Big(\frac{l}{2l+1} \mathbf{S}_{l-1}(t, \boldsymbol{l}, \boldsymbol{p}\boldsymbol{p}_2) \mathbf{S}_l(t, \boldsymbol{k}-\boldsymbol{l}, \boldsymbol{p}'\boldsymbol{p}_1) + \frac{l+1}{2l+1} \mathbf{S}_{l+1}(t, \boldsymbol{l}, \boldsymbol{p}\boldsymbol{p}_2) \mathbf{S}_1(t, \boldsymbol{k}-\boldsymbol{l}, \boldsymbol{p}'\boldsymbol{p}_1) \Big) \\
& + \boldsymbol{l} \cdot \nabla_{\boldsymbol{p}} \boldsymbol{l} \cdot \nabla_{\boldsymbol{p}'} \mathbf{c}_{D1}(l) V_{\boldsymbol{l}} \\
& \times \Big(\frac{l}{2l+1} \mathbf{S}_{l-1}(t, \boldsymbol{k}-\boldsymbol{l}, \boldsymbol{p}\boldsymbol{p}') \mathbf{S}_1(t, \boldsymbol{l}, \boldsymbol{p}_1\boldsymbol{p}_2) + \frac{l+1}{2l+1} \mathbf{S}_{l+1}(t, \boldsymbol{k}-\boldsymbol{l}, \boldsymbol{p}\boldsymbol{p}') \mathbf{S}_1(t, \boldsymbol{l}, \boldsymbol{p}_1\boldsymbol{p}_2) \Big) \Big)
\end{aligned}
\tag{5.5.8}
$$

with $V_{\boldsymbol{l}} = 4\pi/\boldsymbol{l}^2$. We note that for $l = 0$ which is the colorless density channel (5.5.8) involves only $\mathbf{S}_1$ which is the time-dependent charged form factor due to the Coulomb interactions.

5.6 Hydrodynamical Projection

In terms of (5.5.8) , (5.4.2) and

$$
\Sigma_l(z\boldsymbol{k}, \boldsymbol{p}\boldsymbol{p}_1) = \Big(\Sigma_{0l} + \Sigma_{Il} + \Sigma_{Ql} + \Sigma_{Cl} \Big)(z\boldsymbol{k}, \boldsymbol{p}\boldsymbol{p}_1) \tag{5.6.1}
$$

the Fourier and Legendre transform of the kinetic equation (5.3.7) now read

$$z\mathbf{S}_l(z\boldsymbol{k},\boldsymbol{p}\boldsymbol{p}') - \int d\boldsymbol{p}_1\Sigma_l(z\boldsymbol{k},\boldsymbol{p}\boldsymbol{p}_1)\mathbf{S}_l(z\boldsymbol{k},\boldsymbol{p}_1\boldsymbol{p}') = \mathbf{S}_{0l}(\boldsymbol{k},\boldsymbol{p}\boldsymbol{p}') \tag{5.6.2}$$

with $\Sigma_{0l} = L_0$ and $\Sigma_{Sl} = L_{(I+Q)l}$. Specifically

$$\begin{aligned}
\Sigma_{0l}(z\boldsymbol{k},\boldsymbol{p}\boldsymbol{p}_1) &= \boldsymbol{k}\cdot\boldsymbol{v}\delta(\boldsymbol{p}-\boldsymbol{p}_1)\\
\Sigma_{Il}(z\boldsymbol{k},\boldsymbol{p}\boldsymbol{p}_1) &= -n\, f_0(p)\frac{\boldsymbol{k}\cdot\boldsymbol{p}}{m}\,\mathbf{c}_{Dl}(\boldsymbol{k})\\
\Sigma_{Ql}(z\boldsymbol{k},\boldsymbol{p}\boldsymbol{p}_1) &= 0
\end{aligned} \tag{5.6.3}$$

and Σ_{Cl} is defined in (5.5.8). See also Appendix 5.11.2 for an alternative but equivalent derivation using the operator projection method.

(5.6.2) is the key kinetic equation for the colored Coulomb plasma. It still contains considerable information in phase space. A special limit of the classical phase space is the long wavelength or hydrodynamical limit. In this limit, only few moments of the phase space fluctuations δf or equivalently their correlations in $\mathbf{S} \approx \langle \delta f \delta f \rangle$ will be of interest. In particular,

$$\begin{aligned}
\boldsymbol{n}(t,\boldsymbol{r}) &= \int d\boldsymbol{p}d\boldsymbol{Q}\ \delta f(t,\boldsymbol{r},\boldsymbol{p},\boldsymbol{Q})\\
\boldsymbol{p}(t,\boldsymbol{r}) &= \int d\boldsymbol{p}d\boldsymbol{Q}\,\boldsymbol{p}\,\delta f(t,\boldsymbol{r},\boldsymbol{p},\boldsymbol{Q})\\
\mathbf{e}(t,\boldsymbol{r}) &= \int d\boldsymbol{p}d\boldsymbol{Q}\,\frac{p^2}{2m}\,\delta f(t,\boldsymbol{r},\boldsymbol{p},\boldsymbol{Q})
\end{aligned} \tag{5.6.4}$$

The local particle density, 3-momentum and energy (kinetic). The hydrodynamical sector described by the macro-variables (5.6.4) is colorless. An

interesting macro-variable which carries charge representation of SU(2) would be

$$\mathbf{n}_l(t,\boldsymbol{r}) = \frac{1}{2l+1}\sum_m \int d\boldsymbol{r}d\boldsymbol{Q}\, Y_l^m(\boldsymbol{Q})\,\delta f(t,\boldsymbol{r},\boldsymbol{p},\boldsymbol{Q}) \tag{5.6.5}$$

which reduces to the l color density with $l = 0$ being the particle density, $l = 1$ the charged color monopole density, $l = 2$ the charged color quadrupole density and so on. Because of color rotational invariance in the SU(2) colored Coulomb plasma, the constitutive equations for (5.6.5) which amount to charge conservation hold for each l.

To project (5.6.2) onto the hydrodynamical part of the phase space characterized by (5.6.5) and (5.6.4), we define the hydrodynamical projectors

$$\mathcal{P}_H = \sum_{i=1}^{5} |i\rangle\langle i| \qquad\qquad \mathcal{Q}_H = \mathbf{1}_H - \mathcal{P}_H \tag{5.6.6}$$

with $1 =$ l-density, $2, 4, 5 =$ momentum and $3 =$ energy as detailed in Appendix 5.11.4. When the $l = 0$ particle density is retained in (5.6.6) the projection is on the colorless sector of the phase space. When the $l = 1$ charged monopole density is retained in (5.6.6) the projection is on the plasmon channel, and so on. Most of the discussion to follow will focus on projecting on the canonical hydrodynamical phase space (5.6.4) with $l = 0$ or singlet representation. The inclusion of the $l \neq 0$ representations of SU(2) is straightforward.

Formally (5.6.1) can be viewed as a $\boldsymbol{p} \times \boldsymbol{p}_1$ matrix in momentum space

$$(z - \Sigma_l(z\boldsymbol{k}))\ \mathbf{S}_l(z\boldsymbol{k}) = \mathbf{S}_{0l}(\boldsymbol{k}) \tag{5.6.7}$$

The projection of the matrix equation (5.6.7) follows the same procedure as in Appendix 5.11.2. The result is

$$(z - \mathcal{P}_H \Sigma_l(z\boldsymbol{k})\mathcal{P}_H - \mathcal{P}_H \Theta_l(z\boldsymbol{k})\mathcal{P}_H)\, \mathcal{P}_H \mathbf{S}_l(z\boldsymbol{k})\mathcal{P}_H = \mathcal{P}_H \mathbf{S}_{0l}(k)\mathcal{P}_H \tag{5.6.8}$$

with

$$\Theta_l = \Sigma_l(z\boldsymbol{k})\mathcal{Q}_H(z - \mathcal{Q}_H \Sigma_H(z\boldsymbol{k})\mathcal{Q}_H)^{-1}\mathcal{Q}_H \Sigma_l(z\boldsymbol{k}) \tag{5.6.9}$$

If we define the hydrodynamical matrix elements

$$\begin{aligned}
\mathbf{G}_{lij}(z\boldsymbol{k}) &= \langle i|\mathbf{S}_l(z\boldsymbol{k})|j\rangle \\
\Sigma_{lij}(z\boldsymbol{k}) &= \langle i|\Sigma_l(z\boldsymbol{k})|j\rangle \\
\Theta_{lij}(z\boldsymbol{k}) &= \langle i|\Theta_l(z\boldsymbol{k})|j\rangle \\
\mathbf{G}_{0lij}(z\boldsymbol{k}) &= \langle i|\mathbf{S}_{0l}(\boldsymbol{k})|j\rangle
\end{aligned} \tag{5.6.10}$$

then (5.6.8) reads

$$(z\delta_{ii'} - \Omega_{lij}(z\boldsymbol{k}))\ \mathbf{G}_{lji'}(z\boldsymbol{k}) = \mathbf{G}_{0lii'}(\boldsymbol{k}) \tag{5.6.11}$$

with $\Omega_l = \Sigma_l + \Theta_l$. (5.6.11) takes the form of a dispersion for each color partial wave l with the projection operator (5.6.6) set by the pertinent density (5.6.5). The contribution Σ_l to Ω_l will be referred to as *direct* while the contribution Θ_l will be referred to as *indirect*.

5.7 Hydrodynamical Modes

The zeros of (5.6.11) are the hydrodynamical modes originating from the Liouville equation for the time-dependent structure factor. The equation is closed under the free streaming approximation with half renormalized vertices as we detailed above.

We start by analyzing the 2 transverse modes with $i = T$ in (5.6.10) and (5.6.11). We note with [37] that $\mathbf{G}_{lTi} = 0$ whenever $T \neq i$. The hydrodynamical projection (see Appendix 5.11.4) causes the integrand to be odd whatever l. The 2 independent transverse modes in (5.6.11) decouple from the longitudinal $i = L$, the (kinetic) energy $i = E$ and particle density $i = N$ modes for all color projections. Thus

$$\mathbf{G}_{lT}(z\boldsymbol{k}) = \frac{1}{z - \Omega_{lT}(z\boldsymbol{k})} \tag{5.7.1}$$

with $\Omega_{lT} = \langle T|\Omega_l|T\rangle$ and $\mathbf{G}_{lT} = \langle T|\mathbf{G}_l|T\rangle$. The hydro-projected time-dependent l structure factor for fixed frequency $z = \omega + i0$, wavenumber k develops 2 transverse poles

$$z_l(\boldsymbol{k}) = \Omega_{lT}(z\boldsymbol{k}) \approx \mathcal{O}(k^2) \tag{5.7.2}$$

The last estimate follows from O(3) momentum symmetry under statistical averaging whatever the color projection. We identify the transverse poles in (5.7.2) with 2 shear modes of consititutive dispersion

$$\omega + i\frac{\eta_l}{mn}k^2 + \mathcal{O}(k^3) = 0 \tag{5.7.3}$$

with η_l the shear viscosity for the lth color representation. Unlike conventional

plasmas, the classical SU(2) color Coulomb plasma admits an infinite hierarchy of shear modes for each representation l.

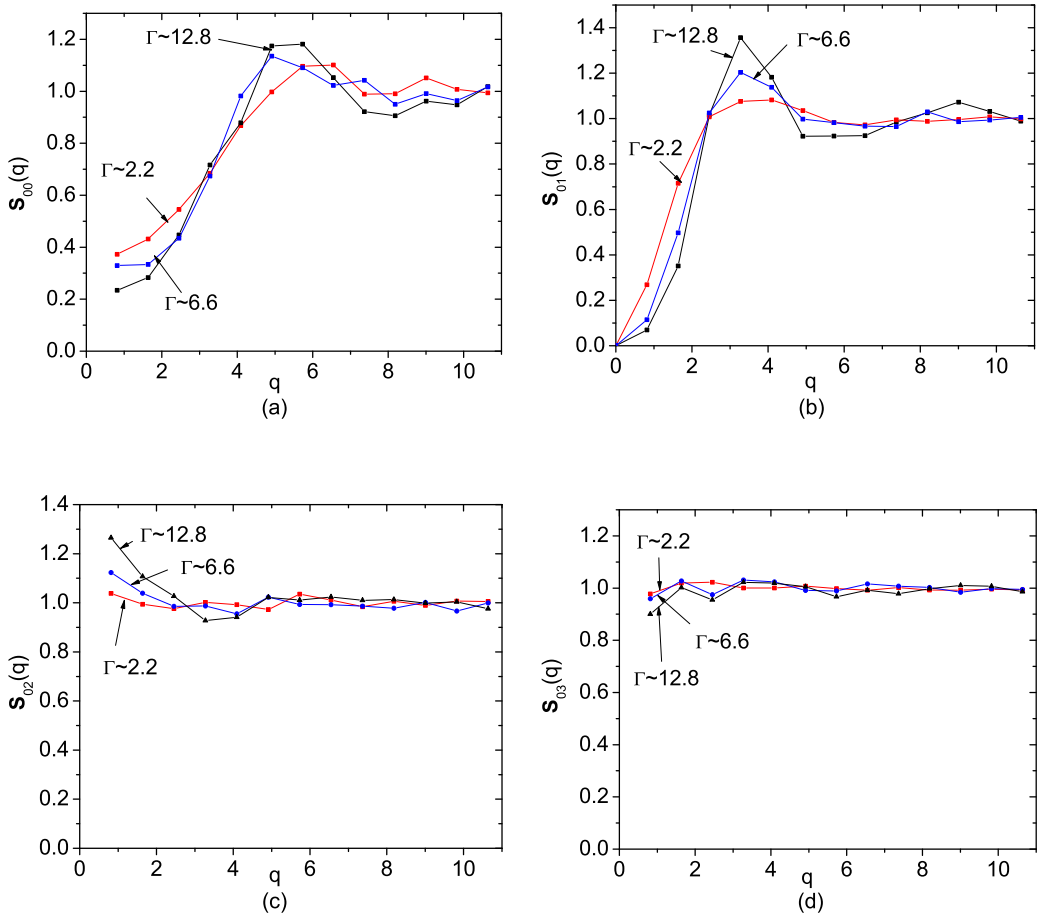

Figure 5.1: $\mathbf{S}_{0l}(q)$ from SU(2) Molecular Dynamics.

The remaining 3 hydrodynamical modes L, E, N are more involved as they mix in (5.6.11) and under general symmetry consideration. Indeed current conservation, ties the L mode to the N mode for instance. Most of the symmetry arguments regarding the generic nature of Ω_l in [37] carry to our case for each color representation. Thus, for the 3 remaining non-transverse modes (5.6.11) reads in matrix form

$$\begin{pmatrix} \mathbf{G}_{lNN} & \mathbf{G}_{lNL} & \mathbf{G}_{lNE} \\ \mathbf{G}_{lLN} & \mathbf{G}_{lLL} & \mathbf{G}_{lLE} \\ \mathbf{G}_{lEN} & \mathbf{G}_{lEL} & \mathbf{G}_{lEE} \end{pmatrix}$$
$$= \begin{pmatrix} z & -\Omega_{lNL} & 0 \\ -\Omega_{lLN} & z-\Omega_{lLL} & -\Omega_{lLE} \\ 0 & -\Omega_{lEL} & z-\Omega_{lEE} \end{pmatrix}^{-1} \begin{pmatrix} 1+n\,\mathbf{h}_l & 0 & 0 \\ 0 & 1 & 0 \\ 0 & 0 & 1 \end{pmatrix} \quad (5.7.4)$$

The 3 remaining hydrodynamical modes are the zeros of the determinant

$$\Delta_l = \begin{vmatrix} z & -\Omega_{lNL}(zk) & 0 \\ -\Omega_{lLN}(zk) & z-\Omega_{lLL}(zk) & -\Omega_{lLE}(zk) \\ 0 & -\Omega_{lEL}(zk) & z-\Omega_{lEE}(zk) \end{vmatrix} = 0 \quad (5.7.5)$$

(5.7.5) admits infinitly many solutions $z_l(k)$. We seek the hydrodynamical solutions as analytical solutions in k for small k, ie. $z(k) = \sum_n z_{ln} k^n$ for each SU(2) color representation l. In leading order, we have

$$\Delta_l \approx z_{l0}\left(z_{l0}^2 - \frac{k^2 T}{m}\,\mathbf{S}_{0l}^{-1}(k \approx 0)\right) \approx 0 \quad (5.7.6)$$

after using the symmetry properties of Ω_l as in [37] for each l. We have also made use of the generalized Ornstein-Zernicke equations for each l representation [31] In Fig. 6.2 we show the molecular dynamics simulation results for 4 typical structure factors [31]

$$\mathbf{S}_{0l}(\boldsymbol{k}) = \left(\frac{4\pi}{2l+1}\right)\left\langle \left| \sum_{jm} e^{i\boldsymbol{k}\cdot\boldsymbol{x}_j(0)}\, Y_l^m(\boldsymbol{Q}_i) \right|^2 \right\rangle \quad (5.7.7)$$

for $l = 0, 1, 2, 3$. We have made use of the dimensionless wavenumber $q =$

$k\,a_{WS}$ with a_{WS} is the Wigner-size radius. In Fig. 5.2 we show the analytical result for $\mathbf{S}_{01}$ which we will use for the numerical estimates below. We note that the $l = 1$ structure factor which amounts to the monopole structure factor vanishes at $k = 0$. All other l's are finite at $k = 0$ with $l = 0$ corresponding to the density structure factor.

(5.7.6) displays 3 hydrodynamical zeros as $k \to 0$ for each l representation. One is massless and we identify it with the diffusive heat mode. The molecular dynamics simulations of the structure factors in Fig. 6.2 implies that all $l \neq 0$ channels are sound dominated with two massless modes, while the $l = 1$ is plasmon dominated with two massive longitudinal plasmon states. Thus

$$z_{l\pm} = \pm\omega_p^2\delta_{l1} \tag{5.7.8}$$

with $\omega_p = k_D\sqrt{T/m}$ the plasmon frequency. The relevance of this channel to the energy loss has been discussed in [38]. We used $\mathbf{S}_{01}(k \approx 0) \approx k^2/k_D^2$ with k_D^2 the squared Debye momentum. All even $l \neq 1$ are contaminated by the sound modes. The SU(2) classical and colored Coulomb plasma supports plasmon oscillations even at strong coupling. These modes are important in the attenuation of soft monopole color oscilations.

5.8 Shear Viscosity

The transport parameters associated to the SU(2) classical and colored Coulomb plasma follows from the hydrodynamical projection and expansion discussed above. This includes, the heat diffusion coefficient, the transverse shear viscosity and the longitudinal plasmon frequency and damping parameters. In this section, we discuss explicitly the shear viscosity coefficient for the SU(2)

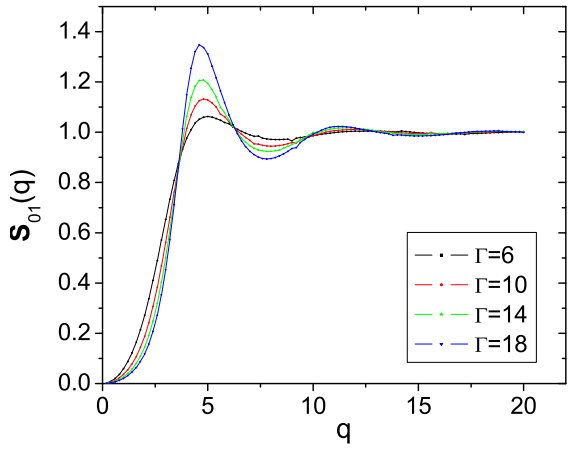

Figure 5.2: $\mathbf{S}_{01}(q)$ for different Γ [31]

.

colored Coulomb plasma.

Throughout, we define $\lambda = \frac{4}{3}\pi(3\Gamma)^{3/2}$, the bare Coulomb interaction $\bar{V}_l = k_0^2/l^2$ in units of the Wigner-size radius $k_0^{-1} = a_{WS}$. While varying the Coulomb coupling

$$\Gamma = \frac{g^2}{4\pi}\beta\frac{C_2}{a_{WS}} \tag{5.8.1}$$

all length scales will be measured in $a_{WS} = (4\pi n/3)^{-1/3}$, all times in the inverse plasmon frequency $1/\omega_p$ with $\omega_p^2 = \kappa_D^2/m\beta = ng^2C_2/m$. All units of mass will be measured in m. The Debye momentum is $\kappa_D^2 = g^2n\beta C_2$ and the plasma density is n. for instance, the shear viscosity will be expressed in fixed dimensionless units of $\eta_* = nm\omega_p a_{WS}^2$.

The transverse shear viscosity follows from (5.7.1) with Σ_l contributing to the direct or hydrodynamical part, and Θ_l contributing to the indirect or single-particle part. For $l = 0$

$$\frac{\eta_0}{\eta^*} = \frac{\eta_{0\,dir}}{\eta^*} + \frac{\eta_{0\,ind}}{\eta^*} \tag{5.8.2}$$

respectively. The direct or hydrodynamical contribution is likely to be dominant at strong coupling, while the indirect or single-particle contribution is likely to take over at weak coupling. We now proceed to show that.

The indirect contribution to the viscosity follows from the contribution outside the hydrodynamical subspace through $\mathcal{Q}_H$ and lumps the single-particle phase contributions. It involves the inversion of $\mathcal{Q}_H\Sigma_{C0}\mathcal{Q}_H$ in (5.11.16) with

$$\eta_{0\text{ind}} = \lim_{k\to 0}\frac{mn}{k^2}\frac{|\langle t|\Sigma_0|tl\rangle|^2}{\langle tl|i\Sigma_0|tl\rangle} = \lim_{k\to 0}\frac{mn}{k^2}\frac{|\langle t|(\Sigma_{00}+\Sigma_{C0})|tl\rangle|^2}{\langle tl|i\Sigma_{C0}|tl\rangle} \tag{5.8.3}$$

In short we expand Σ_{C0} in terms of generalized Hermite polynomials, with the first term identified with the stress tensor due to the projection operator (5.11.21). The inversion follows by means of the first Sonine polynomial expansion. Explicitly

$$\eta_{ind} = \frac{\eta_{0\,ind}}{\eta_*} = nm\lim_{k\to 0}\frac{1}{k^2}\frac{|\langle t|\Sigma_{00}+\Sigma_{C0}(\boldsymbol{k},0)|lt\rangle|^2}{\langle lt|i\Sigma_{C0}(\boldsymbol{k},0)|lt\rangle} = \frac{(1+\lambda I_2)^2}{\lambda I_3} \tag{5.8.4}$$

with

$$\begin{aligned} I_2 &= \frac{1}{60\pi^2}\frac{1}{(3\Gamma)^{1/2}}\int_0^\infty dq\Big(2(\mathbf{S}_{01}(q)^2-1)+(1-\mathbf{S}_{01}(q))\Big) \\ I_3 &= \frac{1}{10\pi^{3/2}}\frac{1}{3\Gamma}\int_0^\infty dqq(1-\mathbf{S}_{01}(q)) \end{aligned} \tag{5.8.5}$$

with the dimensionless wave number $q = ka_{WS}$.

We recall that $\mathbf{S}_{01}$ is the monopole structure factor discussed in [31] both analytically and numerically. In Fig. 5.2 we show the behavior of the static monopole structure factor from [31] for different Coulomb couplings. The larger Γ the stronger the first peak, and the oscillations. These features characterize the onset of the crystalline structure in the SU(2) colored Coulomb plasma. A good fit to Fig. 5.2 follows from the following parametrization

$$1 + C_0 e^{-q/C_1} \sin\left((q - C_2)/C_3\right) \tag{5.8.6}$$

with 4 parameters $C_{0,1,2,3}$. The fit following from (5.8.6) extends to $q \approx 100$ within 10^{-5} accuracy, thanks to the exponent.

The direct contribution to the shear viscosity follows from similar arguments. From (5.7.1) and (5.7.3), we have in the zero momentum limit

$$\eta_{0\,dir} = \lim_{k\to 0} \frac{mn}{k^2} \langle t|i\Sigma_0|t\rangle = \lim_{k\to 0} \frac{mn}{k^2} \langle t|i\Sigma_{C0}(0,0)|t\rangle \tag{5.8.7}$$

with $\Sigma_0 = \Sigma_{00} + \Sigma_{I0} + \Sigma_{C0}$ as defined in (5.6.3) and (5.5.8). Only those nonvanishing contributions after the hydrodynamical projection were retained in the second equalities in (5.8.3) as we detail in Appendix 5.11.4. A rerun of the arguments yields

$$\eta^*_{dir} = \eta_{0\,dir}/\eta_* = \lambda\frac{\omega_p}{\kappa_D^3}\lim_{k\to 0}\frac{1}{\boldsymbol{k}^2}\int\frac{d\boldsymbol{l}}{(2\pi)^3}\int_0^\infty dtn(\boldsymbol{\epsilon}\cdot\boldsymbol{l})^2$$
$$\times \left(\mathbf{c}_{D1}(l)\mathcal{G}_{n1}(\boldsymbol{k}-\boldsymbol{l},t)\mathcal{G}_{n1}(\boldsymbol{l},t)\bar{V}_{\boldsymbol{l}} - \mathbf{c}_{D0}(l)\mathcal{G}_{n1}(\boldsymbol{k}-\boldsymbol{l},t)\mathcal{G}_{n1}(\boldsymbol{l},t)\bar{V}_{\boldsymbol{k}-\boldsymbol{l}}\right) \tag{5.8.8}$$

The projected non-static structure factor is

$$\mathcal{G}_{n1}(\boldsymbol{l},t) = \frac{1}{n}\int d\boldsymbol{p}d\boldsymbol{p}'\,\mathbf{S}_1(\boldsymbol{l},t;\boldsymbol{p}\boldsymbol{p}') = \overline{\mathcal{G}}_{n1}(\boldsymbol{l},t)\,\mathbf{S}_{01}(\boldsymbol{l}) \tag{5.8.9}$$

with the normalization $\overline{\mathcal{G}}_{n1}(\boldsymbol{l},0) = 1$. As in the one component Coulomb plasma studied in [39] we will approximate the dynamical part by its intermediate time-behavior where the motion is free. This consists in solving (5.4.1) with no self-energy kernel or $\Sigma = 0$,

$$\mathcal{G}_{n1}(\boldsymbol{l},t) \approx e^{-(lt)^2/2m\beta}\,\mathbf{S}_{01}(\boldsymbol{l}) \tag{5.8.10}$$

Thus inserting (5.8.10) and performing the integrations with $k \to 0$ yield the direct contribution to the shear viscosity

$$\eta^*_{dir} = \frac{\eta_{dir}}{\eta_0} = \frac{\sqrt{3}}{45\pi^{1/2}}\Gamma^{\frac{1}{2}} \tag{5.8.11}$$

The full shear viscosity result is then

$$\frac{\eta_0}{\eta^*} = \frac{\eta_{0\,dir}}{\eta^*} + \frac{\eta_{0\,ind}}{\eta^*} = \frac{\sqrt{3}}{45\pi^{1/2}}\Gamma^{\frac{1}{2}} + \frac{(1+\lambda I_2)^2}{\lambda I_3} \tag{5.8.12}$$

after inserting (5.8.4) and (5.8.11) in (5.8.2). The result (5.8.12) for the shear

viscosity of the transverse sound mode is analogous to the result for the sound velocity in the one component plasma derived initially in [36] with two differences: 1/ The SU(2) Casimir in Γ; 2/ the occurrence of $\mathbf{S}_{01}$ instead of $\mathbf{S}_{00}$. Since $\mathbf{S}_{01}$ is plasmon dominated at low momentum, we conclude that the shear viscosity is dominated by rescattering against the SU(2) plasmon modes in the cQGP.

Using the fitted monopole structure factor (5.8.6) in (5.8.5) we can numerically assess (5.8.4) for different values of Γ. Combining this result for the indirect viscosity together with (5.8.11) for the direct viscosity yield the colorless or sound viscosity η_0. The values of η_0 are displayed in Table I, and shown in Fig. 5.3 (black). The SU(2) molecular dynamics simulations in [3] which are parameterized as

$$\eta^*_{MD} \simeq 0.001\Gamma + \frac{0.242}{\Gamma^{0.3}} + \frac{0.072}{\Gamma^2} \tag{5.8.13}$$

are also displayed in Table I and shown in Fig. 5.3 (red) for comparison. The sound viscosity dips at about $\Gamma \approx 8$ in our analytical estimate. To understand the origin of the minimum, we display in Fig. 5.4 the scaling with Γ of the direct or hydrodynamical and the indirect part of the shear viscosity. The direct contribution to the viscosity grows like $\Gamma^{1/2}$, the indirect contribution drops like $1/\Gamma^{5/2}$. The latter dominates at weak coupling, while the former dominates at strong coupling. This is indeed expected, since the direct part is the contribution from the hydrodynamical part of the phase space, while the indirect part is the contribution from the non-hydrodynamical or single-particle part of phase space. The crossing is at $\Gamma \approx 4$.

The reduced sound velocity η_* is dimensionless. To restore dimensional-

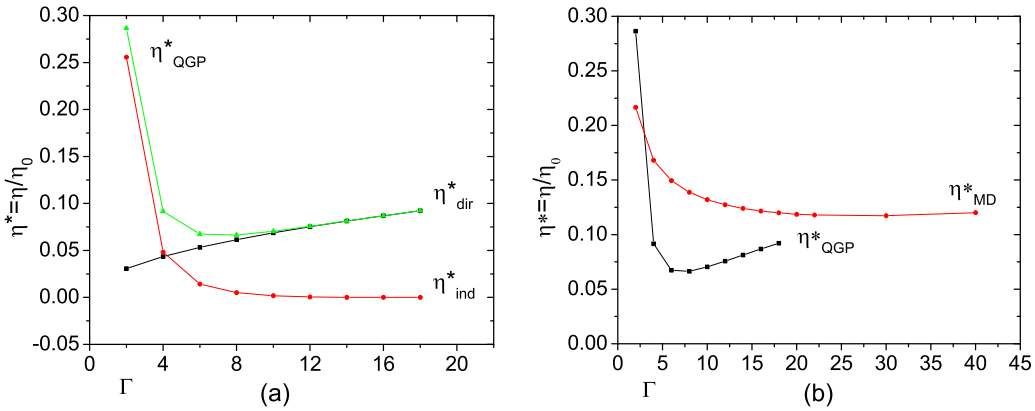

Figure 5.3: The direct and indirect part of the viscosity

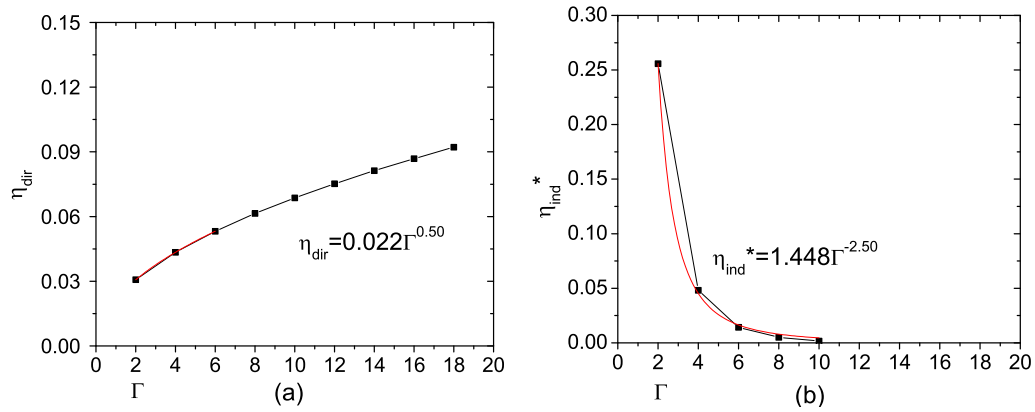

Figure 5.4: The best fit of the direct and indirect part of the viscosity

Table 5.1: Reduced shear viscosity. See text.

Γ	2	4	6	8	10	12	14	16	18
η^*_{QGP}	0.286	0.092	0.067	0.066	0.070	0.076	0.081	0.087	0.092
η_{MD}	0.217	0.168	0.168	0.139	0.132	0.127	0.124	0.122	0.120

ity and compare with expectations for an SU(2) colored Coulomb plasma, we first note that the particle density is about $3 \times 0.244\,T^3 = 0.732\,T^3$. There are 3 physical gluons, each carrying black-body density. The corresponding Wigner-Seitz radius is then $a_{WS} = (3/4\pi n)^{1/3} \approx 0.688/T$. The

Coulomb coupling is $\Gamma \approx 1.453\,(g^2N_c/4\pi)$. Since the plasmon frequency is $\omega_p^2 = \kappa_D^2/m\beta = ng^2N_c/m$, we get $\omega_p^2 \simeq 3.066\,T^2(g^2N_c/4\pi)$ with $m \simeq 3T$. The unit of viscosity $\eta_0 = nm\omega_p a_{WS}^2$ translates to $1.822\,T^3(g^2N_c/4\pi)^{1/2}$. In these units, the viscosity for the SU(2) cQGP dips at about 0.066 which is $\eta^*_{QGP} \approx 0.066\,\eta_0 \approx 0.120\,T^3\,(g^2N_c/4\pi)^{1/2}$. Since the entropy in our case is $\sigma = 6\,(4\pi^2/90)T^3$, we have for the SU(2) ratio $\eta/\sigma|_{SU(2)} = 0.046\,(g^2N_c/4\pi)^{1/2}$. The minimum in the viscosity occurs at $\Gamma = 1.453\,(g^2N_c/4\pi) \approx 8$, so that $(g^2N_c/4\pi)^{1/2} \approx 2.347$. Thus, our shear viscosity to entropy ratio is $\eta/\sigma|_{SU(2)} \simeq 0.107$. A rerun of these estimates for SU(3) yields $\eta/\sigma|_{SU(3)} \simeq 0.078$ which is lower than the bound $\eta/\sigma = 1/4\pi \simeq 0.0795$ suggested from holography.

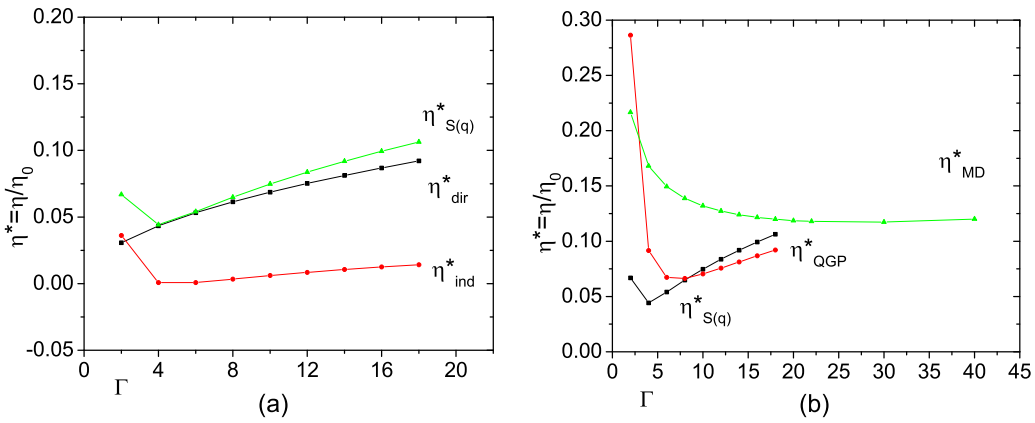

Figure 5.5: Comparison with weak coupling. See text.

Finally, we show in Fig. 5.5 the shear viscosity $\eta*_{S(q)}$ at low Γ (a:green) and large Γ (b:black) assessed using the weak-coupling structure factor $S(k) = k^2/(k^2 + k_D^2)$. The discrepancy is noticeable for Γ near the liquid point. The large discrepancy for small values of Γ reflects on the fact that the integrals in (5.8.5) are infrared sensitive. The sensitivity is tamed by our analytical structure factor and the simulations. We recall that in weak coupling, the Landau viscosity η_L is [40]

$$\frac{\eta_L}{\eta^*} = \frac{5\sqrt{3\pi}}{18}\frac{1}{\Gamma^{5/2}}\frac{1}{\ln(r_D/r_0)} \tag{5.8.14}$$

which follows from a mean-field analysis of the kinetic equation with the plasma dielectric constant set to 1. The logarithmic dependence in (5.8.14) reflects on the infrared and ultraviolet sensitivity of the mean-field approximation. Typically $r_D = 1/k_D$ and $r_0 = (g^2 C_2/4\pi)\beta$ which are the Debye length and the the distance of closest approach. Thus

$$\frac{\eta_L}{\eta^*} \approx \frac{5\sqrt{3\pi}}{27}\frac{1}{\Gamma^{5/2}}\frac{1}{\ln(1/\Gamma)} \tag{5.8.15}$$

or $\eta_L/\eta^* \approx 0.6/(\Gamma^{5/2}\ln(1/\Gamma))$ which is overall consistent with our analysis.

The Landau or mean-field result is smaller for the viscosity than the result from perturbative QCD. Indeed, the unscaled Landau viscosity (5.8.15) reads

$$\eta_L \approx \frac{10}{24}\frac{\sqrt{m}}{(\alpha_s C_2)^2\beta^{5/2}}\frac{1}{\alpha_s} \tag{5.8.16}$$

after restoring the viscosity unit $\eta^* = nm\omega_p a_{WS}^2$ and using $\ln(r_D/r_0) \approx 3\ln(1/\alpha_s)/2$ with $\alpha_s = g^2/4\pi$. While our consituent gluons carry $m \approx \pi T$, in the mean field or weak coupling we can set their masses to $m \approx gT$. With this in mind, and setting $C_2 = N_c = 3$ in (5.8.16) we obtain

$$\eta_L \approx \frac{5\sqrt{2}}{108\pi^{1/4}}\frac{T^3}{\alpha_s^{7/4}\ln(1/\alpha_s)} \approx 0.05\frac{T^3}{\alpha_s^{7/4}\ln(1/\alpha_s)} \tag{5.8.17}$$

which is to be compared with the QCD weak coupling result [41]

$$\eta_{QCD} \approx \frac{T^3}{\alpha_s^2\ln(1/\alpha_s)} \tag{5.8.18}$$

The mean-field result (5.8.17) is $\alpha_s^{1/4} \approx \sqrt{g}$ *smaller* in weak coupling than the QCD perturbative result. The reason is the fact that in perturbative QCD the viscosity is not only caused by collisions with the underlying parton constituents, but also quantum recombinations and decays. These latter effects are absent in our classical QGP.

5.9 Diffusion Constant

The calculation of the diffusion constant in the SU(2) plasma is similar to that of the shear viscosity. The governing equation is again (5.3.7) with Σ and $\mathbf{S}$ replaced by Σ_s, $\mathbf{S}_s$. The label is short for single particle. The difference between $\mathbf{S}$ and $\mathbf{S}_s$ is the substitution of (5.2.7) by

$$f_s(\boldsymbol{r}\boldsymbol{p}\boldsymbol{Q}t) = \sqrt{N}\delta(\boldsymbol{r} - \boldsymbol{r}_1(t))\delta(\boldsymbol{p} - \boldsymbol{p}_1(t))\delta(\boldsymbol{Q} - \boldsymbol{Q}_1(t)) \tag{5.9.1}$$

The diffusion constant follows from the velocity auto-correlator

$$V_D(t) = \frac{1}{3}\langle \boldsymbol{V}(t) \cdot \boldsymbol{V}(0)\rangle \tag{5.9.2}$$

through

$$D = \int_0^\infty dt V_D(t) \tag{5.9.3}$$

Solving (5.3.7) using the method of one-Sonine polynomial approximation as in [39] yields the Langevin-like equation

$$\frac{dV_D(t)}{dt} = -\int_0^t dt' M(t') V_D(t - t') \tag{5.9.4}$$

with the memory kernel tied to Σ^S_{C0},

$$
\begin{aligned}
&n\, f_0(\boldsymbol{p}')\, \Sigma^S_{Cl}(t, \boldsymbol{k}, \boldsymbol{p}\boldsymbol{p}') \\
&= -\frac{1}{\beta} \int d\boldsymbol{p}_1 d\boldsymbol{p}_2 \int \frac{d\boldsymbol{l}}{(2\pi)^3} \boldsymbol{l} \cdot \nabla_{\boldsymbol{p}} \boldsymbol{l} \cdot \nabla_{\boldsymbol{p}'} \mathbf{c}_{D1}(l) V_{\boldsymbol{l}} \\
&\times \Big(\frac{l}{2l+1} \mathbf{S}^S_{l-1}(t, \boldsymbol{k} - \boldsymbol{l}, \boldsymbol{p}\boldsymbol{p}') \mathbf{S}_1(t, \boldsymbol{l}, \boldsymbol{p}_1 \boldsymbol{p}_2) \\
&+ \frac{l+1}{2l+1} \mathbf{S}^S_{l+1}(t, \boldsymbol{k} - \boldsymbol{l}, \boldsymbol{p}\boldsymbol{p}') \mathbf{S}_1(t, \boldsymbol{l}, \boldsymbol{p}_1 \boldsymbol{p}_2) \Big)
\end{aligned}
\tag{5.9.5}
$$

and

$$
\begin{aligned}
&n\, f_0(\boldsymbol{p}')\, \Sigma^S_{C0}(t, \boldsymbol{k} = \mathbf{0}, \boldsymbol{p}\boldsymbol{p}') \\
&= -\frac{1}{\beta} \int d\boldsymbol{p}_1 d\boldsymbol{p}_2 \int \frac{d\boldsymbol{l}}{(2\pi)^3} \boldsymbol{l} \cdot \nabla_{\boldsymbol{p}} \boldsymbol{l} \cdot \nabla_{\boldsymbol{p}'} \mathbf{c}_{D1}(l) V_{\boldsymbol{l}} \mathbf{S}^S_1(t, \boldsymbol{l}, \boldsymbol{p}\boldsymbol{p}') \mathbf{S}_1(t, \boldsymbol{l}, \boldsymbol{p}_1 \boldsymbol{p}_2)
\end{aligned}
\tag{5.9.6}
$$

therefore

$$
M(t) = \frac{\beta}{3m} \int d\boldsymbol{p} d\boldsymbol{p}' \boldsymbol{p} \cdot \boldsymbol{p}' \Sigma^S_{C0}(t, \boldsymbol{k} = \mathbf{0}, \boldsymbol{p}\boldsymbol{p}') f_0(\boldsymbol{p}') \tag{5.9.7}
$$

which clearly projects out the singlet color contribution. If we introduce the dimensionless diffusion constant, $D^* = D/w_p a^2_{WS}$, then (5.9.3) together with (5.9.4) yield

$$
\frac{1}{D} = m\beta \int_0^\infty dt M(t) \rightarrow \frac{1}{D^*} = 3\Gamma \int_0^\infty w_p dt \frac{M(t)}{w_p^2} = 3\Gamma \int_0^\infty d\tau \bar{M}(\tau) \tag{5.9.8}
$$

Using similar steps as for the derivation of the viscosity, we can unwind the self-energy kernel Σ_s in (5.9.8) to give

$$\frac{1}{D^*} = -\Gamma \int \frac{d\boldsymbol{l}}{(2\pi)^3} \int_0^\infty d\tau \boldsymbol{l}^2 \mathbf{c}_{D1}(l) V_{\boldsymbol{l}} \mathcal{G}^S_{n1}(l,t)\, \mathcal{G}_{n1}(l,t) \tag{5.9.9}$$

where we have used the same the half-renormalization method discussed above for the viscosity. The color integrations are done by Legendre transforms. Here again, we separate the time-dependent structure factors as $\mathcal{G}_{n1}(l,t) = \mathbf{S}_{01}(l)\bar{\mathcal{G}}_{n1}(l,t)$ and $\mathbf{S}^S_{01}(l,t) = \bar{\mathcal{G}}_{n1}(l,t)$ in the free particle approximation. Thus

$$\frac{1}{D^*} = \Gamma^{3/2}\Big(\frac{1}{3\pi}\Big)^{\frac{1}{2}} \int_0^\infty dq q(1 - \mathbf{S}_{01}(q)) \tag{5.9.10}$$

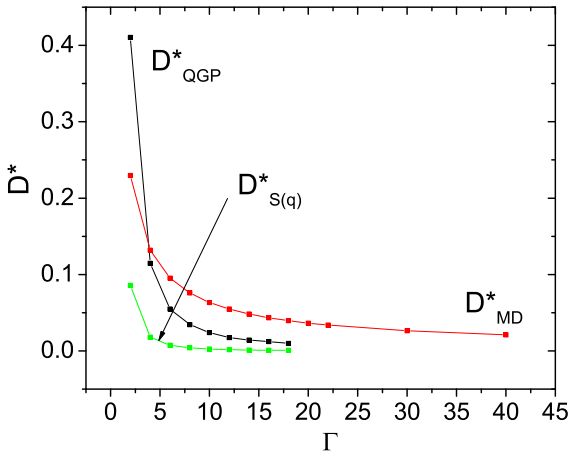

Figure 5.6: Diffusion Constant (black, green) versus molecular dynamics simulations (red). See text.

The results following from (5.9.10) are displayed in Table 5.2 and in Fig. 5.6 (black) from weak to strong coupling. For comparison, we also show the the diffusion constant measured using molecular dynamics simulations with an SU(2) colored Coulomb plasma [3]. The molecular dynamics simulations are

Table 5.2: Diffusion constant. See text.

Γ	2	4	6	8	10	12	14	16	18
D^*_{QGP}	0.410	0.115	0.055	0.034	0.024	0.017	0.014	0.012	0.010
D^*_{MD}	0.230	0.132	0.095	0.076	0.063	0.055	0.048	0.044	0.040

fitted to

$$D^* \simeq \frac{0.4}{\Gamma^{0.8}} \tag{5.9.11}$$

For comparison, we also show the diffusion constant (5.9.10) assessed using the weak coupling or Debye structure factor $S(k) = k^2/(k^2 + k_D^2)$ in Fig. 5.6 (green). The discrepancy between the analytical results at small Γ are similar to the ones we noted above for the shear viscosity. In our correctly resummed structure factor of Fig. 5.2, the infrared behavior of the cQGP is controlled in contrast to the simple Debye structure factor.

Finally, a comparison of (5.9.10) to (5.8.5) shows that $1/D^* \approx 1/\lambda I_3$ which is seen to grow like $\Gamma^{3/2}$. Thus D^* drops like $1/\Gamma^{3/2}$ which is close to the numerically generated result fitted in Fig. 5.7 (left). The weak coupling self-diffusion coefficient scales as $1/\Gamma^{5/2}$ as shown in Fig. 5.7 (right). More importantly, the diffusion constant in the SU(2) colored Coulomb plasma is caused solely by the non hydrodynamical modes or single particle collisions in our analysis. It does not survive at strong coupling where most of the losses are caused by the collective sound and/or plasmon modes. This result is in contrast with the shear viscosity we discussed above, where the hydrodynamical modes level it off at large Γ.

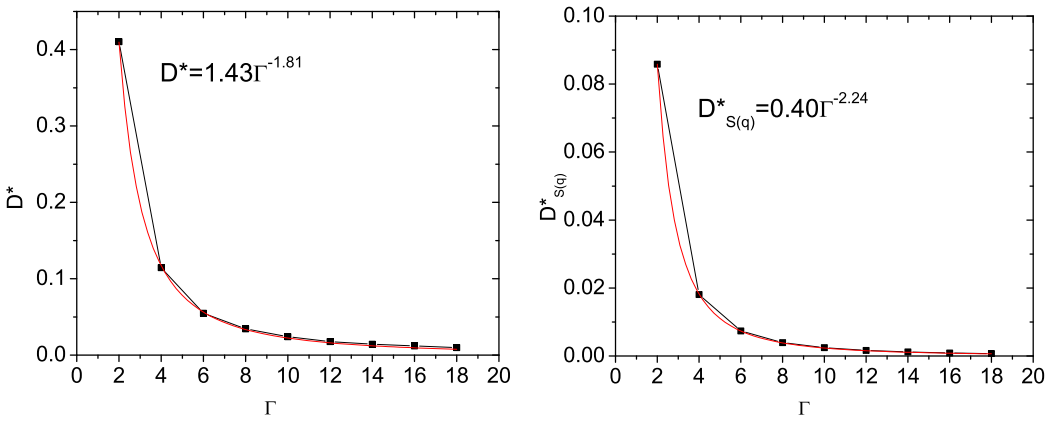

Figure 5.7: Fit to the diffusion constant. See text.

5.10 Conclusions

We have provided a general framework for discussing non-perturbative many-body dynamics in the colored SU(2) Coulomb plasma introduced in [23]. The framework extends the analysis developed intially for one-component Abelian plasmas to the non-Abelian case. In the latter, the Liouville operator is supplemented by a color precessing contribution that contributes to the connected part of the self-energy kernel.

The many-body content of the SU(2) colored Coulomb plasma are best captured by the Liouville equation in phase space in the form of an eigenvalue-like equation. Standard projected perturbation theory like analysis around the static phase space distributions yield a resummed self energy kernel in closed form. Translational space invariance and rigid color rotational invariance in phase space simplifies the nature of the kernel.

In the hydrodynamical limit, the phase space projected equations for the time-dependent and resummed structure factor displays both transverse and longitudinal hydrodynamical modes. The shear viscosity and longitudinal dif-

fusion constant are expressed explicitly in terms of the resummed self-energy kernel. The latter is directly tied with the interacting part of the Liouville operator in color space. We have shown that in the free streaming approximation and half-renormalized Liouville operators, the transport parameters are finite.

We have explicitly derived the shear viscosity and longitudinal diffusion constant of the SU(2) colored Coulomb plasma in terms of the monopole static structure factor and the for all values of the classical Coulomb parameter $\Gamma = V/K$, the ratio of the potential to kinetic energy per particle. The results compare fairly with molecular dynamics simulations for SU(2).

The longitudinal diffusion constant is found to drop from weak to strong coupling like $1/\Gamma^{3/2}$. The shear viscosity is found to reach a minimum for Γ of about 8. The large increase at weak coupling is the result of the large mean free paths and encoded in the direct or driving part of the connected self-energy. The minimum at intermediate Γ is tied with the onset of hydrodynamics which reflects on the liquid nature of the colored Coulomb plasma in this regime.

At larger values of Γ an SU(2) crystal forms as reported in [23]. Our current analysis should be able to account for the emergence of elasticities, with in particular an elastic shear mode. This point will be pursued in a future investigation. The many body analysis presented in this work treats the color degrees of freedom as massive constituents with a finite mass and a classical SU(2) color charge. The dynamical analysis is fully non-classical. In a way, quantum mechanics is assumed to generate the constituent degrees of freedom with their assigned parameters. While this picture is supported by perturbation theory at very weak coupling, its justification at strong coupling is by no means established.

5.11 Appendix

5.11.1 SU(2) color phase space

A useful parametrization of the SU(2) color phase space is through the canonical variables Q^1, π^1 [4, 12]

$$Q^1 = \cos\phi_1\sqrt{J^2 - \pi_1^2}, \quad Q^2 = \sin\phi_1\sqrt{J^2 - \pi_1^2}, \quad Q^3 = \pi^1 \tag{5.11.1}$$

with Q^2 being a constraint variable fixed by J^2 or the quadratic Casimir with $q_2 = \sum_\alpha^{N_c^2-1} Q^\alpha Q^\alpha$. The conjugate set Q^1, π^1 obeys standard Poisson bracket. The associated phase space measure is

$$dQ = c_R d\pi_1 d\phi_1 J dJ \delta(J^2 - q_2) \tag{5.11.2}$$

where c_R is a representation dependent constant. A simpler parametrization of the phase space is to use

$$dQ = \sin\theta d\theta d\phi \tag{5.11.3}$$

with the normalizations $\int dQ = 4\pi$, $\sum_\alpha Q^\alpha Q^\alpha = 1$ and $\int dQ \boldsymbol{Q}\cdot\boldsymbol{Q} = 4\pi$. The SU(2) Casimir is then restored by inspection.

5.11.2 Projection Method

If we define the phase space density, $\delta f_l^m(\boldsymbol{kp}, t)$

$$\delta f_l^m(\boldsymbol{k}\boldsymbol{p},t)=\sum_{i=1}^{N}e^{-i\boldsymbol{k}\cdot\boldsymbol{r}_i(t)}\delta(\boldsymbol{p}-\boldsymbol{p}_i(t))Y_l^m(\boldsymbol{Q}_i)-nf_0(\boldsymbol{p})\delta_{l0}\delta_{m0}\delta_{\boldsymbol{k}\boldsymbol{0}}Y_0^0 \quad (5.11.4)$$

we can construct structure factor $\mathbf{S}_l(t,\boldsymbol{k},\boldsymbol{p}\boldsymbol{p}')$ for lth partial wave

$$\begin{aligned}
&\frac{4\pi}{2l+1}\sum_m(\delta f_l^{m*}(\boldsymbol{k}\boldsymbol{p},t)|\delta f_l^m(\boldsymbol{k}\boldsymbol{p}',0))\\
&\equiv\frac{4\pi}{2l+1}\sum_m\sum_{i,j}^{N}(e^{-i\boldsymbol{k}\cdot(\boldsymbol{r}_i(t)-\boldsymbol{r}_j(t))}\delta(\boldsymbol{p}-\boldsymbol{p}_i(t))\delta(\boldsymbol{p}'-\boldsymbol{p}_j)Y_l^{m*}(\boldsymbol{Q}_i)Y_l^m(\boldsymbol{Q}_j))\\
&-n^2f_0(\boldsymbol{p})f_0(\boldsymbol{p}')\\
&\equiv\mathbf{S}_l(t,\boldsymbol{k},\boldsymbol{p}\boldsymbol{p}') \qquad (5.11.5)
\end{aligned}$$

Here a scalar product $(A|B)$ is defined as $\langle A^*B\rangle_{eq}$. We follow [37, 42, 43] and recast the formal Liouville equation (5.3.4) in the form of a formal eigenvalue-like equation in phase space

$$\mathbf{S}_l(\boldsymbol{k}z;\boldsymbol{p}\boldsymbol{p}')=(\delta f_l^{m*}(\boldsymbol{k}\boldsymbol{p})|(z-\pounds)^{-1}|\delta f_l^m(\boldsymbol{k}'\boldsymbol{p}')) \quad (5.11.6)$$

The color charge effect by partial waves is represented as l,m in Eq. (5.11.6). If we introduce the projection operator

$$\mathcal{P}=4\pi\sum_{l,m,\boldsymbol{k}}\int d\boldsymbol{p}_1d\boldsymbol{p}_2|\delta f_l^m(\boldsymbol{k},\boldsymbol{p}_1))\mathbf{S}_{0l}^{-1}(\boldsymbol{k},\boldsymbol{p}_1,\boldsymbol{p}_2)\langle\delta f_l^{m*}(\boldsymbol{k},\boldsymbol{p}_2)|=1-\mathcal{Q} \quad (5.11.7)$$

we can check that this projection operator satisfies $\mathcal{P}^2=\mathcal{P}$

$$\begin{aligned}\mathcal{P}^2 &= 4\pi \sum_{l,m,\boldsymbol{k}} \sum_{l',m',\boldsymbol{k}'} \int d\boldsymbol{p}_1 d\boldsymbol{p}_2 d\boldsymbol{p}'_1 d\boldsymbol{p}'_2 |\delta f_l^m(\boldsymbol{k},\boldsymbol{p}_1))\mathbf{S}_{0l}^{-1}(\boldsymbol{k},\boldsymbol{p}_1,\boldsymbol{p}_2) \\ &\times 4\pi(\delta f_l^{m*}(\boldsymbol{k},\boldsymbol{p}_2)|\delta f_{l'}^{m'}(\boldsymbol{k},\boldsymbol{p}'_1))\mathbf{S}_{0l}^{-1}(\boldsymbol{k},\boldsymbol{p}'_1,\boldsymbol{p}'_2)(\delta f_{l'}^{m'*}(\boldsymbol{k},\boldsymbol{p}'_2)| = \mathcal{P}\end{aligned} \tag{5.11.8}$$

because of the translational invariance in space and the rotational invariance in color space,

$$4\pi(\delta f_l^{m*}(\boldsymbol{k},\boldsymbol{p}_2)|\delta f_{l'}^{m'}(\boldsymbol{k},\boldsymbol{p}'_1)) \equiv \delta_{\boldsymbol{k}\boldsymbol{k}'}\delta_{ll'}\delta_{mm'}\mathbf{S}_{0l}(\boldsymbol{k},\boldsymbol{p}_2,\boldsymbol{p}'_1) \tag{5.11.9}$$

The off-diagonal elemenets vanish in the equilibrium averaging due to phase incoherence. Therefore, the projection operator in Eq. (5.11.8) satisfies also $\mathcal{Q}^2 = \mathcal{Q}$ and $\mathcal{P}\mathcal{Q} = \mathcal{Q}\mathcal{P} = 0$. If we define $|F_l^m(\boldsymbol{k}\boldsymbol{p};z))$ as $|F_l^m(\boldsymbol{k}\boldsymbol{p};z)) = (z-\mathcal{L})^{-1}|\delta f_l^m(\boldsymbol{k}\boldsymbol{p}))$ from Eq. (5.11.6), we have

$$\mathcal{P}(z-\mathcal{L})|F_l^m(\boldsymbol{k}\boldsymbol{p};z)) = \mathcal{P}|\delta f_l^m(\boldsymbol{k}\boldsymbol{p})) \tag{5.11.10}$$

$\mathcal{P}$ in Eq. (5.11.8) is the operator which projects phase space function of a multipartle state with l'th partial wave into a single particle state of the same parial wave, $|\delta f_{l'}^{m'}(\boldsymbol{k}\boldsymbol{p}))$, $\mathcal{P}|g_{l'}^{m'}(\boldsymbol{k}\boldsymbol{p})) = |\delta f_{l'}^{m'}(\boldsymbol{k}\boldsymbol{p}))$. Therefore $\mathcal{Q}|\delta f_l^m(\boldsymbol{k}\boldsymbol{p})) = (1-\mathcal{P})|\delta f_l^m(\boldsymbol{k}\boldsymbol{p})) = 0$. With these in mind, we can modify the above equation further using $\mathcal{P}+\mathcal{Q} = I$

$$\begin{aligned}(\mathcal{P}z - \mathcal{P}\mathcal{L}\mathcal{P} - \mathcal{P}\mathcal{L}\mathcal{Q})|F_l^m(\boldsymbol{k}\boldsymbol{p};z)) &= \mathcal{P}|\delta f_l^m(\boldsymbol{k}\boldsymbol{p})) \\ (\mathcal{Q}z - \mathcal{Q}\mathcal{L}\mathcal{P} - \mathcal{Q}\mathcal{L}\mathcal{Q})|F_l^m(\boldsymbol{k}\boldsymbol{p};z)) &= 0\end{aligned} \tag{5.11.11}$$

From these equations, we can extract

$$z\mathcal{P}|F_l^m(\boldsymbol{kp};z)) - \mathcal{P}\mathcal{L}\mathcal{P}|F_l^m(\boldsymbol{kp};z)) - \mathcal{P}\mathcal{L}\mathcal{Q}(z-\mathcal{Q}\mathcal{L}\mathcal{Q})^{-1}\mathcal{Q}\mathcal{L}\mathcal{P}|F_l^m(\boldsymbol{kp};z))$$
$$= \mathcal{P}|\delta f_l^m(\boldsymbol{kp})) \tag{5.11.12}$$

By multiplying $(\delta f(\boldsymbol{kp})|$ we finally obtain,

$$z\mathbf{S}_l(\boldsymbol{k}z;\boldsymbol{pp}') - \int d\boldsymbol{p}_1 d\Sigma_l(\boldsymbol{k}z;\boldsymbol{pp}_1)\mathbf{S}_l(\boldsymbol{k}z;\boldsymbol{p}_1\boldsymbol{p}') = \mathbf{S}_l(\boldsymbol{k}0;\boldsymbol{pp}') \tag{5.11.13}$$

where the memory function, or the evolution operator $\Sigma_l(\boldsymbol{k}z;\boldsymbol{pp}_1)$ is

$$\Sigma_l(\boldsymbol{k}z;\boldsymbol{pp}') = \frac{4\pi}{2l+1}\sum_m \int d\boldsymbol{p}_1(\delta f_l^{m*}(\boldsymbol{k},\boldsymbol{p})|\mathcal{L}+\Psi|\delta f_l^m(\boldsymbol{k},\boldsymbol{p}_1))\mathbf{S}_{0l}^{-1}(\boldsymbol{k},\boldsymbol{p}_1,\boldsymbol{p}') \tag{5.11.14}$$

with

$$\Psi = \mathcal{P}\mathcal{L}\mathcal{Q}(z-\mathcal{Q}\mathcal{L}\mathcal{Q})^{-1}\mathcal{Q}\mathcal{L}\mathcal{P} \tag{5.11.15}$$

Since the Liouville operator $\mathcal{L}$ can be split into $\mathcal{L}_0+\mathcal{L}_I+\mathcal{L}_Q$, Eq. (5.2.9), the evolution operator can also be split into four terms; the free streaming term(Σ_l^0), the self consistent term(Σ_l^s), the color charge term(Σ^Q) and the non-local collision term(Σ^c).

$$\Sigma_{0l}(\boldsymbol{k}z;\boldsymbol{p}\boldsymbol{p}') = \frac{\boldsymbol{k}\cdot\boldsymbol{p}}{m}\delta(\boldsymbol{p}-\boldsymbol{p}')$$
$$\Sigma_{Il}(\boldsymbol{k}z;\boldsymbol{p}\boldsymbol{p}') = -n\frac{\boldsymbol{k}\cdot\boldsymbol{p}}{m}f_0(\boldsymbol{p})\mathbf{c}_{Dl}(\boldsymbol{k})$$
$$\Sigma_{Ql}(\boldsymbol{k}z;\boldsymbol{p}\boldsymbol{p}') = 0$$
$$\Sigma_{Cl}(\boldsymbol{k}z;\boldsymbol{p}\boldsymbol{p}') = \frac{1}{nf_0(\boldsymbol{p})}\frac{4\pi}{2l+1}\sum_m(\delta f_l^{m*}(\boldsymbol{k}\boldsymbol{p})|\mathcal{L}\mathcal{Q}(z-\mathcal{Q}\mathcal{L}\mathcal{Q})^{-1}\mathcal{Q}\mathcal{L}|\delta f_l^m(\boldsymbol{k}\boldsymbol{p}')) \tag{5.11.16}$$

5.11.3 Collisional Color Contribution

In this Appendix we detail the calculation that leads to a zero contribution from the colored Liouville operator in the collisional part of the self energy in the free streaming approximation. A typical contribution to (5.5.1) and (5.5.4) is

$$\begin{aligned} &L_Q(\boldsymbol{q},\boldsymbol{q}_1)\,L_Q^R(\boldsymbol{q}',\boldsymbol{q}_2)\,\mathbf{S}(t,\boldsymbol{q},\boldsymbol{q}_2)\,\mathbf{S}(t,\boldsymbol{q}',\boldsymbol{q}_1) = \frac{1}{\beta}\\ &\times\Big(V(\boldsymbol{r}-\boldsymbol{r}_1)\,\boldsymbol{Q}\times\boldsymbol{Q}_1\cdot(\boldsymbol{\nabla}_Q-\boldsymbol{\nabla}_{Q_1})\Big)\\ &\times\Big(\mathbf{c}_D'(\boldsymbol{r}'-\boldsymbol{r}_2,\boldsymbol{Q}'\cdot\boldsymbol{Q}_2))\,\boldsymbol{Q}'\times\boldsymbol{Q}_2\cdot(\boldsymbol{\nabla}_{Q'}-\boldsymbol{\nabla}_{Q_2})\Big)\\ &\times\mathbf{S}(t,\boldsymbol{q},\boldsymbol{q}_2)\,\mathbf{S}(t,\boldsymbol{q}',\boldsymbol{q}_1) \end{aligned} \tag{5.11.17}$$

which can be reduced to

$$
\begin{aligned}
&L_Q(\boldsymbol{q},\boldsymbol{q}_1)\, L_Q^R(\boldsymbol{q}',\boldsymbol{q}_2)\, \mathbf{S}(t,\boldsymbol{q},\boldsymbol{q}_2)\, \mathbf{S}(t,\boldsymbol{q}',\boldsymbol{q}_1) \\
&= -\frac{1}{\beta}\, V(\boldsymbol{r}-\boldsymbol{r}_1)\, \mathbf{c}_D'(\boldsymbol{r}'-\boldsymbol{r}_2, \boldsymbol{Q}'\cdot\boldsymbol{Q}_2)) \\
&\times\Bigg(\mathbf{S}'(\boldsymbol{Q}\cdot\boldsymbol{Q}_2)\mathbf{S}'(\boldsymbol{Q}'\cdot\boldsymbol{Q}_1)(\boldsymbol{Q}_1\times\boldsymbol{Q}_2)\cdot\boldsymbol{Q}\,(\boldsymbol{Q}_1\times\boldsymbol{Q}_2)\cdot\boldsymbol{Q}' \\
&\quad \times\mathbf{S}''(\boldsymbol{Q}\cdot\boldsymbol{Q}_2)\mathbf{S}(\boldsymbol{Q}'\cdot\boldsymbol{Q}_1)(\boldsymbol{Q}_1\times\boldsymbol{Q}_2)\cdot\boldsymbol{Q}\,(\boldsymbol{Q}\times\boldsymbol{Q}')\cdot\boldsymbol{Q}_2 \\
&\quad \times\mathbf{S}(\boldsymbol{Q}\cdot\boldsymbol{Q}_2)\mathbf{S}''(\boldsymbol{Q}'\cdot\boldsymbol{Q}_1)(\boldsymbol{Q}\times\boldsymbol{Q}')\cdot\boldsymbol{Q}_1\,(\boldsymbol{Q}_1\times\boldsymbol{Q}_2)\cdot\boldsymbol{Q}' \\
&\quad \times\mathbf{S}'(\boldsymbol{Q}\cdot\boldsymbol{Q}_2)\mathbf{S}'(\boldsymbol{Q}'\cdot\boldsymbol{Q}_1)(\boldsymbol{Q}\times\boldsymbol{Q}')\cdot\boldsymbol{Q}_1\,(\boldsymbol{Q}\times\boldsymbol{Q}')\cdot\boldsymbol{Q}_2 \Bigg)
\end{aligned}
\tag{5.11.18}
$$

The derivatives on $\mathbf{c}_D$ and $\mathbf{S}$ are on their color argument. We note that (5.11.18) contribute to the collisional part of the self energy in (5.11.9) after the integration over Q_1 and Q_2, which is then zero. This is expected. Indeed, the colored Liouville operator is a 3-body force that requires 3 distinct color charges to not vanish. While (5.11.18) contributer to the unintegrated collisional operator, it does not in the integrated one which is the self-energy on the 2point function. It does contribute in the Liouville hierarchy in the 3-body structure factors and higher.

5.11.4 Hydrodynamical subspace

The projection method onto the hydrodynamical subspace has been discussed by many [32, 33, 37]. This consists in dialing the projector in (5.6.2) onto the hydrodynamical modes. We choose Hermite polynomials as a basis set with the Maxwell-Boltzman distribution $f_0(\boldsymbol{p})$ as a Gaussian weight function. The Hermite polynomials are the the generalized ones in 3D [45]. Specifically

$$H_{1(n)}(\boldsymbol{p}) = 1 \qquad H_{2(l)}(\boldsymbol{p}) = p_z \qquad H_{3(\epsilon)}(\boldsymbol{p}) = \frac{1}{\sqrt{6}}(p^2 - 3)$$
$$H_{4(t_1)}(\boldsymbol{p}) = p_x \qquad H_{5(t_2)}(\boldsymbol{p}) = p_y \tag{5.11.19}$$

These polynomials are orthonormal for the inner product

$$\langle m|n\rangle = \int d\boldsymbol{p} a_m H_m(\boldsymbol{p}) a_n H_n(\boldsymbol{p}) n f_0(\boldsymbol{p}) = \delta_{mn}$$
$$\langle m|F(k,t)|n\rangle = \int d\boldsymbol{p} d\boldsymbol{p}' a_m H_m(\boldsymbol{p}) F(k,t;\boldsymbol{p}\boldsymbol{p}') a_n H_n(\boldsymbol{p}') n f_0(\boldsymbol{p}') \tag{5.11.20}$$

Here a_m and a_n set the normalizations. We chose the longitudinal momentum direction along $\boldsymbol{k}$ in Fourier space, $\langle l| = a_m \hat{k} \cdot \boldsymbol{p}$. The transverse directional is chosen orthogonal to $\boldsymbol{k}$, $\langle t| = a'_m \boldsymbol{\epsilon} \cdot \boldsymbol{p}$ with a unit vector satisfying $\boldsymbol{\epsilon}^2 = 1$ and $\boldsymbol{\epsilon} \cdot \hat{k} = 0$.

The hydrodynamical projection operators $\mathcal{P}_H$ restricted to the five states (5.11.19) are

$$\mathcal{P}_H = \sum_i^5 |i\rangle\langle i| \qquad \mathcal{Q}_H = 1 - \mathcal{P}_H = 1 - \sum_i^5 |i\rangle\langle i| \tag{5.11.21}$$

While in general these 5 statesare enough to characterize the hydrodynamical modes in the SU(2) phase space, we need additional states to work out the shear viscosity as it involves in general correlations in the stress tensor through the Kubo relation [1]. For that we need additionally,

$$H_6(\boldsymbol{p}) = p_x p_y \qquad H_7(\boldsymbol{p}) = p_x p_z \qquad H_8(\boldsymbol{p}) = p_y p_z \tag{5.11.22}$$

With the definition of $G_{ij}(\boldsymbol{k}z) = \langle i|\mathbf{S}(\boldsymbol{k}z;\boldsymbol{p}\boldsymbol{p}')(nf_0(\boldsymbol{p}))^{-1}|j\rangle$ we can rewrite (5.6.2) as

$$\Big(z - \sum_k \langle i|\Omega(\boldsymbol{k}z;\boldsymbol{p}\boldsymbol{p}')|k\rangle\Big)G_{kj}(\boldsymbol{k}z) = G_{ij}(\boldsymbol{k}0) \tag{5.11.23}$$

where i, j are short for: n(density), ϵ(energy), l(longitudinal momentum) and t(transverse momentum).

Chapter 6

Energy Loss

6.1 Introduction

Parton energy loss at RHIC is widely viewed as a way to probe the properties of the medium created during the first few fm/c of the collision. The medium is suspected to be a strongly coupled liquid [46] with near perfect fluidity and strong energy loss.

There have been a number of calculations involving parton collisional [47–50] and radiative [51, 52] energy loss at RHIC with the chief consequence of jet quenching [53]. The measured jet quenching at RHIC exceeds most current theoretical predictions, most of which are based on a weakly coupled quark-gluon plasma (wQGP).

The QCD matter probed numerically using lattice simulations and at RHIC using heavy ion collisions, is likely to be dominated by temperatures in the few T_c range making it de facto non-perturbative. Non-perturbative methods are therefore welcome for analyzing the QCD matter conditions in this temperature range. An example being the holographic method as a tool for jet

quenching analysis [54, 55].

In this chapter, we follow the approach suggested in [3] to model the strongly coupled quark and gluon plasma, by classical colored constituents interacting via strong Coulomb interactions. This model has been initially analyzed using Molecular Dynamics (MD) simulations mostly for the SU(2) version with species of constituents (gluons). The MD results reveal a strongly coupled liquid at $\Gamma = V/K \approx 3$ the ratio of the kinetic to Coulomb energy. The fractional energy loss is also found to be considerably larger than most leading order QCD estimates.

Here, we will provide the analytical framework to analyze the MD simulation results for partonic energy loss in the cQGP. In section 6.2, we outline a formal derivation of the energy loss in the cQGP for arbitrary values of Γ. In section 6.3, we use linear response theory and the fluctuation-dissipation theorem to tie the energy loss to the non-static colored structure factor. In section 6.4, we derive explicitly the non-static structure factor using the Liouville equation. Some useful aspects of the plasmon excitations in the cQGP are discussed in section 6.5. In section 6.6, we analyze the energy loss for both charm and bottom for Γ =2,3 and 4 in the liquid phase and compare them to the recent SU(2) MD simulations [25]. In section 6.7, we discuss the relevance of our results to RHIC and holographic QCD.

6.2 Energy Loss

Consider an SU(2) colored particle of charge q^a travelling with velocity v in the strongly coupled colored plasma [3]. The equation of motion of this *extra* particle in phase space follows from the Poisson bracket

$$\frac{d\boldsymbol{p}_i}{dt} = -\{H, \boldsymbol{p}_i\} = q^a \cdot \boldsymbol{E}^a_{in} \tag{6.2.1}$$

with the longitudinal colored electric field

$$\boldsymbol{E}^a_{in} = -\boldsymbol{\nabla} \sum_i \frac{Q^a_i(t)}{|\boldsymbol{r} - \boldsymbol{r}_i(t)|} = -\boldsymbol{\nabla}_i \Phi^a_{in}(t, \boldsymbol{r}) \tag{6.2.2}$$

We note that in [3] the SU(2) plasma is considered mostly electric with massive constituents $m\beta \approx 3$. As a result the transverse electric contribution is absent in (6.2.2). Also, (6.2.1) does not involve the magnetic part of the Lorentz force for the same reasons. The latter is irrelevant for the energy loss per travel length $\boldsymbol{r} = \boldsymbol{v}t$

$$\frac{dK}{dr} = \boldsymbol{v} q^a \boldsymbol{E}^a_{in}(t, \boldsymbol{r} = \boldsymbol{v}t) \tag{6.2.3}$$

even in the ultrarelativistic case since the magnetic force does not perform work.

The induced colored Coulomb potential Φ_{ind} follows from the total colored potential Φ_{tot} through

$$\Phi^a_{tot}(\omega, \boldsymbol{k}) = \Phi^a_{ind}(\omega, \boldsymbol{k}) + \Phi^a_{ex}(\omega, \boldsymbol{k}) = \frac{\Phi^a_{ex}(\omega, \boldsymbol{k})}{\epsilon_L(\omega, \boldsymbol{k})} \tag{6.2.4}$$

The last relation defines the longitudinal dielectric constant with $\boldsymbol{\Phi}_{ex}(\omega, \boldsymbol{k}) = \frac{4\pi}{k^2} 2\pi \boldsymbol{q} \delta(\omega - \boldsymbol{k} \cdot \boldsymbol{v})$, the colored potential caused by the *extra* particle in the probe approximation (ignoring back reaction). Thus

$$\Phi^a_{ind}(t, \boldsymbol{r}) = q^a \int \frac{d\boldsymbol{k}}{(2\pi)^3} \left(\frac{1}{\epsilon_L(k \cdot v, \boldsymbol{k})} - 1 \right) \frac{4\pi}{k^2} e^{i\boldsymbol{k}\cdot\boldsymbol{r} - i\boldsymbol{k}\cdot\boldsymbol{v}t} \tag{6.2.5}$$

Using (6.2.2) and (6.2.3) we have for the energy loss of a fast moving probe

SU(2) charge

$$-\frac{dK}{dr} = -\frac{\boldsymbol{q}^2}{\pi v^2}\int\frac{dk}{k}\int_{-kv}^{kv}\omega d\omega\,\mathrm{Im}\left(\frac{1}{\epsilon_L(\omega+i0,\boldsymbol{k})}\right) \tag{6.2.6}$$

after using the analytical property of $\epsilon_L(z,k) = \epsilon_L(-z^*,-k)$ which follows from the causal character of the longitudinal dielectric function as detailed below. (6.2.6) is identical in form to the one derived for the Abelian one component colored Coulomb plasma in [14], to the exception of the SU(2) classical Casimir $\boldsymbol{q}^2$ in (6.2.6). It is different in content through the longitudinal dielectric constant ϵ_L which now should be derived for a colored SU(2) Coulomb plasma. Our derivation is *fully* non-Abelian in the probe approximation.

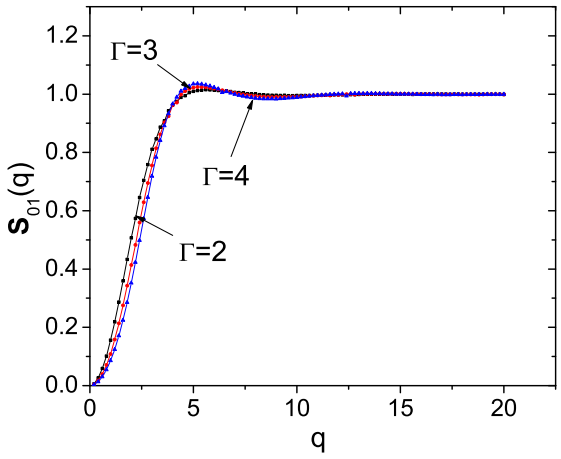

Figure 6.1: Static structure factors for $\Gamma = 2, 3, 4$

Below we show that for the SU(2) colored Coulomb plasma at strong Coulomb coupling, (6.2.6) reads

$$-\frac{dK}{dr} = -\frac{\boldsymbol{q}^2}{\pi v^2}\int\frac{dk}{k^3}\frac{k_D^2\,\mathbf{S}_{01}(k)}{1-\mathbf{S}_{01}(k)}\int_{-kv}^{+kv}d\omega\,\omega\;\mathrm{Im}\left(\frac{1}{\epsilon_1(\omega+i0,\boldsymbol{k})}\right) \tag{6.2.7}$$

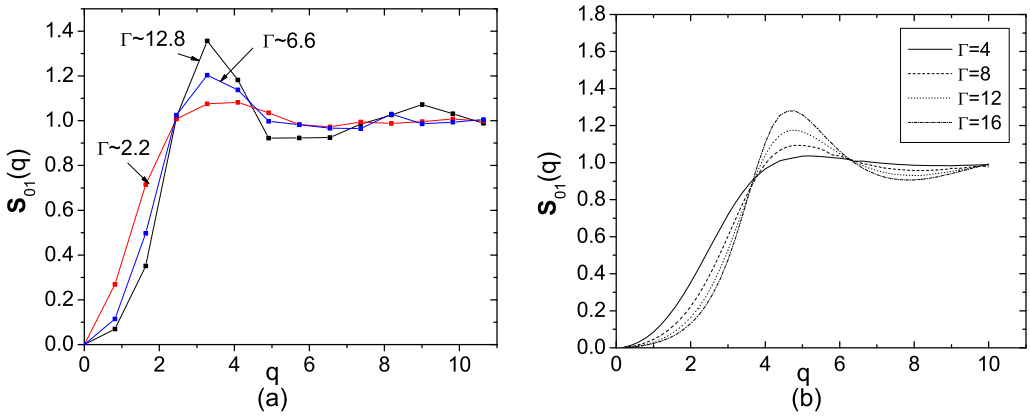

Figure 6.2: $\mathbf{S}_{01}(q)$: molecular dynamics simulation (a) and analytic (b). See text.

with k_D^2 the SU(2) Debye wave number squared. Here

$$\epsilon_1(z, \boldsymbol{k}) = 1 - n\, \mathbf{c}_{D1}(\boldsymbol{k})\, \mathbf{W}(z/\omega_T) \tag{6.2.8}$$

with the thermal frequency $\omega_T = v_T k$ and velocity $v_T = \sqrt{T/m}$ and

$$\mathbf{W}(z/\omega_T) = \frac{1}{\sqrt{2\pi}} \int_{-\infty}^{+\infty} dt\, \frac{t}{t - z/\omega_T}\, e^{-t^2/2} \tag{6.2.9}$$

The l=1 static structure factor $\mathbf{S}_{01}$ [31]

$$\mathbf{S}_{01}(k) = \left\langle \left| \sum_{j=1}^{N} e^{i\boldsymbol{k}\cdot\boldsymbol{r}_j}\, Q_j^a \right|^2 \right\rangle \tag{6.2.10}$$

satisfies the generalized Ornstein-Zernicke equation

$$\mathbf{S}_{01}(k) = \frac{1}{1 - n\mathbf{c}_{D1}(k)} \tag{6.2.11}$$

in the colored Coulomb plasma with 1 species density $n = N/V$. In Fig. 6.1 we

show analytical results for (6.2.10) around the liquid point [31]. In Fig. 6.2a we show the behavior of (6.2.10) using SU(2) molecular dynamics simulations with the dimensionless wavenumber $q = k\, a_{WS}$ where a_{WS} is the Wigner-Seitz radius through $1/n = 4\pi\, a_{WS}^3/3$. In Fig. 6.2b we show the analytical results for the same range of Γ in [31].

The $l = 1$ contribution ϵ_1 plays the role of a generalized longitudinal dielectric constant in the SU(2) Coulomb plasma. Indeed, for weak Coulomb coupling $\Gamma \ll 1$, $-n\mathbf{c}_{D1} \approx k_D^2/k^2$ so that $\mathbf{S}_{01} \approx k^2/(k^2 + k_D^2)$. The energy loss (6.2.7) reduces to (6.2.6) with $\epsilon_L \to \epsilon_1$. At weak coupling ϵ_1 in (6.2.8) is the standard Vlasov dielectric function in [14]. The only difference is in the SU(2) Debye wave number.

6.3 Linear Response

To construc the longitudinal dielectric constant for the SU(2) Coulomb plasma we will make use of the Liouville kinetic equations for the time dependent structure factors derived in [31]. For that we recall that in linear response, the induced color charge density $\rho^a_{ind} = \nabla \cdot E^a_{ind}/4\pi$ ties with the external potential Φ^b_{ext} through the retarded correlator

$$\rho^a_{ind}(t, \boldsymbol{r}) = i \int dt'\, d\boldsymbol{r}'\, \left\langle \mathbf{R}\left(\mathbf{J}^a_0(t, \boldsymbol{r}) \mathbf{J}^b_0(t', \boldsymbol{r}')\right)\right\rangle\, \Phi^b_{ext}(t', \boldsymbol{r}') \tag{6.3.1}$$

where $\mathbf{J}^a_0$ are the pertinent color charge densities. In Fourier space we have

$$\Phi^a_{ind} = -\frac{4\pi}{k^2}\, \Delta^{ab}_R(\omega, \boldsymbol{k})\, \Phi^b_{ext} \tag{6.3.2}$$

with

$$\Delta_R^{ab}(\omega,\boldsymbol{k}) = -i\int e^{-i\omega t+i\boldsymbol{k}\cdot\boldsymbol{r}}\,\left\langle \mathbf{R}\left(\mathbf{J}_0^a(t,\boldsymbol{r})\mathbf{J}_0^b(t',\boldsymbol{r}')\right)\right\rangle \tag{6.3.3}$$

A comparison of (6.3.2) with (6.2.4) yields

$$\left(\frac{1}{\epsilon_L(\omega,\boldsymbol{k})}-1\right)\,\delta^{ab} = -\frac{4\pi}{k^2}\,\Delta_R^{ab}(\omega,\boldsymbol{k}) \tag{6.3.4}$$

which defines the longitudinal dielectric constant.

The retarded correlator (6.3.3) is in general a quantum object, we now show how to extract it from the correlations in the classical and strongly coupled SU(2) colored Coulomb plasma. For that, we note that the colored charge density in the SU(2) phase space is

$$\mathbf{J}_0^a(t,\boldsymbol{r}) = \int dQ\,d\boldsymbol{p}\,Q^a\delta f(t,\boldsymbol{r},\boldsymbol{p},\boldsymbol{Q}) \tag{6.3.5}$$

and that the SU(2) charge-charge correlator is

$$\left\langle \mathbf{J}_0^a(t,\boldsymbol{r})\mathbf{J}_0^b(t',\boldsymbol{r}')\right\rangle = \frac{1}{3}\delta^{ab}\int dQ\,dQ'\,d\boldsymbol{p}\,d\boldsymbol{p}'\,\boldsymbol{Q}\cdot\boldsymbol{Q}'\,\mathbf{S}(t-t',\boldsymbol{r}-\boldsymbol{r}',\boldsymbol{p}\boldsymbol{p}',\boldsymbol{Q}\cdot\boldsymbol{Q}') \tag{6.3.6}$$

where global time, space and color invariances were used thanks to the statistical averaging. The time dependent structure factor $\mathbf{S} = \langle\delta f\delta f\rangle$ was defined in [31] . Using the color Legendre transform of $\mathbf{S}$ yields

$$\left\langle \mathbf{J}_0^a(t,\boldsymbol{r})\mathbf{J}_0^b(t',\boldsymbol{r}')\right\rangle = \delta^{ab}\int d\boldsymbol{p}\,d\boldsymbol{p}'\,\mathbf{S}_1(t-t',\boldsymbol{r}-\boldsymbol{r}',\boldsymbol{p}\boldsymbol{p}') \tag{6.3.7}$$

Only the $l=1$ partial wave in the Legendre transform of the color part of $\mathbf{S}$

contributes to the SU(2) charge-charge correlation function.

The fluctuation-dissipation theorem in the *classical limit* ties the retarded correlator Δ_R in (6.3.3) to the Fourier transform of the classical phase space fluctuations (6.3.7) as

$$\mathrm{Im}\,\Delta_R^{ab}(\omega,\boldsymbol{k}) = \delta^{ab}\frac{n\omega}{2T}\,\mathbf{S}_1(\omega,\boldsymbol{k}) \equiv -\delta^{ab}\frac{n\omega}{T}\;\mathrm{Im}\,\mathbf{S}_1(z,\boldsymbol{k}) \tag{6.3.8}$$

The last relation follows from $\mathbf{S}_1(\omega,\boldsymbol{k}) = -2\,\mathrm{Im}\,\mathbf{S}_1(\omega,\boldsymbol{k})$ between the Laplace transform and Fourier transform of $\mathbf{S}_1$ with $z = \omega + i0$.

6.4 Non-Static Structure Factor

We have shown in [22] that the l-color partial wave of the Laplace transform of $\mathbf{S}_l$ obeys the Liouville equation

$$z\mathbf{S}_l(z\boldsymbol{k};\boldsymbol{p}\boldsymbol{p}') - \int d\boldsymbol{p}_1\Sigma_l(z\boldsymbol{k};\boldsymbol{p}\boldsymbol{p}_1)\,\mathbf{S}_l(z\boldsymbol{k};\boldsymbol{p}_1\boldsymbol{p}') = \mathbf{S}_{0l}(\boldsymbol{k};\boldsymbol{p}\boldsymbol{p}') \tag{6.4.1}$$

$\mathbf{S}_{0l}$ is the l static structure factor introduced in [31]

$$\mathbf{S}_{0l}(\boldsymbol{k};\boldsymbol{p}\boldsymbol{p}') = n\,f_0(\boldsymbol{p})\,\delta(\boldsymbol{p}-\boldsymbol{p}') + n^2 f_0(\boldsymbol{p})\,f_0(\boldsymbol{p}')\,\mathbf{h}_l(\boldsymbol{k}) \tag{6.4.2}$$

with the Maxwell-Boltzmann distribution $f_0(\boldsymbol{p})$. The structure factor $\mathbf{h}_l(\boldsymbol{k})$ relates to the standard structure factor $\mathbf{S}_{0l}(k)$ by the generalized Ornstein-Zernicke equations

$$\frac{1}{n}\int d\boldsymbol{p}\,d\boldsymbol{p}'\,\mathbf{S}_{0l}(k;\boldsymbol{p}\boldsymbol{p}') = \mathbf{S}_{0l}(k) = 1 + n\,\mathbf{h}_l(k) = (1 - n\,\mathbf{c}_{Dl}(k))^{-1} \tag{6.4.3}$$

The self-energy kernel Σ_l in (6.4.1) splits into a static and collisional contribution in each color partial wave l [22].

We note that

$$\mathbf{S}_l(zk) = \frac{1}{n} \int d\boldsymbol{p}\, d\boldsymbol{p}'\, \mathbf{S}_l(z\boldsymbol{k}; \boldsymbol{p}\boldsymbol{p}') \tag{6.4.4}$$

with $l = 1$ is what is needed in (6.3.8). For that, we solve (6.4.1) in the collisionless limit with

$$\Sigma_l(z\boldsymbol{k}; \boldsymbol{p}\boldsymbol{p}') \approx \frac{1}{m} \boldsymbol{k}\cdot\boldsymbol{p}\, \delta(\boldsymbol{p}-\boldsymbol{p}') - \frac{1}{m} \boldsymbol{k}\cdot\boldsymbol{p}\, n\, f_0(\boldsymbol{p})\, \mathbf{c}_{Dl}(\boldsymbol{k}) \tag{6.4.5}$$

We recall that the SU(2) color part of the Liouville operator is a genuine 3-body force that only enters the collisional contribution. [22]. Inserting (6.4.5) into (6.4.1) and using (6.4.5) and (6.4.3) yield in the collisionless limit

$$\mathbf{S}_l(z, \boldsymbol{k}) = \frac{\mathbf{S}_{0l}(k)}{\epsilon_l(z, \boldsymbol{k})} \int d\boldsymbol{p}\, \frac{f_0(p)}{z - \boldsymbol{k}\cdot\boldsymbol{p}/m} \tag{6.4.6}$$

with

$$\epsilon_l(z, \boldsymbol{k}) = 1 + n\, \mathbf{c}_{Dl}(k) \int d\boldsymbol{p}\, \frac{\boldsymbol{k}\cdot\boldsymbol{p}/m}{z - \boldsymbol{k}\cdot\boldsymbol{p}/m}\, f_0(p) \tag{6.4.7}$$

and

$$\int d\boldsymbol{p}\, \frac{f_0(p)}{z - \boldsymbol{k}\cdot\boldsymbol{p}/m} = \frac{1}{\omega}\Big(1 - \mathbf{W}(z/\omega_T)\Big) \tag{6.4.8}$$

If we insert (6.4.6) into (6.3.8) and then use (6.3.4), we find for $l = 1$

$$\mathrm{Im}\, \frac{1}{\epsilon_L(z, \boldsymbol{k})} = -\frac{k_D^2}{k^2} \frac{1}{n\mathbf{c}_{D1}(k)}\, \mathrm{Im}\, \frac{1}{\epsilon_1(z, \boldsymbol{k})} \tag{6.4.9}$$

Inserting (6.4.9) into (6.2.6) yields the announced relation (6.2.7).

6.5 SU(2) Plasmon

Before analyzing the energy loss in (6.2.8) for heavy charged probes, it is instructive to discuss the zeros of the longitudinal dielectric constant $\epsilon_1(\omega, k) = 0$ in (6.2.8) as they reflect on the longitudinal excitations in the $l = 1$ channel. For that, we need the behavior of $\mathbf{W}(x)$ as defined in (6.2.9) with $x = \omega/v_T k$ for small and large ratio k/k_D. $v_T = \sqrt{T/m}$ is the velocity of the the particles in the SU(2) heat bath. In weak coupling QCD $m \approx gT$, while in strong coupling $m \approx \pi T$.

In general,

$$\mathbf{W}(x) = \mathbf{W}_R(x) + i\mathbf{W}_I(x) = 1 - xe^{-x^2/2}\,\psi(x) + i\sqrt{\frac{\pi}{2}}\,x\,e^{-x^2/2} \tag{6.5.1}$$

with $\psi(x) = \int_0^x dx\, e^{y^2/2}$ the incomplete exponential function. For $k \ll k_D$ or $x \gg 1$,

$$\mathbf{W}(x) \approx -\frac{1}{x^2} + i\frac{\sqrt{\pi}}{2}\,xe^{\,-x^2} \tag{6.5.2}$$

while for $k \gg k_D$ or $x \ll 1$

$$\mathbf{W}(x) \approx 1 - x^2 + i\frac{\sqrt{\pi}}{2}\,xe^{\,-x^2} \tag{6.5.3}$$

So in the long wavelength limit with $k \ll k_D$, (6.2.8) expands to

$$\epsilon_1(\omega, \boldsymbol{k}) \approx 1 + \frac{n\mathbf{c}_{D1}(k)}{x^2}\left(1 - i\frac{\sqrt{\pi}}{2}x^3 e^{-x^2/2}\right) \tag{6.5.4}$$

For small k, $n\mathbf{c}_{D1}(k) \approx \mathbf{S}_{01}(k) \approx k_D^2/k^2$ whatever the coupling in the SU(2) colored plasma. Thus

$$\epsilon_1(\omega, \boldsymbol{k}) \approx 1 - \frac{\omega_p^2}{\omega^2}\left(1 - i\frac{\sqrt{\pi}}{2}x^3 e^{-x^2/2}\right) \tag{6.5.5}$$

with the plasmon frequency $\omega_p = v_T\, k_D$. So for $k \ll k_D$, the zero of (6.5.5) is

$$\omega_1^2(k) \approx \omega_p^2\left(1 - i\frac{\sqrt{\pi}}{2}\frac{k_D^3}{k^3}e^{-k_D^2/2k^2}\right) \tag{6.5.6}$$

The SU(2) colored Coulomb plasma supports a plasmon with frequency ω_p with an exponentially small width $e^{-\omega^2/2v_T^2k^2}$ both at weak and strong SU(2) Coulomb coupling Γ. This result agrees with our analytic and leading kinetic analysis in the hydrodynamical limit [22] . The current analysis provides the non-analytic imaginary part as well.

The high $k \gg k_D$ limit is metallic whatever Γ with

$$\epsilon_1(x) \approx 1 - in\mathbf{c}_{D1}(k)\, x\sqrt{\frac{\pi}{2}}\, e^{-x^2/2} \tag{6.5.7}$$

with a metallic conductivity $x = \omega/\omega_T = \omega/v_T k$

$$\sigma_1(\omega, \boldsymbol{k}) = \frac{n\,\mathbf{c}_{D1}(k)}{\sqrt{32\pi}}\,\frac{\omega^2}{v_T k}\, e^{-\omega^2/2v_T^2k^2} \tag{6.5.8}$$

We note that the plasmon branch disappears at high k in (6.5.7) as the plasma turns metallic i.e. a collection of free colored SU(2) particles with a classical thermal spectrum. Also the plasmon in (6.5.5) broadens substantially at $k \approx k_D$ with its real part comparable to its imaginary part. This point causes

the plasmon contribution to drop from the energy loss in the colored SU(2) Coulomb plasma as we show below.

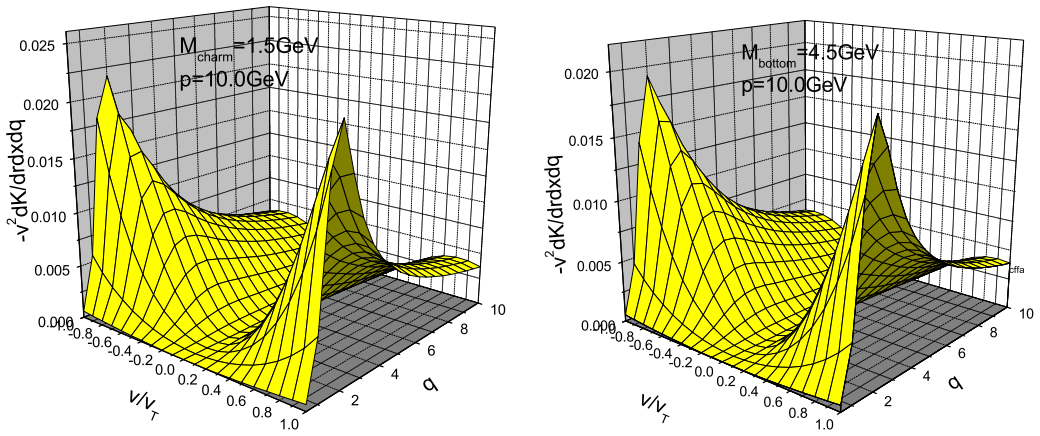

Figure 6.3: Surface plot of $-v^2 dK/drdxdq$ for charm and bottom. See text.

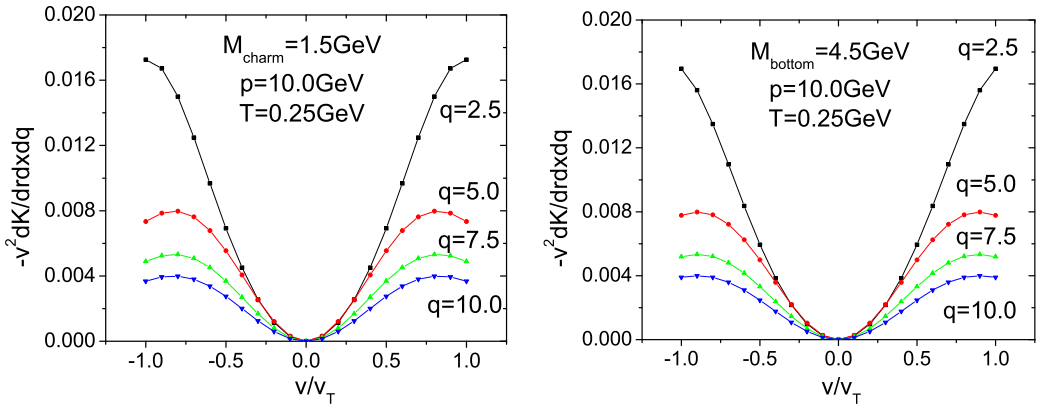

Figure 6.4: $-v^2 dK/drdxdq$ versus v/v_T for charm and bottom quark for fixed q. See text.

6.6 Charm and Bottom Loss

Inserting (6.2.8) into (6.2.7) and using the explicit form (6.5.1) yields the energy loss in the SU(2) Coulomb plasma

$$-\frac{dK}{dr} = \frac{g^2\, C_F}{4\pi}\frac{\omega_p^2}{v^2}\int_0^{k_{max}} dk\,\frac{1}{k}\,\frac{1}{\sqrt{2\pi}}\int_{-v/v_T}^{v/v_T} dx\, e^{x^2/2}$$
$$\times\left(\left(\left(1-n\mathbf{c}_{D1}(k)\right)e^{x^2/2}/x - n\mathbf{c}_{D1}(k)\,\psi(x)\right)^2 + \pi\, n^2\mathbf{c}_{D1}^2(k)/2\right)^{-1} \tag{6.6.1}$$

For an SU(2) probe charge after the substitution $\boldsymbol{q}^2 \to g^2 C_F/4\pi$ with C_F the SU(2) Casimir. We note that (6.6.1) is cutoff in the infrared by the Debye wave number since $\mathbf{S}_{01}(k) \approx k^2/k_D^2$. So the main contribution to the energy loss in (6.6.1) stems from the region $k > k_D$ for which the SU(2) plasmon is too broad to contribute as we noted earlier. Most of the loss stems from the metallic part of the SU(2) plasma which is the analogue as rescattering against the *free* thermal spectrum explicit in (6.5.8).

In Fig. 6.3 we display the integrand in (6.6.1) versus the jet velocity v/v_T and the dimensionless momentum $q = ka_{WS}$. This is a weighted plot of the longitudinal spectral function along the jet velocity. The two wings at small q are the two plasmons peaks, which progressively turns into the thermal distribution at larger q. In Fig. 6.4 we show the same integrand for fixed q versus the jet velocity v/v_T normalized to the thermal velocity V_T. We note again the 2 plasmon poles around $v \approx v_T$ at small q. The vanishing of the termal distribution at $q = 0$ follows from the extra x^2 weight arising from the denominator of (6.6.1) for $\mathbf{c}_{D1}(k) \approx 0$ at large k.

Since the loss is colored with only $l = 1$ contributing and is metallic with only $k > k_D$ contributing, we do not see colored Cherenkov radiation stemming from plasmon emission [56], nor the ubiquitous Mach cone stemming from

coupling to the sound mode [57]. While the sound mode contributes to $\mathbf{S}$ in (6.3.6) it drops in the statistical averaging as only $l = 1$ or plasmon channel contributes. The energy loss in the classical colored SU(2) Coulomb plasma is mostly metallic with $k > k_D$ and soundless due to the color quantum numbers of the fast moving probe charge.

A qualitative estimate for the energy loss follows by using $\mathbf{S}_{01}(k) \approx k^2/(k^2 + k_D^2)$ and saturating the integrand by $k > k_D$,

$$-\frac{dK}{dr} \approx \frac{g^2\, C_F}{4\pi}\frac{\omega_p^2}{v^2}\left(\sqrt{\frac{2}{\pi}}\int_0^{v/v_T} x^2\, e^{-x^2/2}\right)\, \ln\left(\frac{k_{max}}{k_D}\right) \tag{6.6.2}$$

The upper divergence is manifest in (6.6.1) at $k \gg k_D$ since $\mathbf{S}_{01}(k) \approx 1$ and $\mathbf{c}_{D1}(k) \approx k_D^2/k^2$ through the generalized Ornstein-Zernicke equation for all Coulomb couplings. The upper cutoff $k_{max} \approx 2\gamma\, mv$ which is set by the maximum momentum transfer to the thermal particle of mass m in the rest frame of the probe particle $M \gg m$. Typically M is charm and bottom, while $m \approx gT$ in weak coupling and $m \approx \pi T$ in strong coupling for a QCD plasma near the critical point. For the former $v/v_T \approx v\sqrt{g}$ (weak coupling) while for the latter $v/v_T \approx v\sqrt{\pi}$ (strong coupling). For $v/v_T \gg 1$ (6.6.2) reduces further to

$$-\frac{dK}{dx} \approx \frac{g^2\, C_F}{4\pi}\frac{\omega_p^2}{v^2}\, \ln\left(\frac{2\gamma\, m\, v}{k_D}\right) \tag{6.6.3}$$

For the SU(2) colored Coulomb plasma. Aside from the Casimirs, this result is analogous to the energy loss in the classical and Abelian Coulomb plasma.

To assess the energy loss for varying Coulomb coupling $\Gamma = (g^2 C_2/4\pi)(\beta/a_{WS})$, we will rewrite the energy loss (6.6.1) as

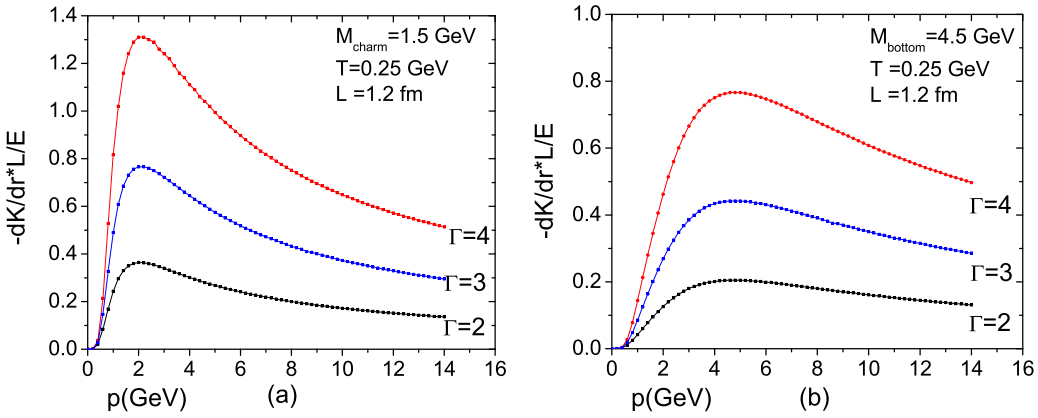

Figure 6.5: Energy loss for charm (left) and bottom (right) in the cQGP: $\Gamma = 2, 3, 4$.

$$-\frac{dK}{dr} = 3\Gamma^2 \left(\frac{C_F}{C_2}\right) \frac{v_T^2}{v^2} \frac{T}{a_{WS}} \int_0^{q_{max}} dq \, \frac{1}{q} \frac{1}{\sqrt{2\pi}} \int_{-v/v_T}^{v/v_T} dx \, e^{x^2/2} \times \left(\left((1 - n\mathbf{c}_{D1}(q)) \, e^{x^2/2}/x - n\mathbf{c}_{D1}(q) \, \psi(x) \right)^2 + \pi \, n^2 \mathbf{c}_{D1}^2(q)/2 \right)^{-1} \tag{6.6.4}$$

where $q = ka_{WS}$ and a_{WS} is the Wigner-size radius. The units for the energy loss per length in (6.6.4) follows from T/a_{WS}. For SU(2), $C_F = 3/4$ for a heavy quark, and $C_2 = 2$ for thermal constituent gluons of mass $m \approx \pi T$. $a_{WS} = (3/4\pi n)^{1/3} = (\frac{3}{4\pi} \frac{\beta^3}{0.244\times 3})^{1/3} = 0.6883\beta$ for a density dominated by black-body (gluon) radiation $n = 0.244(N_c^2 - 1)/\beta^3 = 0.244 \times 3/\beta^3$.

In Fig. 6.5 we show the dimensionless energy loss following from (6.6.4) for charm and bottom as a function of the probe momentum $\gamma M v$, for different $\Gamma = 2, 3, 4$ around the SU(2) liquid point. The numerics have been carried using the analytic structure factor of Fig. 6.1. The energy loss is normalized to the total kinetic energy in length L, $E/L = (\gamma - 1)M/L$. Since the quark

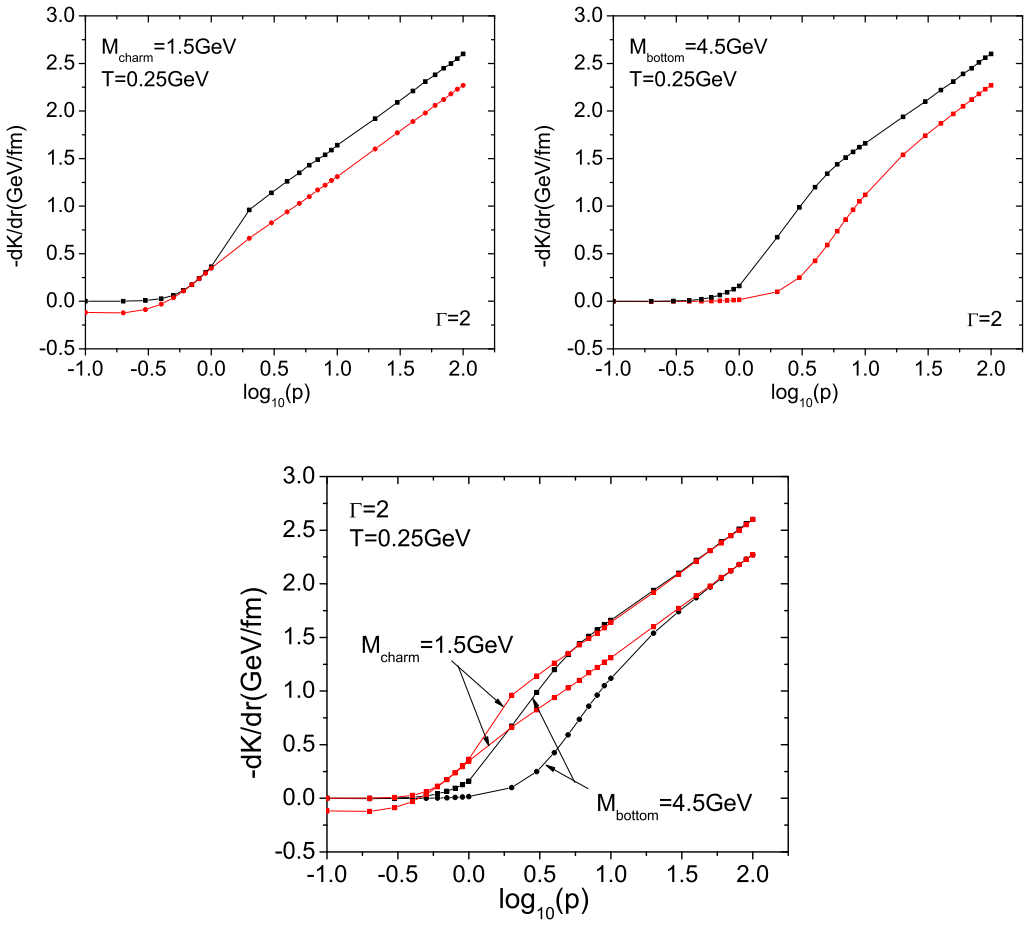

Figure 6.6: Logarithmic energy loss for charm (left) and bottom (right) in absolute units. See text.

velocity is maintained constant, the energy loss is seen to exceed 1 for $\Gamma = 4$. The loss is very sensitive to the Coulomb coupling Γ in the liquid phase.

In Fig. 6.6 we show the energy loss on a logarithmic momentum scale for both charm and bottom. The upper curve (black) is the total loss from (6.6.4), while the lower curve (red) is just the metallic loss following from (6.6.3). The difference is a measure of the energy loss due to collisions with the low momentum part of the excitational spectrum of the SU(2) plasma which is plasmon dominated. These are the wings shown in Fig. 6.4. Charm

and bottom jets with low momenta say $p \approx 3$ GeV experience energy loss through broad plasmons. The energy loss for jets with p larger than 10 GeV is mostly linear and therefore metallic.

In Fig. 6.7 we compare our analytical results for the energy loss (blue curve) to recent SU(2) numerical simulations (black curve) using the same model [25]. The analytical results appear to undershoot the SU(2) molecular dynamics simulations by an overall factor of 2 for the heaviest quarks in the liquid phase with $\Gamma = 3$. They are comparable to the energy loss for charm till about $p = 4$ GeV. This discrepancy between our analysis and the simulations at high momentum and for heavy quarks maybe due to the hard core necessary to carry the SU(2) molecular dynamics simulations in [25].

6.7 Conclusions

We have analyzed the energy loss of fast moving charm and bottom quarks in an SU(2) color Coulomb plasma for a broad range of the Coulomb coupling. The Coulomb character of the underlying interaction retained classically make the energy loss entirely described by the longitudinal part of the dielectric function. We have used linear response theory to derive an explicit expression for the imaginary part of the dielectric function in terms of the Laplace transform of the time-dependent structure factor in the SU(2) Coulomb plasma.

We have shown that the probe initial color and statistical averaging causes the longitudinal dielectric function to select the $l = 1$ color channel of the time-dependent structure factor which is the plasmon channel. The sound channel dominates the low momentum of the $l = 0$ color channel, and decouples from the longitudinal part of the dielectric function. While the SU(2) plasmon

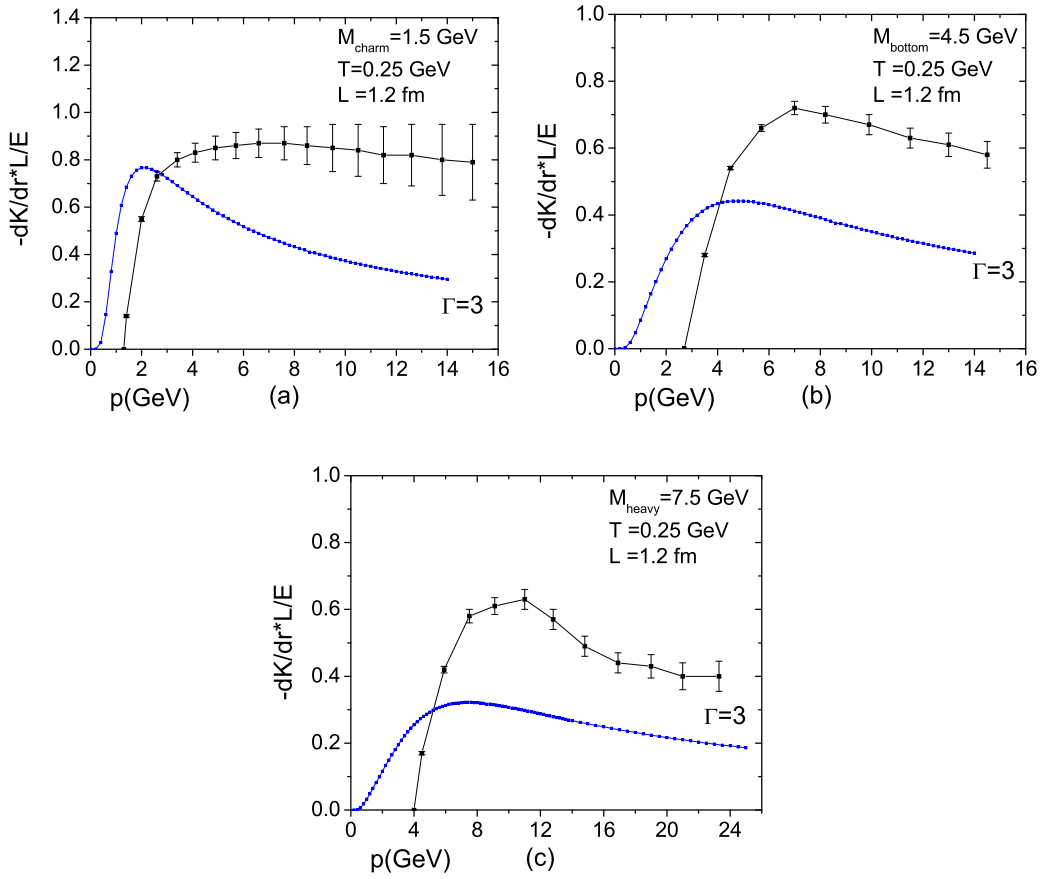

Figure 6.7: Energy loss: (blue) analytical versus (black) SU(2) molecular dynamics [25].

survives at strong coupling, its width for $k > k_D$ is substantial and therefore causes it to thermally decay.

The energy loss of fast moving charm and bottom quarks is mostly due to the metallic aspect of the SU(2) colored Coulomb plasma which is dominated by thermal particles. There is no colored Cerenkov cone as the plasmon is dwarfed in the metallic limit, nor a colorless Mach cone as the sound decouples due to the probe initial colors. The energy loss is soundless. Our results are of course only classical. They apply for a broad range of Γ near the liquid point. The comparison to the MD simulations show that our energy loss is about half

the energy loss reported numerically. The latter is sensitive to the choice of the regulating core at short distances.

Strong coupling assessment of jet energy loss in gauge theories have been carried out in the context of holographic QCD [58]. The fact that a Mach cone was reported in these calculations [59], maybe due to the fact that the probe jet is actually colorless. Indeed, most of the holographic jets are inserted with an external hand that maintains a constant velocity and perhaps even balance the color charge. Clearly colorless (mesonic) jets of the type $\overline{Q}Q$ do couple to the sound channel in our case through the $\mathbf{S}_{00}(k)$ structure factor [31], and are expected to be trailed by a Mach cone.

Finally, to carry our analysis of charm and bottom at RHIC and perhaps even LHC, require an assessment of the heavy quark composition in the prompt phase of the heavy ion collision which we have not carried out. Also, we need to address more carefully the correspondence between our classical SU(2) QGP and the quantum SU(3) QGP. These issues will be addressed next.

Chapter 7

Conclusion

In this conclusion, we summarize what we have learned through the study about classical strongly coupled QGP.

In chapter 2, we have analyzed the equilibrium properties of the classical QGP in three different ways. First we have defined the grand partition function of the classical liquid QGP by considering the long range Coulomb field and the short range hardcore potential. Then the cumulant expansion and the high temperature of it have been worked out. The loop expansion of the grand partition function defined by a similar but quite different point of view has been worked out. We have shown that these expansions for both SU(2) and SU(3) are valid in a weak coupling limit.

In chapter 3, we have constructed the energy density of the SU(2) cQGP valid for all values of the plasma constant Γ by combining the analytic result obtained in chapter 2 through the loop expansion with the result from the molecular dynamics simulation of SU(2) colored particle. We have extracted a running coupling constant by fitting our result to the lattice energy density and have found that ours is smaller than the one directly calculated by the

lattice but is large enough to reflect the nature of the strongly coupled QGP.

We have shown that QGP is strongly coupled near the critical temperature T_C and its coupling constant changes significantly across the transition temperature. We have expected transport properties such as diffusion and viscosity, as well as energy loss to be significantly affected in the transition region from strong to weak coupling in the cQGP.

In chapter 4, we have considered correlation functions of a system composed of strongly coupled cQGP. At first, we have obtained a generalized Ornstein-Zernicke equation valid also for colored particles. Then, for simplicity, we have restricted our interest to SU(2) cQGP of which color components are describable by 3 coordinates of a point in a sphere with a radius of the second Casimir. We have shown that correlation functions of colored particles yield multiple correlation functions characterizing color correlations originated by Legendre polynomials.

We have applied the Debye-Hückel plus Hole (DHH) theory to Debye charging process and the linearized Poisson-Boltzman equation to obtain the structure factor, the density correlation function in an analytic form. Also, we have proven by the SU(2) molecular dynamics simulations the split of the correlation function of color charges to correlation functions of different channels. We have shown that the density and charge structure factors are characterized by the sound and plasmon mode. We have emphasized important roles of structure factors in describing the strongly coupled cQGP.

In chapter 5, we have analyzed the kinetic properties of strongly coupled cQGP. Starting from constructing the Liouville equation in phase space we have derived the generalized Langevin equation containing a non-local collision term, the self-energy kernel. We have shown that the self-energy kernel can

be re-expressed in terms of correlation functions and contributes mainly to transport coefficients in the hydrodynamical limit. We have seen that our results compare fairly with molecular dynamics simulations for SU(2) and have concluded from the dependence of the transport coefficients on the plasma constant Γ that colored Coulomb plasma in this regime is in the liquid state.

Finally, in chapter 6, We have investigated the energy loss of heavy quarks travelling through an SU(2) cQGP. We have used linear response theory and fluctuation-dissipation theorem to tie the energy loss of a fast moving particle to the charge density response, or the structure factor, of the medium composed of strongly coupled cQGP. We have shown that only the $l = 1$ color channel of the structure factor survives for the longitudinal part of the dielectric function. We have considered the energy loss in a various limit and concluded that the energy loss is soundless in the classical limit. We also have compared ours to molecular dynamics simulations and seen that ours is about half the energy loss obtained from simulation.

7.1 Outlook

We have explained so far various aspects of physics related to sQGP with the model of classical sQGP. This research is meaningful by the fact that it has tried to investigate the classical aspects of non-Abelian plasma. It has helped us in understanding real sQGP and also has given us a guideline for a future research. But it is also true that we still have many problems that should be solved before we develop more the theory of the classical sQGP.

The current analysis has been, mostly in the non-equilibrium part, based on the classical treatment of SU(2) QGP. Even though we have succeeded in

extracting the core properties of sQGP with this model, we have to decrease the gap between the SU(3) sQGP and the model since we might have missed the important effects originated by another Casimir, cubic Casimir.

We also have to extend our classical sQGP to consider the effects caused by many components. As we have pointed out in chapter 4, we have observed the multi-component effect of the structure factor even though we have considered only one-component classical colored plasma. What can be observed when the effects of the multi-component classical colored plasma are considered is not yet known.

Moreover, we need to consider various quantum effects to reduce the difference between real SU(3) multi-component sQGP and our model. To treat classical sQGP quantum mechanically, we need to include the spin, the magnetic fields, the running coupling constant and so on. These consideration would make the model of classical sQGP richer. We hope that the classical sQGP would also suggest a guideline even for the new research triggered by the experiment at LHC.

Bibliography

[1] J. P. Hansen and I. R. McDonald, *Theory of simple liquids* (Academic Press, 2006)

[2] R. R. Nets and H. Orland, Eur. Phys. J. E **1**, 67 (2000)

[3] B. A. Gelman, E. V. Shuryak and I. Zahed, Phys. Rev. C **74**, 044908 (2006)

[4] K. Johnson, Annals Phys. **192**, 101 (1989)

[5] S. K. Wong, Nuovo Cimento A **65**, 689 (1970)

[6] J. Liao and E. Shuryak, Phys. Rev. C **75**, 054907, (2007)

[7] J.-M. Caillol and J.-L. Raimbault, J. Stat. Phys. **103**, 753 (2001)

[8] B. A. Gelman, E. V. Shuryak and I. Zahed, Phys. Rev. C **74**, 044909 (2006)

[9] J.-L. Raimbault and J.-M. Caillol, J. Stat. Phys. **103**, 777 (2001)

[10] L. S. Brown and L. G. Yaffe, Phys. Rept. **340**, 1 (2001)

[11] S. Cho and I. Zahed, Phys. Rev. C **80** 014906 (2009)

[12] D. F. Litim and C. Manuel, Phys. Rept. **364**, 451 (2002)

[13] S. Jeon and R. Venugopalan Phys. Rev. D **70**, 105012 (2004)

[14] S. Ichimaru, Rev. Mod. Phys. **54**, 1017 (1982)

[15] J. Hansen, I. McDonald and E. Pollock, Phys. Rev. A **11**, 1025 (1975)

[16] S. Cho and I. Zahed, Phys. Rev. C **79**, 044911 (2009)

[17] S. Ichimaru, *Statistical Plasma Physics Vol II:Condensed Plasmas* (Westview Press, 2004)

[18] V. Bannur, Eur. Phys. J. C **11**, 169 (1999)

[19] S. Nordholm, Chem. Phys. Lett. **105**, 302 (1984)

[20] J. Engels, F. Karsch and H. Satz, Phys. Lett. B **101**, 89 (1981)

[21] O. Kaczmarek, F. Karsch, F. Zantow and P. Petreczky, Phys. Rev. D **70**, 074505 (2004)

[22] S. Cho and I. Zahed, `arXiv:0910.2666`

[23] E. V. Shuryak and I. Zahed, Phys. Rev. C **70**, 021901 (2004)
E. V. Shuryak and I. Zahed, Phys. Rev. D **70**, 054507 (2004)

[24] D. Teaney, J. Lauret and E. V. Shuryak, Phys. Rev. Lett. **86**, 4783 (2001)
D. Teaney, J. Lauret and E. V. Shuryak, `nucl-th/0110037`
P. F. Kolb, P. Huovinen, U. Heinz, H. Heiselberg, Phys. Lett. B **500**, 232 (2001)
P. F. Kolb and U. Heinz, `nucl-th/0305084`

[25] K.Dusling and I.Zahed, `arXiv:0904.0169`

[26] D. A. McQuarrie, *Statistical Mechanics* (Harper and Row, 1976)

[27] M. N. Tamashiro, Y. Levin and M. C. Barbosa, Physica A **268**, 24 (1999)

[28] B. P. Lee and M. E. Fisher, Phys. Rev. Lett. **76**, 302 (1996)

[29] B. P. Lee and M. E. Fisher, Europhys. Lett. **39**, 611 (1997)

[30] J.P.Hansen and I.R.McDonald, Phys. Rev. A **11**, 2111 (1975)

[31] S. Cho and I. Zahed, `arXiv:0909.4725`

[32] D. Foster and P. C. Martin, Phys. Rev. A **2**, 1575 (1970)

[33] D. Foster, Phys. Rev. A **9**, 943 (1974)

[34] G. F. Mazenko, Phys. Rev. A. **7**, 209 (1973)

[35] G. F. Mazenko, Phys. Rev. A. **9**, 360 (1974)

[36] J. Wallenborn and M. Baus, Phys. Rev, A **18**, 1737 (1978)

[37] M. Baus, Physica A **79**, 377 (1975)

[38] S. Cho and I. Zahed, `arXiv:0910.1548`

[39] H. Gould and G. F. Mazenko, Phys. Rev. A **15**, 1274 (1977)

[40] S. Ichimaru, *Statistical Plasma Physics Vol I:Basic Principles* (Westview Press, 2004)

[41] H. Heiselberg, Phys. Rev. D **49**, 4739 (1994)

[42] H. Mori, Prog. Theor. Phys. **33**, 423 (1965)

[43] A. Z. Akcasu and J. J. Duderstadt, Phys. Rev. **188**, 479 (1969)

[44] J. Wallenborn and M. Baus, J. Stat. Phys. **16**, 91 (1977)

[45] H. Grad, Comm. Pure Appl. Maths, **2**, 331 (1949)

[46] E. V. Shuryak, Prog. Part. Nucl. Phys. **62**, 48 (2009)

[47] M. H. Thoma and M. Gyulassy, Nucl. Phys. B **351**, 491 (1991)

[48] E. Braaten and M. H. Thoma, Phys. Rev. D **44**, 1298 (1991)

[49] E. Braaten and M. H. Thoma, Phys. Rev. D **44**, R2625 (1991)

[50] M. Djordjevic, Phys. Rev. C **74**, 064907 (2006)

[51] M. Djordjevic and U. Heinz, Phys. Rev. Lett. **101** 022302 (2008)

[52] M. Djordjevic and U. Heinz, Phys. Rev. C **77** 024905 (2008)

[53] A. Dumitru, Y. Nara, B. Schenke and M. Strickland, Phys. Rev. C **78** 024909 (2008)

[54] S. Sin and I. Zahed, Phys. Lett. B **608**, 265 (2005)

[55] H. Liu, K. Rajagopal and U. A. Wiedemann, Phys. Rev. Lett. **97**, 182301 (2006)

[56] J. Ruppert and B. Muller, Phys. Lett. B **618**, 123 (2005)

[57] J. Casalderrey-Solana, E. V. Shuryak and D. Teaney, Nucl. Phys. A **774**, 577 (2006)

[58] C. P. Herzog, A. Karch, P. Kovtun, C. Kozcaz and L. G. Yaffe, JHEP. **07**, 013 (2006)

[59] P. M. Chesler and L. G. Yaffe, Phys. Rev. Lett. **99**, 152001 (2007)